ANALYSES OF STRONG-MOTION RECORDS FROM A PARKING STRUCTURE DURING THE 17 JANUARY 1994 NORTHRIDGE EARTHQUAKE

by

Said Hilmy, Stuart Werner, Ahmed Nisar and James Beck

Dames and Moore
Santa Ana, California

Data Utilization Report CSMIP/00-04 (OSMS 00-06)

California Strong Motion Instrumentation Program

March 2000

CALIFORNIA DEPARTMENT OF CONSERVATION
DIVISION OF MINES AND GEOLOGY
OFFICE OF STRONG MOTION STUDIES

THE RESOURCES AGENCY
MARY NICHOLS
SECRETARY FOR RESOURCES

STATE OF CALIFORNIA
GRAY DAVIS
GOVERNOR

DEPARTMENT OF CONSERVATION
DARRYL YOUNG
DIRECTOR

DIVISION OF MINES AND GEOLOGY
JAMES F. DAVIS
STATE GEOLOGIST

DISCLAIMER

The content of this report was developed under Contract No. 1093-554 from the Strong Motion Instrumentation Program in the Division of Mines and Geology of the California Department of Conservation. This report has not been edited to the standards of a formal publication. Any opinions, findings, conclusions or recommendations contained in this report are those of the authors, and should not be interpreted as representing the official policies, either expressed or implied, of the State of California.

ANALYSES OF STRONG-MOTION RECORDS FROM A PARKING STRUCTURE DURING THE 17 JANUARY 1994 NORTHRIDGE EARTHQUAKE

by

Said Hilmy, Stuart Werner, Ahmed Nisar and James Beck

Dames and Moore
Santa Ana, California

Data Utilization Report CSMIP/00-04 (OSMS 00-06)

California Strong Motion Instrumentation Program

March 2000

This study was conducted at Dames and Moore, Inc. in Santa Ana, California from June 1994 to June 1996 and was supported by the Department of Conservation under Contract No. 1093-554.

California Department of Conservation
Division of Mines and Geology
Office of Strong Motion Studies
801 K Street, MS 13-35
Sacramento, California 95814-3531

PREFACE

The California Strong Motion Instrumentation Program (CSMIP) in the Division of Mines and Geology of the California Department of Conservation promotes and facilitates the improvement of seismic codes through the Data Interpretation Project. The objective of the this project is to increase the understanding of earthquake strong ground shaking and its effects on structures through interpretation and analysis studies of CSMIP and other applicable strong motion data. The ultimate goal is to accelerate the process by which lessons learned from earthquake data are incorporated into seismic code provisions and seismic design practices.

The specific objectives of the CSMIP Data Interpretation Project are to:

1. Understand the spatial variation and magnitude dependence of earthquake strong ground motion.

2. Understand the effects of earthquake motions on the response of geologic formations, buildings and lifeline structures.

3. Expedite the incorporation of knowledge of earthquake shaking into revision of seismic codes and practices.

4. Increase awareness within the seismological and earthquake engineering community about the effective usage of strong motion data.

5. Improve instrumentation methods and data processing techniques to maximize the usefulness of SMIP data. Develop data representations to increase the usefulness and the applicability to design engineers.

This report is part of CSMIP data utilization reports designed to transfer recent research findings on strong-motion data to practicing seismic design professionals and earth scientists. CSMIP extends its appreciation to the members of the Strong Motion Instrumentation Advisory Committee and its subcommittees for their recommendations regarding the Data Interpretation Research Project.

Anthony F. Shakal
CSMIP Program Manager

Moh J. Huang
CSMIP Data Interpretation
Project Manager

FORWARD

The investigation described in this report has been sponsored by the Strong Motion Instrumentation Program, of the California Department of Mines and Geology. It was implemented under Contract Number 1093-554 for the data interpretation project entitled "Analyses of Strong Motion Records from Parking Structures during the January 17th Northridge Earthquake".

Co-Principal Investigators for the project were Dr. Said Hilmy and Mr. Stuart Werner from Dames & Moore, Inc. Significant contributors to this work were Mr. Ahmed Nisar from Dames & Moore, Inc., who carried out the system identification of the recorded earthquake motions at the parking structure, and Professor James Beck of California Institute of Technology, who was a special consultant to the project and provided invaluable assistance throughout the investigation. The authors are grateful to the assistance provided by Dr. Moh Huang of the SMIP data interpretation program and the useful suggestions provided by the members of the appointed review committee of the project.

TABLE OF CONTENTS

TABLE OF CONTENTS
(Continued)

1.0 INTRODUCTION

1.1 STATEMENT OF THE PROBLEM

Of all modern concrete buildings that were subjected to strong shaking during the Northridge earthquake, parking structures appear to have suffered the greatest degree of damage. During the earthquake, eight parking structures at heavily used shopping malls, hospitals, and colleges either partly or completely collapsed. Four were built between 1986 and 1992, and the others were built between 1965 and 1982. Damaged or severely cracked columns, beams, and shear walls caused building inspectors to close at least 24 other parking structures in the San Fernando Valley, and in Glendale, Santa Monica and West Los Angeles. Many of the damaged parking structures will take months and millions of dollars to repair.

This extensive damage to parking structures during the Northridge earthquake, resulted from several unique characteristics of such structures which are summarized below:

Precast Concrete Construction. Many of the damaged parking structures were constructed from precast concrete components which lacked adequate strength, ductility and redundancy. Current code design procedures do not penalize this type of construction. Examples of severely damaged structures with conventional precast concrete construction include the recently constructed, 2,500-car, three-story parking structure at California State University in Northridge and the Northridge Fashion Center's north and south parking structures with parking spaces of 750 cars and 650 cars, respectively. In addition, parking structures with patented precast systems were also vulnerable (e.g., the precast table system used in Community hospital parking structure in Granada Hills, and Glendale Fashion Center's parking structure, which experienced severe damage at the base of the columns and the supporting pedestals).

Short Column Effects. The architectural configuration of the sloped ramps in parking structures and the existence of the deep spandrels attached to the perimeter columns result in short effective lengths of the columns. The shear demands for these short columns increase significantly as plastic hinges form at the columns ends. Several cases of this failure mechanism occurred in the Northridge Earthquake, with shear failure of short columns associated with the loss of the capacity of the columns to resist vertical loads. The damage to these columns was catastrophic in cases where non-ductile reinforcing details were used. Examples include Glendale Fashion Center parking structure, which collapsed and Westside Pavilion parking structure, which experienced severe damage.

Concrete Ramps. The concrete ramps in parking structures form a connecting link between floors that is not typically modeled in the seismic design and analysis process. Sloped ramps with a large span-width ratio may experience large floor accelerations and may result in more flexible response and high seismic stresses in certain members. Damage due to sloped ramps

occurred at parking structures in Granada Hills and Sherman Oaks. Helical ramps in a Westside parking structure experienced major damage, with heavily cracked columns which shifted out of plumb.

Long Spans and Open Architecture. Parking structures typically feature long spans and open architecture, both to reduce construction cost and to increase parking space. Interior partitions and walls are kept to a minimum. In other types of buildings, partitions and other nonstructural elements have the beneficial effect of increasing the building's dissipation of the energy from the seismic shaking. However, because parking structures typically lack these nonstructural elements, they are subjected to effectively larger forces and deformations. Parking structures with multi-bay post-tensioned moment frames experienced damage during the Northridge Earthquake (e.g., parking structures in Westside, Sherman Oaks, and Canoga Park).

Deterioration and Corrosion. Because of the relatively large exposed surface of parking structures and their traditionally low maintenance, the potential for deterioration and corrosion will be increased. Significant Corrosion may be found at the interface between slabs and walls and at the connections of precast elements and peripherals. Several failures of these elements can be attributed to corrosion problems.

Penthouse and peripherals Damage. During the Northridge Earthquake several parking structures had penthouses and attached peripherals, such as elevator cores and stairwells, suffered severe damage or collapse. This can be attributed to amplified acceleration levels at the top levels and the traditionally low ductility code requirements in the design of these peripherals.

Pounding at Separation Joints. Separation joints in older parking structures were often insufficient to prevent pounding, which was observed in many instances. Such pounding caused dropping of the sealants and flashing, and cracking in adjacent floors and columns. The resulting horizontal and vertical distortions at adjacent slabs near separation joints, was often significant and beyond repair at several parking structures.

The poor performance of many parking structures during the Northridge earthquake demonstrates that current seismic evaluation and design procedures for such structures require further improvement. An important vehicle for improving these procedures and the understanding of the seismic response characteristics of parking structures is the compilation and analysis of strong motion records from such structures using sound analysis procedures. Unfortunately, there has been relatively few arrays of recorded motions in parking structures during past earthquakes, and no known examples of the use of such motions to assess and improve seismic evaluation and design procedures. However, during the Northridge Earthquake, a set of 14 strong motion records was obtained at a 6-story parking structure in Los Angeles (CSMIP Station No. 24655). Detailed analysis of this structure based on these recorded motions can provide important insights for assessing seismic performance and improving seismic design procedures for parking

structures. The research project described in this report is directed toward meeting these objectives.

1.2 SCOPE OF RESEARCH

The objectives of this project are to use state-of-the-practice system identification and engineering analysis procedures in conjunction with the recorded earthquake at the parking structure in order to:

- evaluate the seismic performance characteristics of this structure;
- assess the adequacy of current seismic design and analysis procedures for such structures; and
- recommend directions for improving these procedures in the future.

In particular, the project will address the following key issues:

- How do the base shear forces and overturning moments and the interstory shear forces, torsional moments, and drifts developed in the structure during the Northridge Earthquake compare to the original design values of the quantities and to the design values given in the 1994 Uniform Building Code (UBC)? How consistent are these various comparisons with the observed seismic performance of the structure?
- How do the dynamic characteristics of the structure (such as mode shapes and natural periods) identified from the recorded earthquake motions compare with the values obtained from finite elements computer models and the values recommended by the building code?
- What was the degree of nonlinearity in the structures response to the Northridge earthquake and how did it affect the structural response? What were the seismic demand/capacities (D/C) ratios experienced by the parking structure, and what are the acceptable levels D/C ratios recommended for future seismic design?
- What is the effect of the ground acceleration of the behavior of upper beams and parapets, and can their behavior can be reasonably well predicted using analytical models?

1.3 REPORT ORGANIZATION

Chapter 2 of this report includes a building description, the important structural features, and the site assessment of the structural behavior during the Northridge Earthquake. Chapter 3 presents

the recorded strong motion data for this structure as provided by the Strong Motion Instrumentation Program. It also outlines the main dynamic characteristics of these recorded motions.

Chapter 4 of this report features the use of system identification of the recorded motions in the parking structure, in order to estimate normal modes of vibration excited in the structure during the Northridge Earthquake. The chapter provides a description of the MODE-ID methodology and a comparison between computed model motions and recorded motions. The description of the finite elements computer model is given in Chapter 5. A comparison between the recorded motions and the computed results is also provided.

Chapter 6 includes an assessment of the structural behavior and comparison with seismic design provisions. Computer models to study the response of vertical vibration of the roof girder and the roof parapets are also presented. Chapter 7 provides a comparison of the structural behavior of the parking structure under investigation, and the response of similar parking structures during the Northridge earthquake. Finally, concluding remarks of this investigation are outlined in Chapter 8.

2.0 BUILDING DATA

2.1 BUILDING DESCRIPTION

The parking structure is located near downtown Los Angeles. It is a six story reinforced concrete structure that is rectangular in plan, and has plan dimensions of approximately 307 feet in the east-west direction and 260 feet in the north-south direction. The structure has seven levels of parking with a total usable area of approximately 550,000 square feet.

Appendix A includes several structural Drawings for the as-built condition of the parking strucure. Drawings #1, #2, and #3 provide details of the typical plans and elevations of the structure. There are 17 bays along the east-west direction (the typical span of the interior bays is 18 feet, and the span of the two end bays is 17.75 feet). There are four (4) bays along the north-south direction which each span 65 feet. The traffic circulates between parking levels through two interior ramps which slope upward and downward between adjacent floors. The typical floor height of the structure is 10 feet, and it's total height is 60 feet.

The building was constructed in two phases. The 1977 "Phase I" construction consisted of only three stories (see Drawing # 4). A 5-inch cast-in-place post-tensioned concrete slab spans between adjacent precast concrete beams, which are spaced at 18 ft. o.c. These post-tensioned beams have a cross section area of 14" x 30" and span 65 feet along the north-south direction. The beams are supported on the corbels of precast concrete columns (Drawing # 5). The dimensions of the columns are 24" square at the interior, 16" square at the exterior north and south sides of the structure (Grid lines A and E), and 16" x 17" at the exterior east and west sides (Grid Lines 1 and 18). The slab thickness increases from 5" to 5.75" at the second level of the structure, and the column schedule and reinforcing details are shown in Drawing # 6.

The lateral load resisting system consists of cast-in-place shear walls. As shown in Drawing # 1, there are six separate walls at the exterior east and west sides of the buildings (three walls at Grid line (1) and three similar walls at grid line (18): Each wall is 32.5 feet wide, and 14" thick). There are two interior walls (72'long and 16" thick) along the east-west direction at grid lines B and D. The reinforcing steel of the North-South walls and the East-West walls is summarized in Tables #2.1 and #2.2, respectively.

The soil at the site consists of alluvium soil on a deep layer of firm sand (the depth of the sand layer was not indicated in the drawings). All columns are supported on drilled bell caissons. As shown in Drawing # 7, the shaft diameter of the bell caissons varies from 3.5 feet to 5.0 feet and the bell diameter varies from 7.0 feet to 15.0 feet. Typically, the bell caissons penetrate from 2-3 feet into the firm sand, whereas at the ends of the shear walls, the penetration of the caissons into the firm sand is 6 feet.

The drawings indicate that the allowable soil bearing pressure is 8.0 ksf for dead load plus live load with 2.0 feet penetration into the firm sand layer, and 10 ksf with 6 feet penetration. The allowable soil bearing is increased to 20 ksf for combined dead, live and seismic loads.

In 1979, a "Phase II" construction project resulted in the additional levels above the original parking structure. This construction included three additional levels to the parking structure with a similar architectural layout to the existing structure. However, during this phase, cast-in-place concrete was used for all additional columns and walls. The thickness of the shear walls along the east-west direction was reduced from 16" to 11" at the fifth and sixth levels and between Grid lines 8 and 10 at the fourth level. The thickness of the shear walls at the east and west sides of the buildings was reduced from 14" to 11".

The specified 28-day concrete strength was 5,000 psi for the precast concrete walls, columns and beams, and 4000 psi for the cast-in-place concrete and precast panels. The initial design live load is 50 psf for the parking floor with no reduction allowed.

The following are important characteristics of the parking structure under investigation:

(1) At the four corners of the structure there are four (4) exterior stair towers that are of steel construction. Each tower is attached to two masonry veneer walls as shown in Photo #3. These walls are 8" reinforced clay block walls and are attached to the main structure through dowels at the floor levels. The details shown in Drawing # 8 indicate that the steel dowels are embedded in plastic tubes to provide only out-of-plane resistance (i.e., the masonry walls do not provide additional resistance to the seismic shear forces from the main structure).

(2) The architectural veneer attached to the exterior of the building consists of 3" tied veneer brick anchored to the adjacent walls with 14 gage galvanized dovetailed anchors that are 1.00 inch wide and are placed at 12" on center (See Drawing # 9). Therefore, in this investigation the veneer was considered to add to the mass of the main structure, but not to increase the structure's total stiffness.

(3) The exterior spandrels at the south and north sides are separated from the columns as shown in Drawing # 6, Detail # 5. However, the spandrels at the east and west sides are connected to the shear walls with continuous steel dowels to provide flexural continuity at the beam-wall joints (Drawing # 10). The top beam at the east and west side is a 6 foot deep beam and provides coupling between the adjacent shear walls.

(4) The interior prestressed beams are seated on neoprene bearing pads at the columns corbels, with no positive ties between the beams and columns. The slabs are connected to the columns with 3/4 inch diameter coil inserts that are embedded 6 inches into the columns and are connected to 3/4 inch diameter threaded rods that are embedded three feet into the slab (See Drawing # 6, Detail # 7).

(5) The precast concrete columns are embedded in 18 inch deep pockets in the poured-in-place caissons. The gaps were filled with non-shrink grout. The connection between the columns at the ends of the shear walls and the caissons consists of additional reinforcing steel that extends from the precast concrete columns to the poured-in-place concrete caissons (See Drawing # 7, Detail # 6).

(6) The typical connection between the precast concrete columns and cast-in-place walls is provided through steel dowels and shear keys (See Drawing # 10). Jamb steel at the wall ends is also indicated in Drawing # 10.

(7) The typical joints between the floors and the east and west walls are cast-in-place concrete as shown in Drawing # 11 a. The connection between the floors and north and south walls for Phase I construction is provided through shear keys, as shown in Drawing # 11 b.

(8) The typical interface between Phase I and II construction is provided by roughening the existing concrete surface and by providing full strength butt welding of existing and new 75 ksi reinforcements.

(9) Diaphragm chord reinforcement was provided in both the Phase I and Phase II construction. This reinforcement consisted of 3#7 rebars at the lower levels and 5#7 rebars at the upper levels. (see Drawing # 12, Detail C).

10) Rooms for facility offices were provided at the first level of the parking structure between Grid lines 11, 18, C and D. These rooms have 8 inch thick reinforced block walls that are connected to slab-on-grade with steel dowels (Drawing # 12).

11) Typical parapet details are shown in Drawing # 13. One of the roof parapets at the North side of the garage was instrumented during the Northridge Earthquake and experienced severe levels of shaking with a recorded peak acceleration that exceeded 1.0 g.

2.2 SITE REVIEW

On September 29, 1994, Mr. Stuart Werner and Dr. Said Hilmy visited the structure to visually observe and photograph the structure and its damage due to the Northridge Earthquake, and to speak to personnel from the parking structure regarding its performance during the earthquake. The information that we compiled during this visit indicated that the structure's overall seismic performance during the Northridge Earthquake was good. The only earthquake damage experienced by the structure was as following:

(a) Diagonal hairline cracking at some beams that interconnect the perimeter shear walls at the east and west sides of the structure.

(b) Some cracking and spalling of brick veneer along the stairwells at the upper levels. However, most of this damage apparently existed prior to the Northridge Earthquake.

(c) Some movement of precast concrete wheel stops at the roof.

There was no obvious signs of patching or damage at the roof or at the interface of Phase I and Phase II construction. Photos 1 through 18, which were taken during our site visit show outside views of the parking structure, locations of sensors, and others views for structural elements inside the structure.

Table # 2.1
Steel Reinforcements in N-S Shear Walls

Level	Wall Length	Wall Thickness	Horiz. Steel in wall each face of wall	Vertical Steel in each face of wall	Boundary column Dimensions	Vertical Steel in B/C columns	Confinmen t Reinfs.
6th	32.5'	11.0"	#5 @ 18"	#5 @ 18"	16 x 17	6 # 10	# 3@14
5th	32.5'	11.0"	#6 @ 18"	#6 @ 18"	16x17	6 # 10	# 3@14
4th	32.5'	11.0"	#6 @ 10"	#7 @ 16"	16x17	8 # 11	# 3@14
3rd	32.5'	14.0"	#6 @ 14"	#6 @ 14"	16x17	12 # 11	# 3@14
2nd	32.5'	14.0"	#7 @ 14"	#7 @ 14"	16x17	18 # 11	# 3@14
1st	32.5'	14.0"	#7 @ 14"	#7 @ 14"	16x17	23 # 11	# 3@14

Table # 2.2
Steel Reinforcements in E-W Shear Walls

Level	Wall Length	Wall Thickness	Horiz. Steel in wall each face of wall	Vertical Steel in each face of wall	Boundary column Dimensions	Vertical Steel in B/C columns	Confinmen t Reinfs.
6th	72.0	11.0"	#5 @ 18"	#5 @ 18"	24x24	6 # 10	# 3@14
5th	72.0	11.0"	#6 @ 18"	#6 @ 18"	24x24	6 # 10	# 3@14
4th	72.0	11.0"	#6 @ 10"	#7 @ 16"	24x24	12 # 11	# 3@14
3rd	72.0	16.0"	#7 @ 14"	#7 @ 14"	24x24	12 # 11	# 3@14
2nd	72.0	16.0"	#8 @ 14"	#8 @ 14"	24x24	18 # 11	# 3@14
1st	72.0	16.0"	#8 @ 14"	#8 @ 14"	24x24	23 # 11	# 3@14

PHOTO 1: View looking northeast.

PHOTO 2: View from the top of adjacent tower looking northeast.

PHOTO 3: View looking northwest.

PHOTO 4: View of south side of parking structure.

PHOTO 5: West side of parking structure.

PHOTO 6: East side of parking structure.

PHOTO 7: Sensor location #1 to measure vertical motion at west end of north wall.

PHOTO 8: Sensor locations #2 & #5 to measure vertical and horizontal motion at east end of north wall.

PHOTO 9: Sensor locations #10 & #12 to measure lateral motion at center of north wall below roof.

PHOTO 10: Sensor location #7 to measure lateral motion at 14" concrete wall at east side.

PHOTO 11: Sensor location #13 to measure vertical motion at the middle of a 65 foot long prestressed beam at roof level.

PHOTO 12: Sensor location #14 to measure lateral motion at top of parapet at roof (north end).

PHOTO 13: Sloping ramps at roof.

PHOTO 14: Interface between interior columns and sloping ramps.

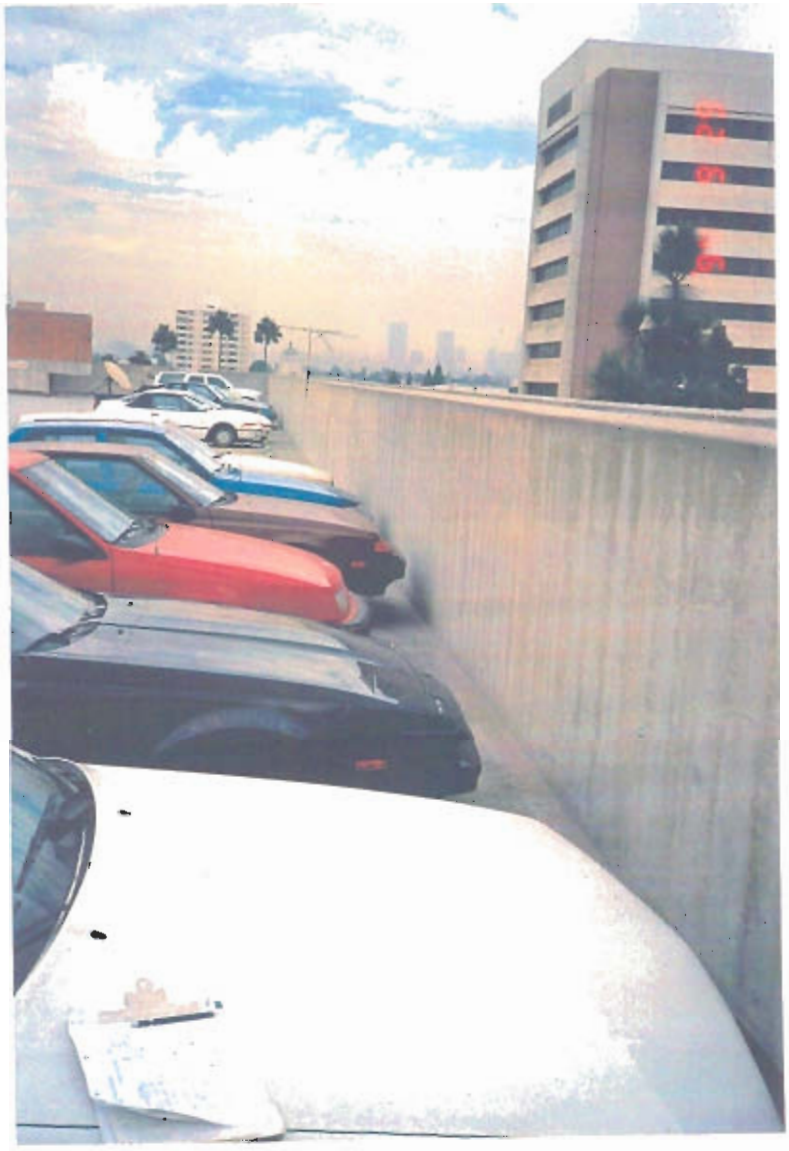

PHOTO 15: Deep beam at the top of shear walls (east side).

PHOTO 16: View of 24" X 24" interior columns.

PHOTO 17: Previous spalling at block walls of stair towers.

PHOTO 18: Cracks at top of block walls of stair towers.

3.0 STRONG MOTION DATA

3.1 EARTHQUAKE CHARACTERISTICS

The Northridge Earthquake occured at 4:30 a.m. on the morning of January 17, 1994, and had a moment magnitude (MW) of 6.7. The epicenter of the earthquake was located about 32 km northwest of the downtown Los Angeles, in the densely populated San Fernando Valley. The earthquake was caused by rupture along a thrust fault with a strike N60°W and a dip of 35-45°S. The fault rupture initiated about 19 km below the San Fernando Valley, propagated upward toward the northeast on this plane, and stopped about 5 km below the ground surface.

3.2 BUILDING INSTRUMENTATION

The 6-story parking structure in downtown Los Angeles is the first parking structure from which significant strong-motion data has been obtained during earthquake shaking. It is located approximately 31 km from the epicenter of the Northridge earthquake. The California Division of Mines and Geology deployed a total of 14 strong motion accelerometers within the structure whose locations along the first floor, fourth floor, and roof are shown in Figure #3.1 and in Photos #2, #3, #4 and #15. This instrumentation system has been designed to measure (a) horizontal translations (in two orthogonal directions) and torsional rotations of each instrumented floor, (b) vertical translations of the first floor, together with rocking rotations of the floor about the north-south axis; (c) in-plane diaphragm deformations in the north-south direction, and (d) out-of-plane bending deformations of the parapet on the north side of the roof. In addition, a single vertical accelerometer is located on the roof.

3.3 CDMG STRONG MOTION DATA

The recorded motion time-history and response spectra at all the sensors of the parking structure were supplied by CDMG. The time-history records include displacement, velocity, and acceleration time-history for the main-shock's 60 seconds duration. The number of digitized points is 6001. The response spectra curves correspond to different damping levels of 0%, 2%, 3%, 5%, 7%, and 10%. A comparison of the acceleration time-history plots of the different stations is shown in Figure 3.2. Generated response spectra curves of recorded motion are given in Figure 3.3. Plots of individual acceleration time histories are givin in Appendix B.

3.4 CHARACTERISTICS OF RECORDED MOTIONS

The motions recorded at the base of structure was moderately strong, with peak horizontal accelerations of 0.29 g and 0.15 g in the north-south and east-west directions respectively and peak accelerations of the two vertical accelerograms of 0.22 g and 0.11 g. These motions were amplified substantially over the height of the structure, attaining peak horizontal accelerations at the roof of 0.55 g in the north-south direction (along the west and east walls) and 0.31 g in the east-west directions. The north-south accelerations measured at the mid-length of the roof diaphragm was amplified still further, allowing a peak acceleration of 0.84 g. In addition very

strong horizontal motions were recorded on the north parapet (with peak acceleration of 1.21 g), and strong vertical motions of a roof girder were also recorded (peak acceleration = 0.52 g). The duration of the strong shaking segement of the recorded motions was in the order of 12-13 Sec.

Preliminary inspection of all of the structure's recorded motions indicated significant rocking of the structure about its north-south axis, prominent in-plane deformations of the roof diaphragm, and relatively small torsional rotations. There does not appear to be significant nonlinearity of the structural response, since the widths of the acceleration cycles do not change appreciably overtime.

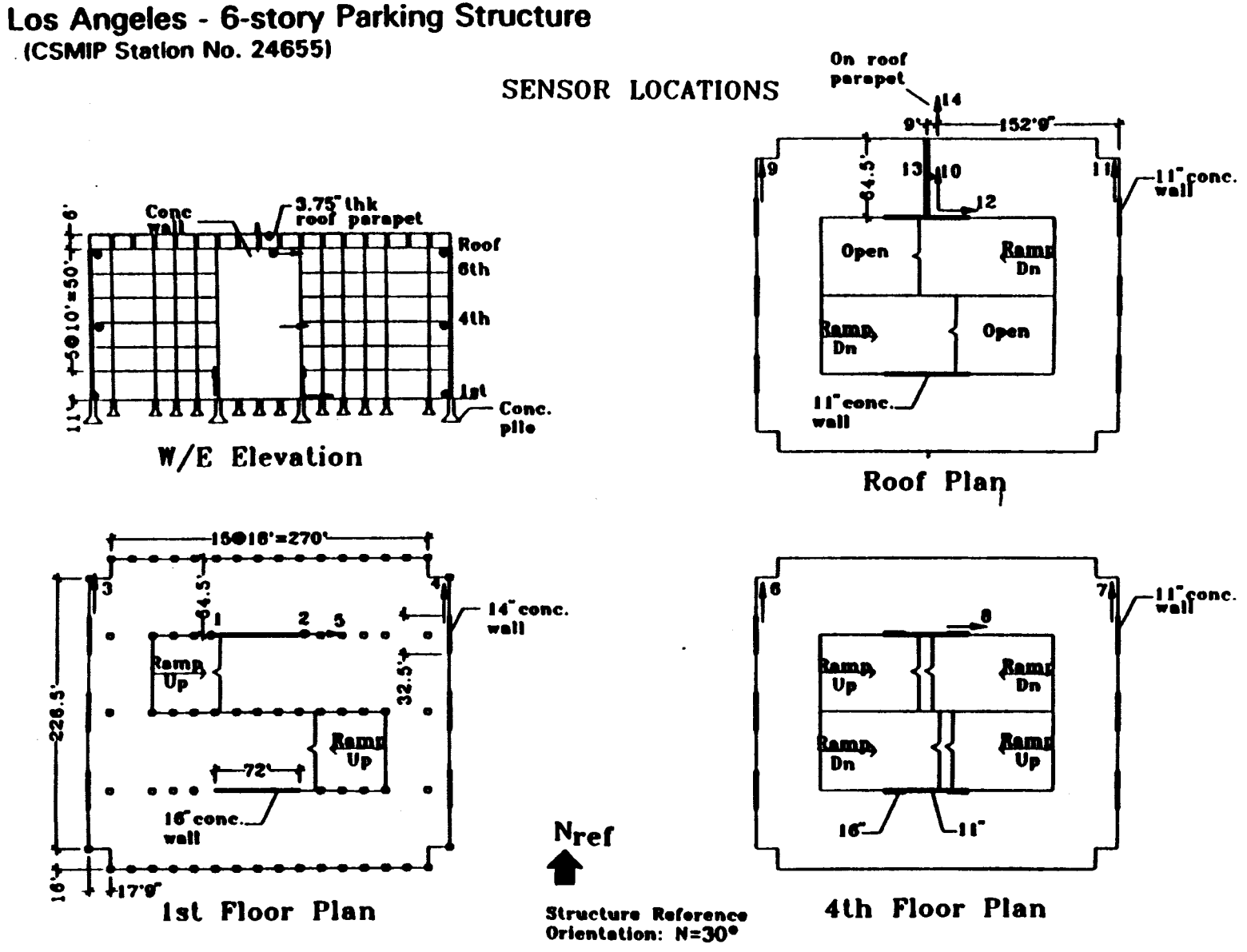

Figure 3.1 Locations of the Accelerometers

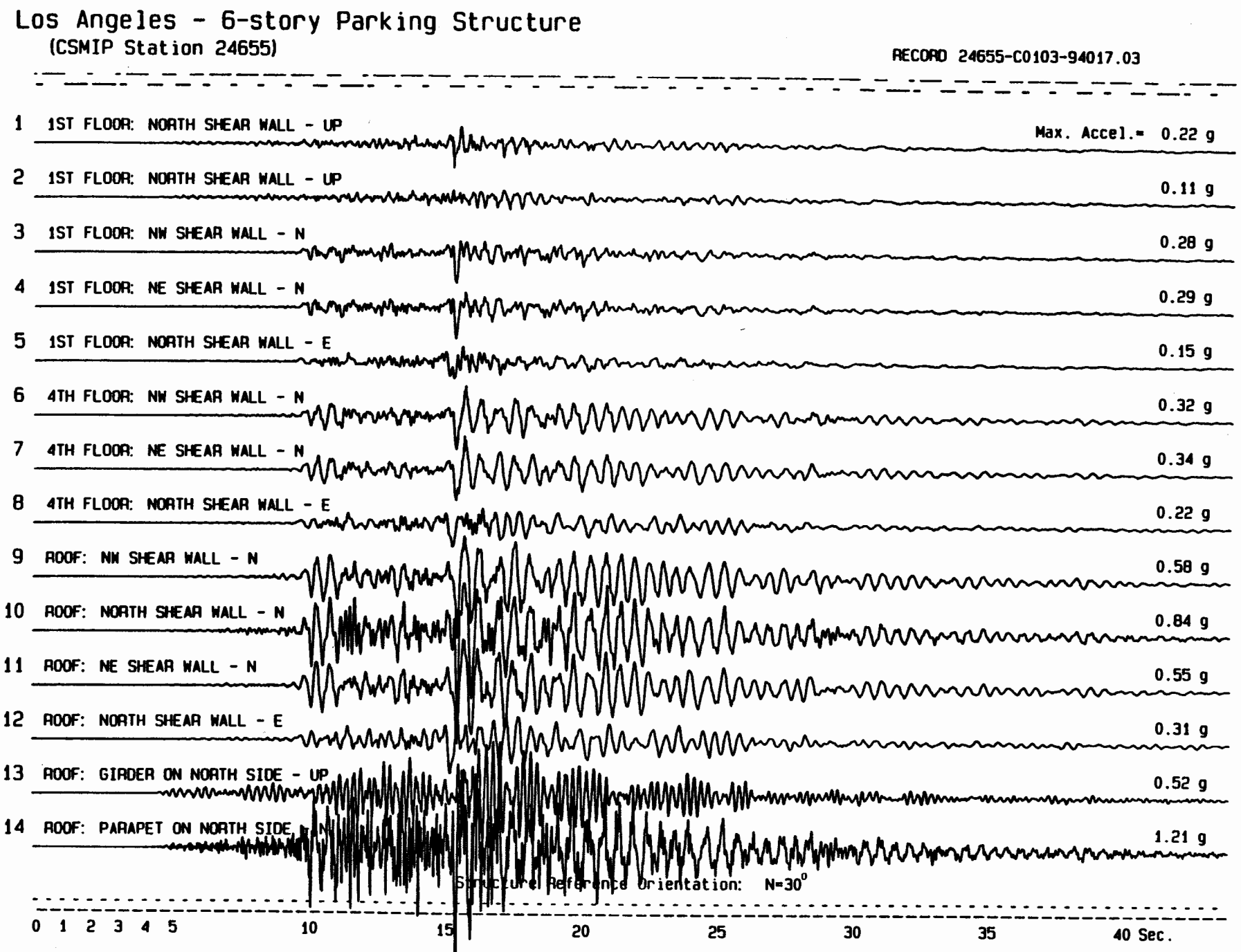

Figure 3.2 **A Comparison Between the Time-History Acceleration Records at Different Stations**

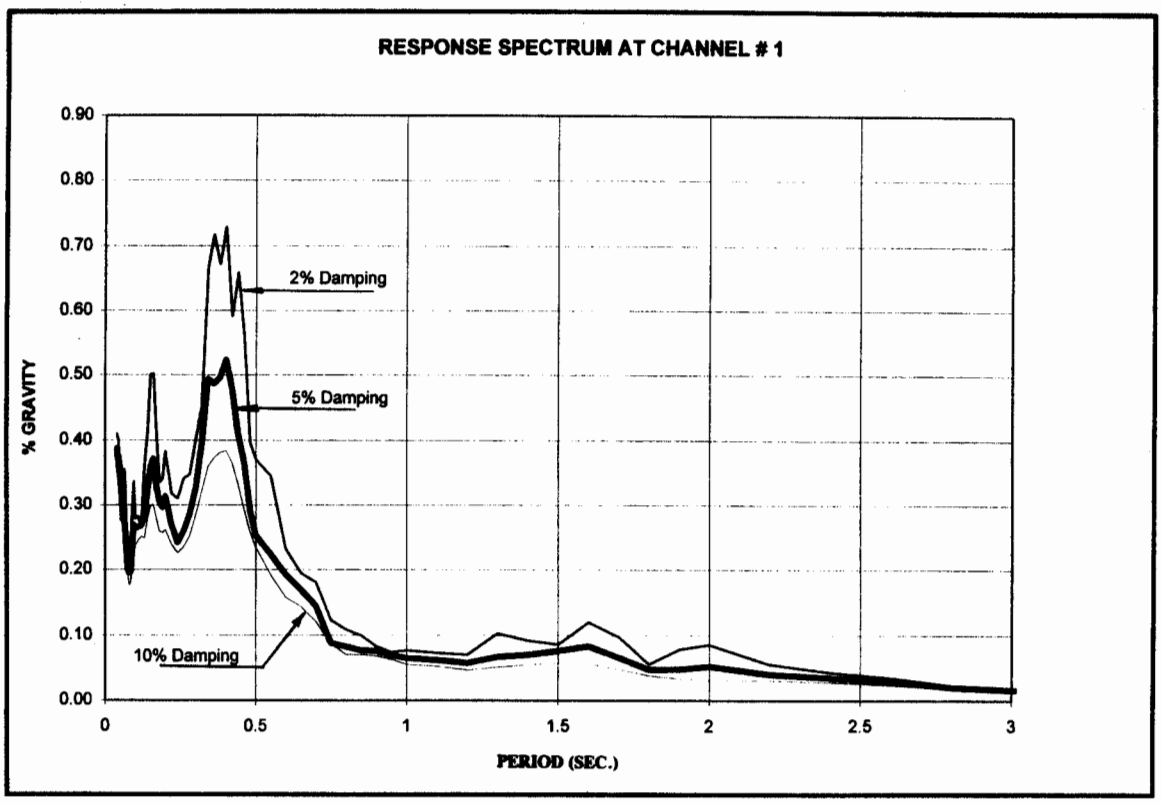

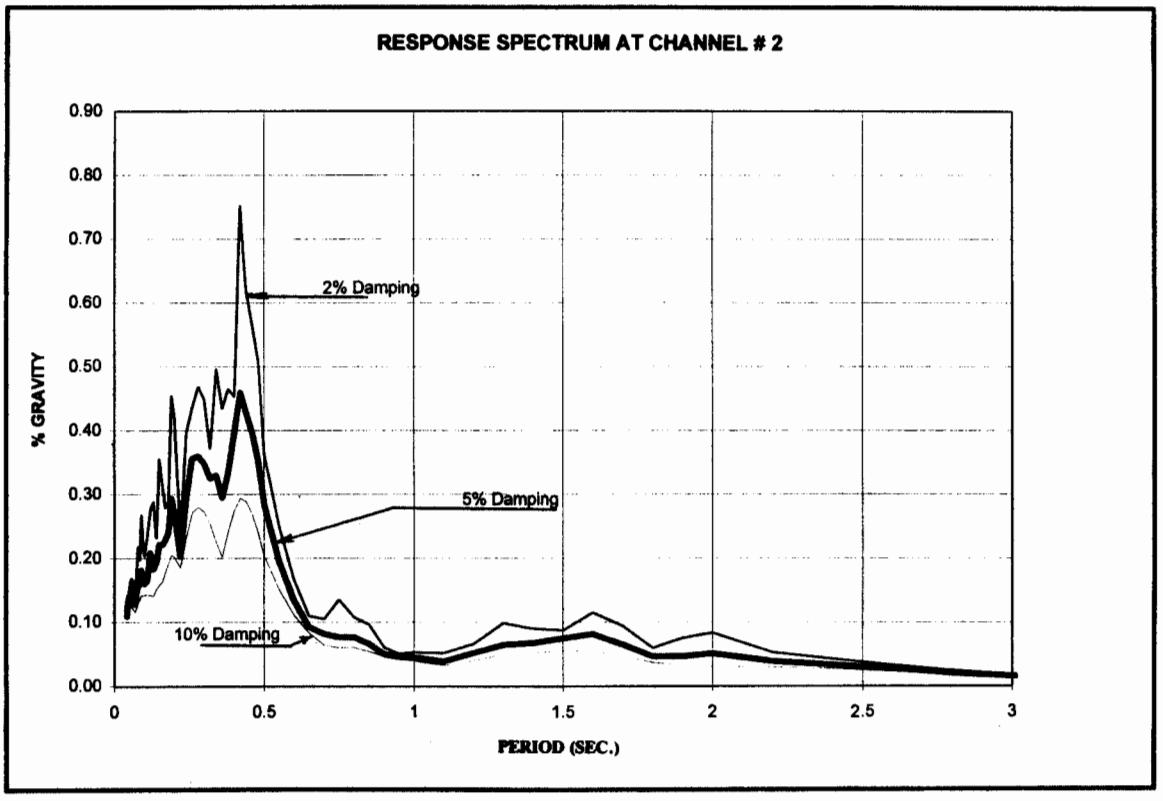

Figure 3.3 Generated Response Spectra Curves of Recorded Motions

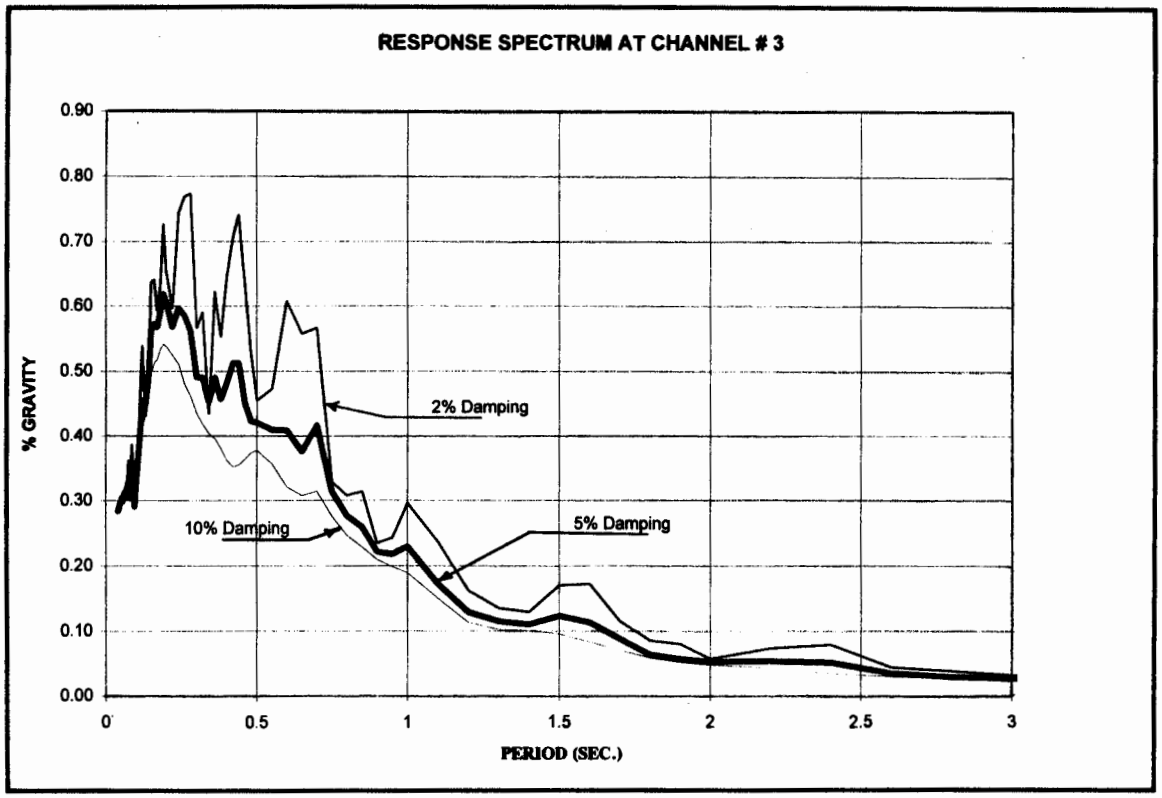

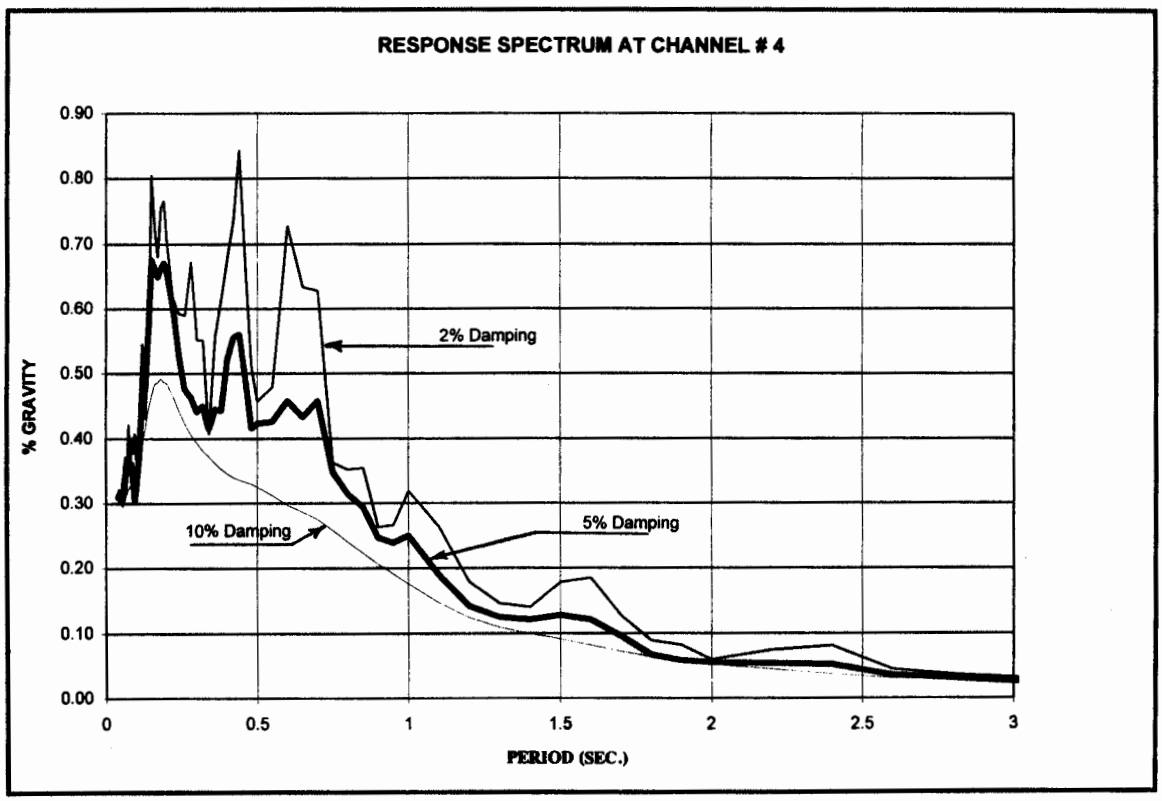

Figure 3.3 (continue) **Generated Response Spectra Curves of Recorded Motions**

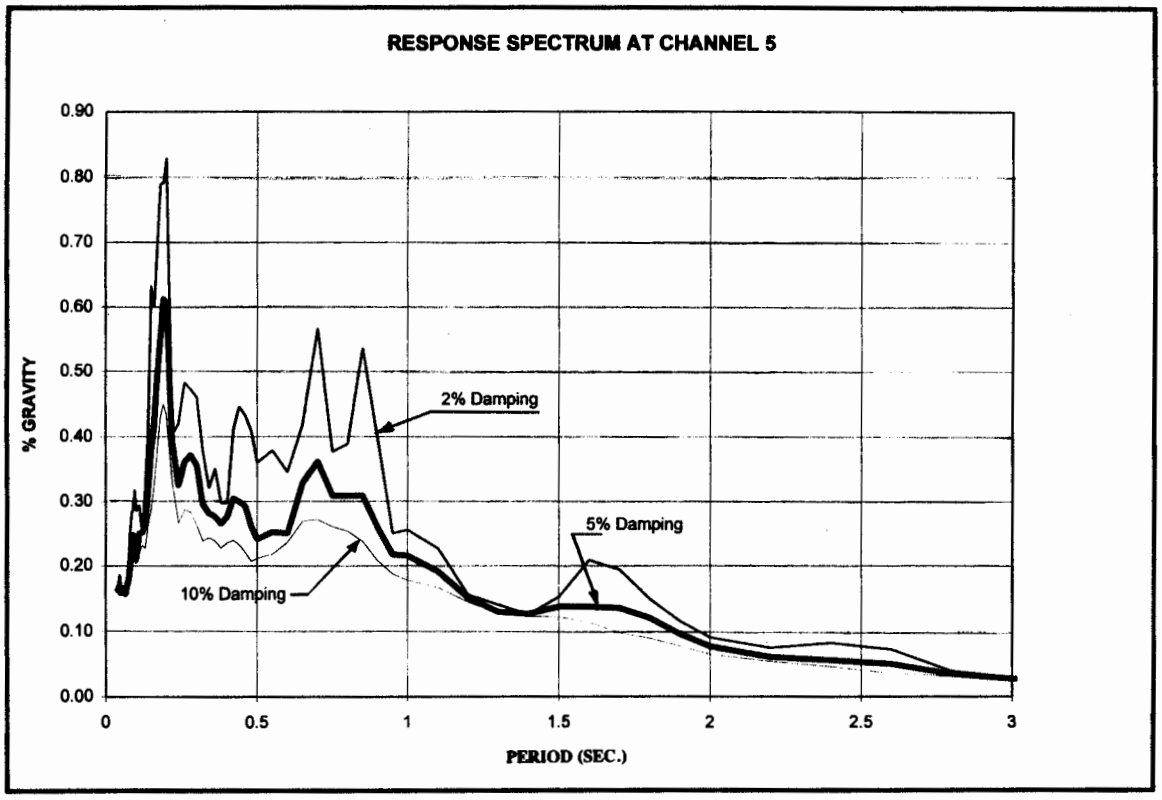

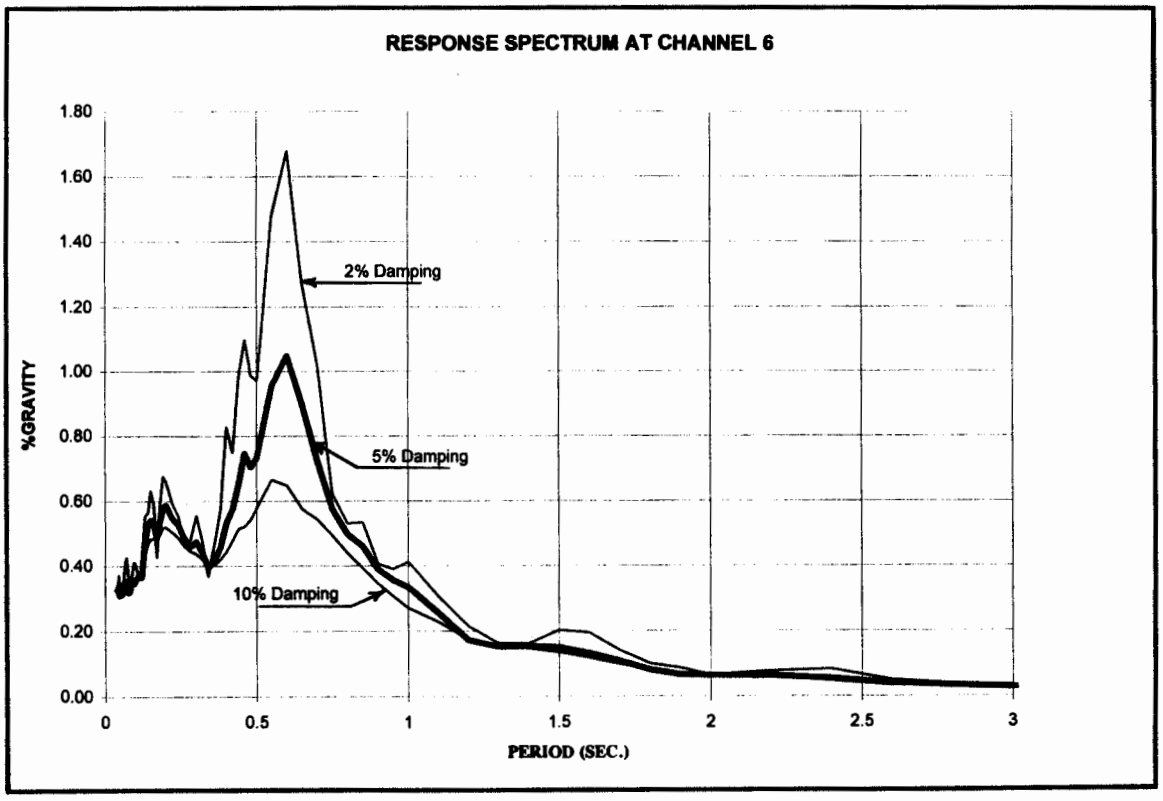

Figure 3.3 (continue) **Generated Response Spectra Curves of Recorded Motions**

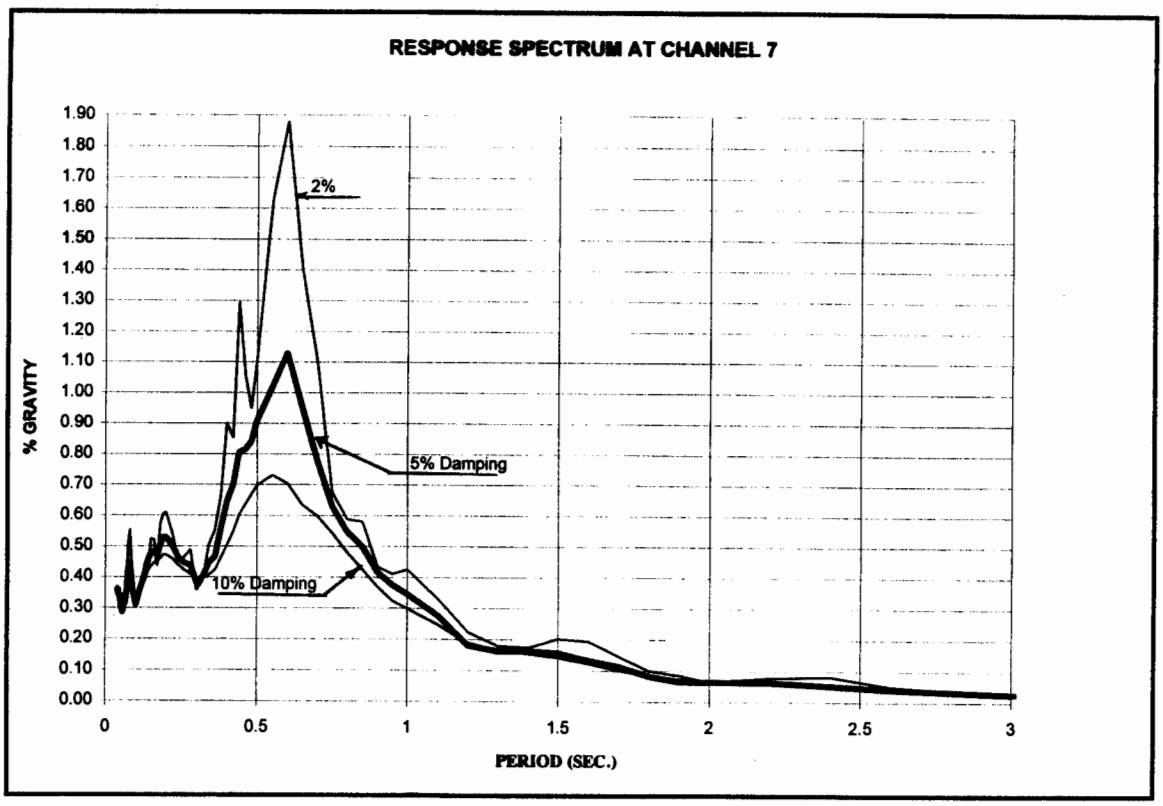

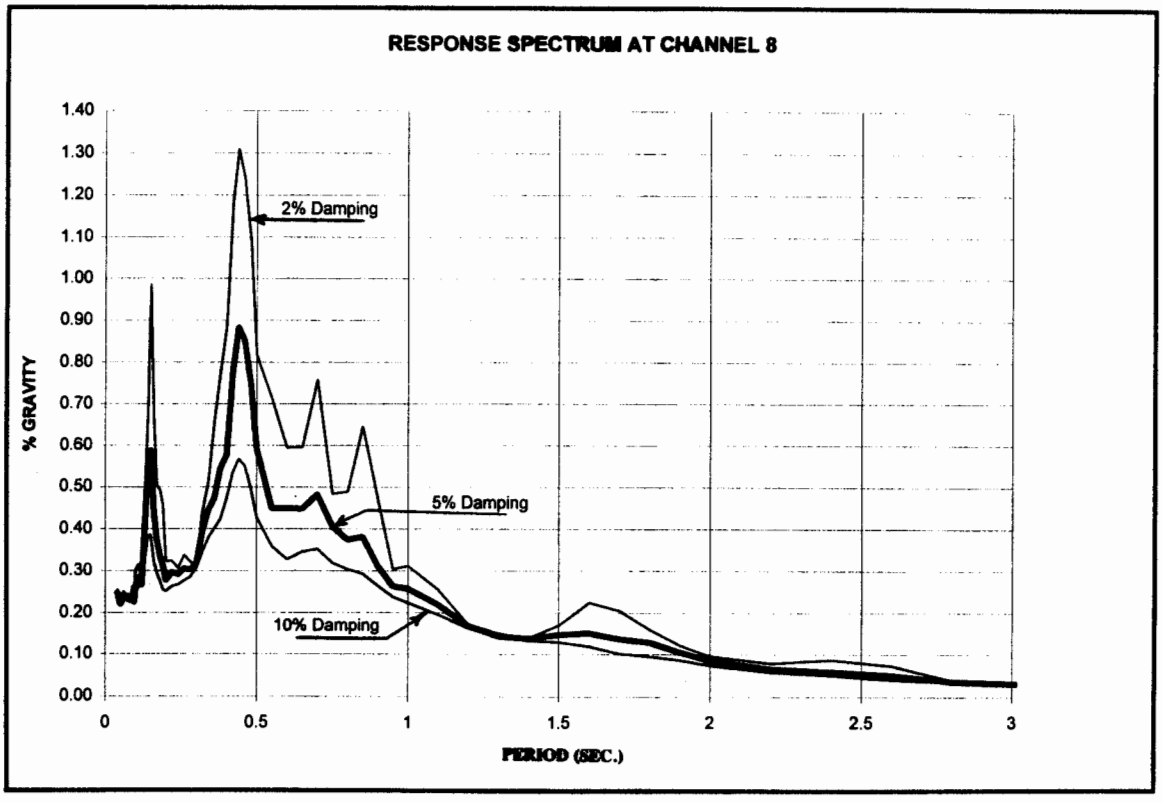

Figure 3.3 (continue) **Generated Response Spectra Curves of Recorded Motions**

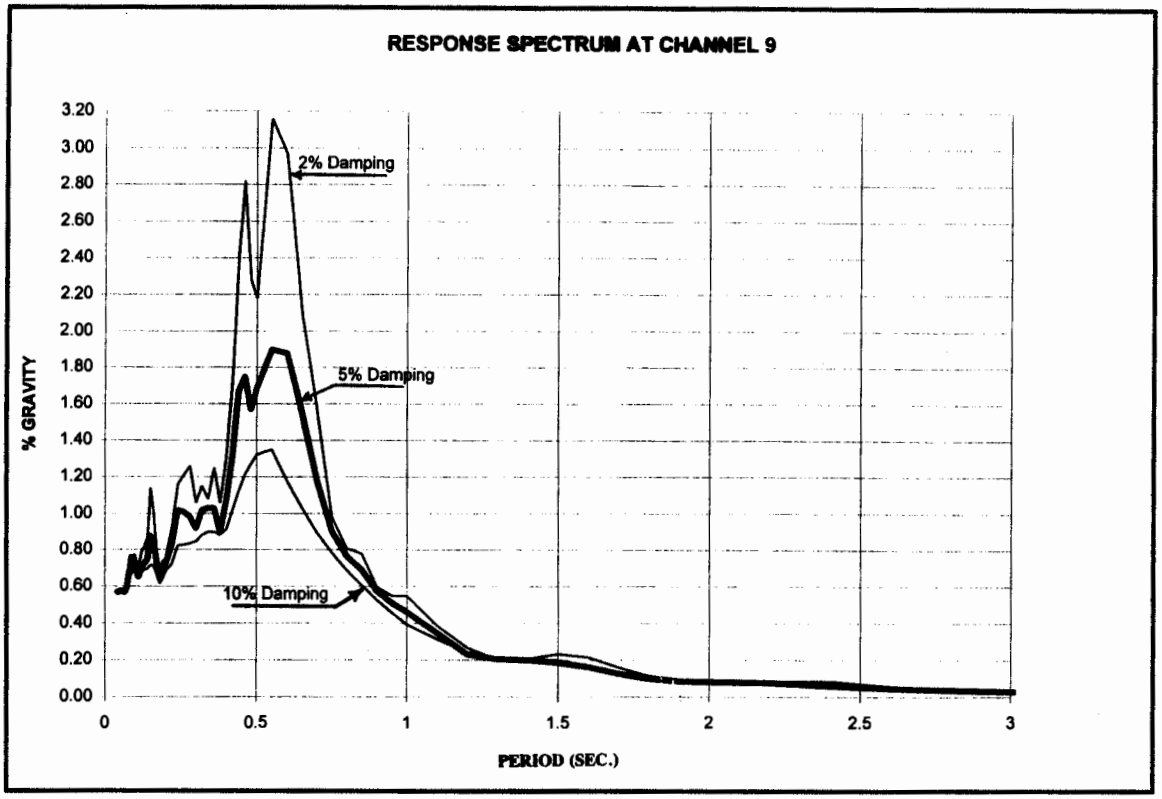

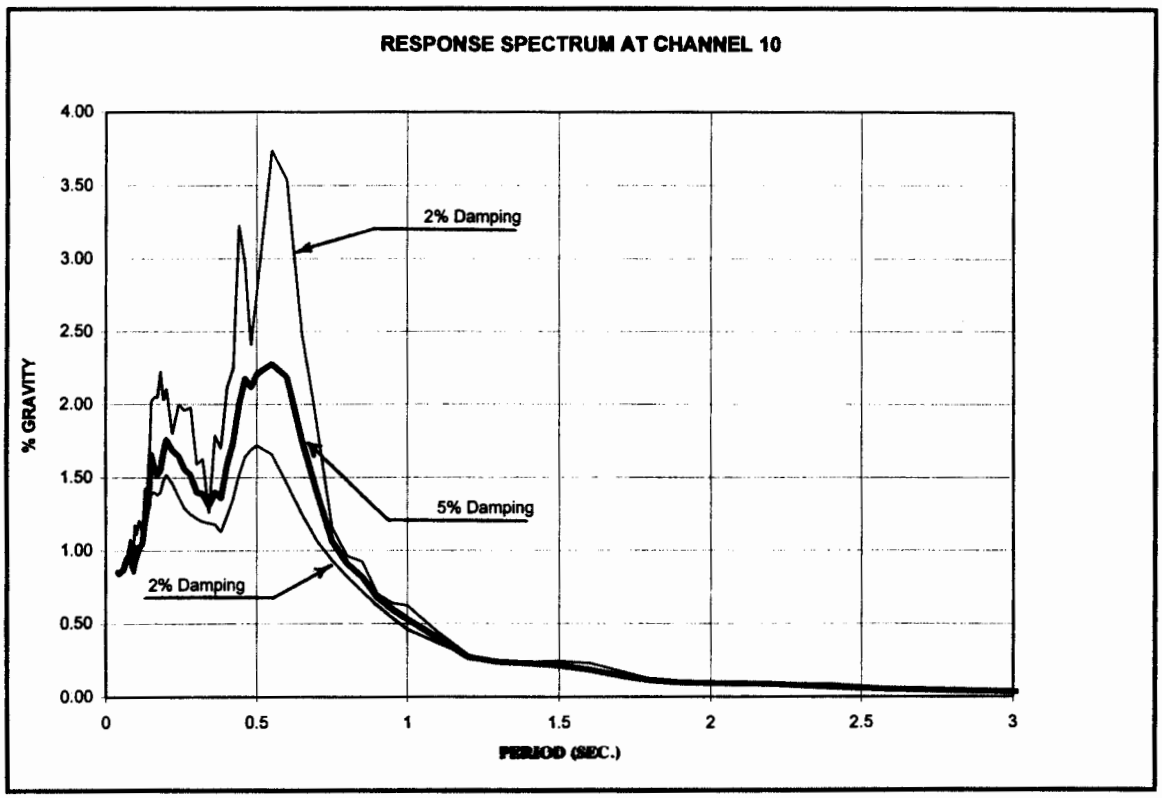

Figure 3.3 (continue) **Generated Response Spectra Curves of Recorded Motions**

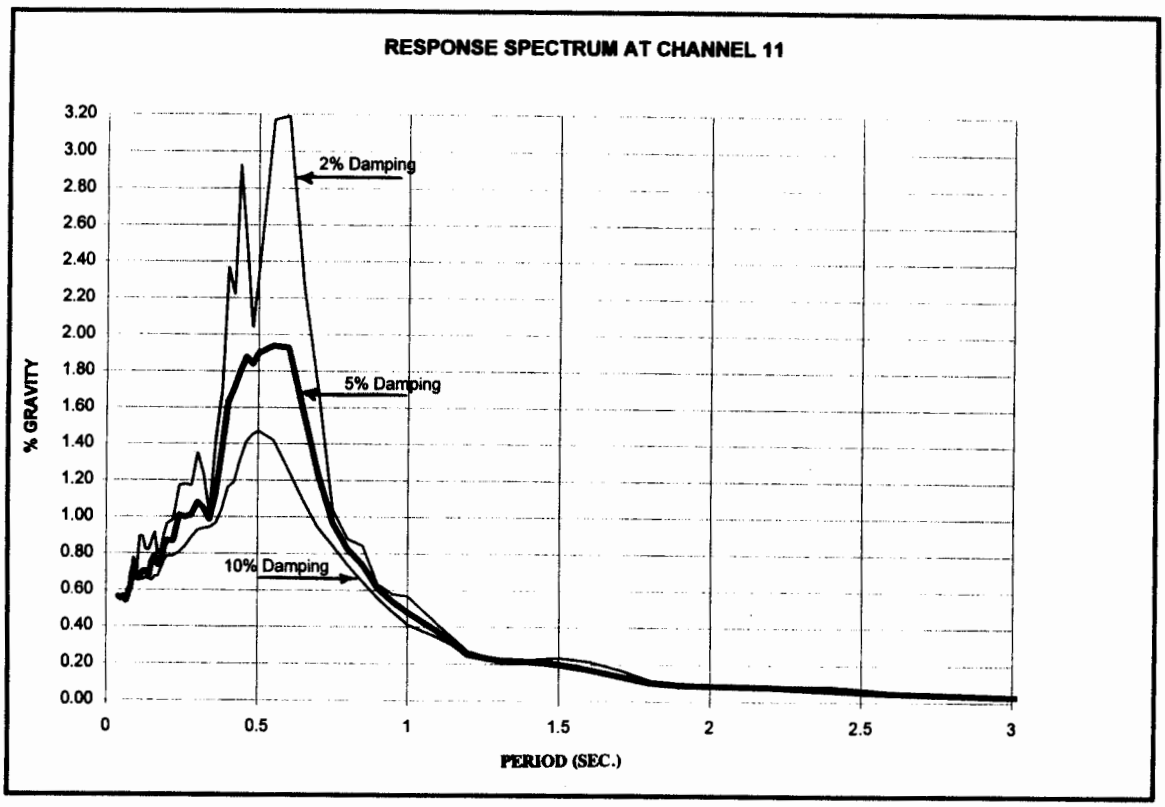

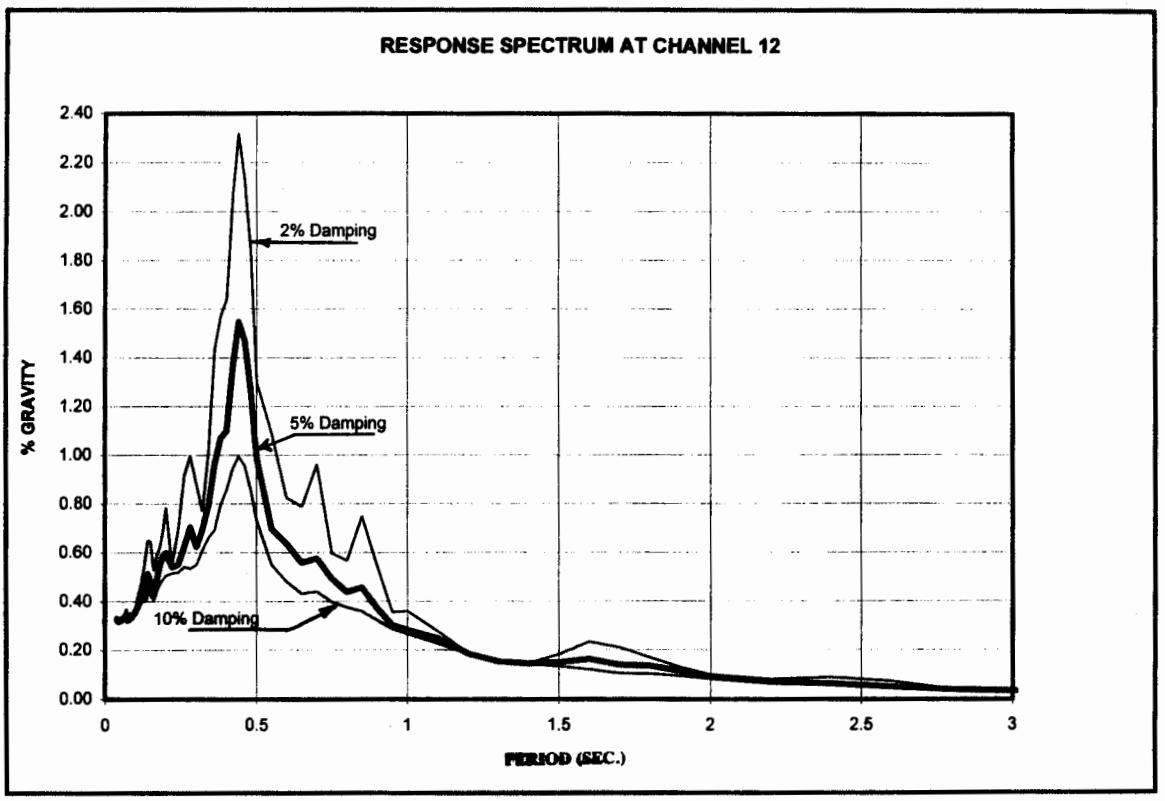

Figure 3.3 (continue) **Generated Response Spectra Curves of Recorded Motions**

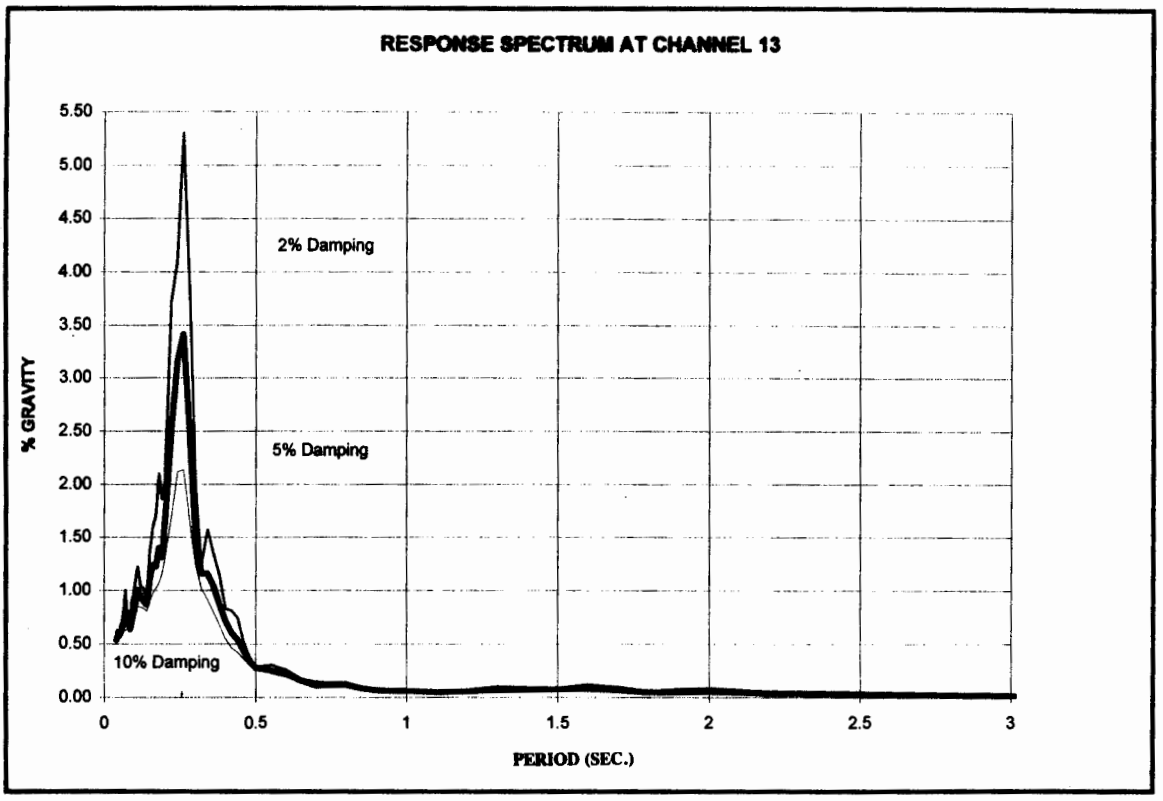

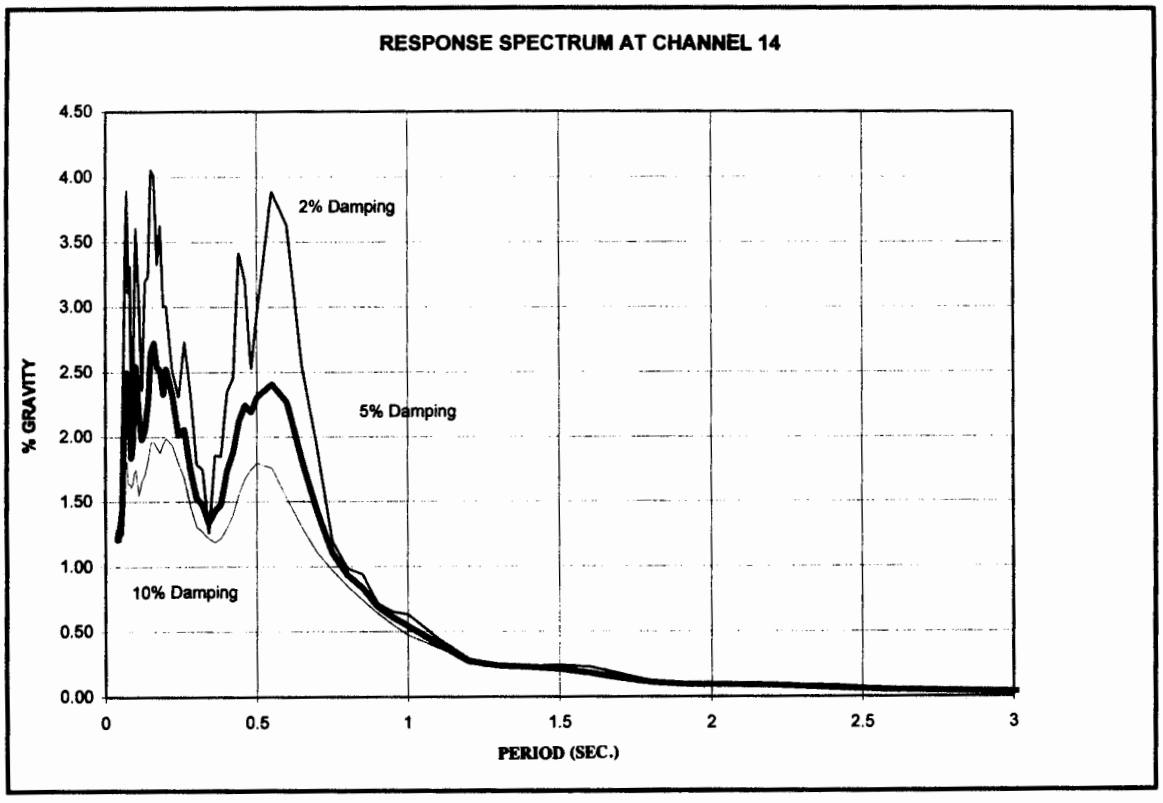

Figure 3.3 (continue) **Generated Response Spectra Curves of Recorded Motions**

4.0 SYSTEM IDENTIFICATION OF RECORDED MOTIONS

4.1 PROCEDURE

4.1.1 Overview

An important element of this research project was the use of system identification of the recorded motions in the parking structure, in order to estimate normal modes of vibration excited in the structure during the Northridge Earthquake. These normal modes were then used to calibrate a detailed finite element model of the structure which, in turn, was used to carry out detailed seismic analyses of the structure (see Chap. 5).

The system identification process involved three main steps. First, initial evaluation of the structure's seismic response was carried out by visually examining the accelerogram records and by computing transfer functions from the records. These transfer functions were computed as ratios of the Fourier Amplitude Spectra (FAS) of the recorded motions at the upper floors of the structure to the FAS of the motions of the ground floor. The natural periods at which major peaks occurred in these transfer functions were used in Step 2 of the process as first estimates of the periods of the structure's significant modes of vibrations.

The second step in the system identification process consisted of the application of the MODE-ID methodology to the recorded motions, in order to estimate a model of the parking structure that results in computed motions that are a "best-fit" to the recorded earthquake motions. The model parameters that were identified by MODE-ID were the natural period, mode shape, damping ratio, and participation factors for each significant normal mode of vibration excited by the ground shaking.

In the third and final step in the process, we evaluated the parking structure models estimated in Step 2. This evaluation consisted of: (a) assessment of the adequacy of the identified model, by comparing the computed model motions to the recorded motions of the parking structure; (b) assessment of the relative contributions of the structure's pseudostatic response and its response in each mode of vibration to its total response; and (c) interpretation of the relative translational, torsional, and rocking contributions to the response of the structure in each mode.

4.1.2 MODE-ID Methodology

The MODE-ID system identification procedure was applied to the strong motion records measured in the parking structure during the Northridge Earthquake, in order to estimate the modal parameters for the normal modes of vibration excited in the structure during the earthquake. This procedure was originally developed by one of the authors of this report (J.L. Beck), and has been applied to a variety of bridges and buildings subjected to seismic or forced-vibration excitations (e.g., Beck,1978; Werner, et. al, 1987, 1990, 1992a, 1992b, and 1993).

MODE-ID is a modal identification procedure for any structure that is modeled as having classical normal modes. It does not require a structural model to be developed, and is applied to an array of corresponding input (excitation) and output (response) measurements. The input can be multiple support motions or force-time histories, and there can be arbitrary initial conditions at the beginning of the time window of data. The structural response to the input motions is assumed to consist of the following components:

- *Pseudostatic Component.* The pseudostatic response component represents the "quasi-static" contributions of the individual support motions to the building's total response (neglecting inertial and damping effects). It can be visualized as a time-dependent "reference" position of the structure whose deformed shape at each instant of time depends on the instantaneous position of the structure's supports. This pseudostatic response is represented as the product of a pseudostatic matrix and the vector of input motions. For structures with multiple input support motions, MODE-ID can estimate the pseudostatic matrix or, alternatively, a theoretical pseudostatic matrix can be used.

- *Dynamic Component.* The dynamic response component represents the contributions of the structure's modal vibrations about its pseudostatic reference position. The model parameters that are used to compute the dynamic component are the natural period, damping ratio, input participation factors, and mode shape for each significant mode excited by the earthquake. MODE-ID estimates each of these modal parameters for each significant mode of vibration.

The above pseudostatic and normal mode parameters are estimated by a least-squares output-error method, in which MODE-ID uses an optimization algorithm to compute the "best" matching of the measured response (Beck, 1978). Within a Bayesian probability framework, the parameters estimated by MODE-ID can be viewed as most probable values based on the given data (Beck, 1990).

In these particular applications, it was not necessary to identify the pseudostatic matrix for the parking structure using MODE-ID; rather, the matrix was calculated directly based on the assumption that the base of the structure was rigid. This assumption simplified the calculation of the pseudostatic matrix; i.e., the i^{th} column of the matrix could be computed as the rigid body displacements at each output measurement location due to a unit displacement at the location of the i^{th} input motion measurement, with zero displacements assumed at all other input measurement locations. Following this, MODE-ID was applied on a step-by-step basis to identify the modal parameters for the significant modes of vibration excited in the structure during the Northridge Earthquake. In this, the pseudostatic matrix and then one mode at a time were successively incorporated into the model, and the modal parameters identified from each MODE-ID run were used as input to the next run with one additional mode included. This process led to the identification of the modal parameters for each significant mode (i.e., the mode's natural period, damping ratio, participation factor matrix, and mode shape amplitude at each accelerometer location), such that the resulting building model (which also includes the pseudostatic matrix) minimized a measure-of-fit parameter $J(\theta)$. This parameter is defined as the ratio of the sum of the output errors to the sum of the squares of the measured accelerations, i.e.,

$$J(\theta) = \frac{1}{V} \sum_{i=1}^{NR} \sum_{n=0}^{NT} [a_i(n\Delta t) - \ddot{y}_i(n\Delta t, \theta)]^2 \qquad (4\text{-}1)$$

where

$$V = \sum_{i=1}^{NR} \sum_{n=0}^{NT} [a_i^2(n\Delta t)] \qquad (4\text{-}2)$$

and

a_i, $\ddot{y}_i$ = Measured acceleration and computed model acceleration for the ith output degree of freedom (where i = 1,2,- - - - - NR, which is the total number of output channels). In MODE-ID, the Beck-Dowling (1988) algorithm was used to efficiently compute modal accelerations from the modal equations of motion, and the resulting modal accelerations at the ith output degree of freedom were then superimposed to obtain $\ddot{y}_i$.

θ = Pseudostatic matrix elements and identified modal parameters.

Δt = Time step at which the recorded motions in the parking structure have been digitized (= 0.01 sec.).

n = Time step number ranging from 0 to NT, which corresponds to a total time duration of NT x Δt sec.

V = Sum of the squares of the recorded accelerations.

Further description of the MODE-ID methodology is provided in Beck (1978) and in Werner, Beck, and Levine (1987).

4.1.3 Model Characteristics

This subsection summarizes the following elements of our modeling process that will be important when interpreting the system identification results: (a) our estimation of time-invariant and time-varying models; (b) our use of "rocking base" models, in which the effects of rocking of the parking structure are included in the modes of vibration, rather than in the pseudostatic matrix; (c) our estimation of three-dimensional mode shapes of the structure that include its translational, rocking, and torsional response; and (d) our process for evaluating the identified models of the parking structure and the relative contributions of each model element to the structure's total seismic response. These aspects are discussed below.

4.1.3.1 Time-Invariant and Time-Varying Models

We used MODE-ID to identify both time-invariant and time-varying models of the parking structure's seismic response during the Northridge Earthquake. These two different model types were used to show how the modal parameters vary over time (as the intensity of the ground shaking varies). Therefore, they enabled us to assess the degree to which nonlinear behavior may have played a roll in the structure's seismic response.

Because of the extremely fine digitization of the recorded motions at the parking structure (at a time step of 0.01 sec.), it was not possible for us to develop a single time-invariant model for the entire 60+ sec. duration of the shaking; i.e., the large number of digitized acceleration points exceeded the capacity of MODE-ID. Therefore, we instead identified time invariant models for four time segments over which the strength of the shaking appeared to be clearly different: (a) 10-15 sec., which corresponds to the time frame within which the shaking was increasing from very minimal levels to strong motions; (b) 15-30 sec., which corresponds to the duration of the strongest shaking of the parking structure during the earthquake; (c) 30-40 sec., when the shaking is decaying down to very small intensity levels; and (d) 40-60 sec., when the seismic excitation has ceased and the structure is essentially undergoing free vibrations at very low intensity levels.

In addition to the time-invariant models, time-varying models were identified using overlapping sliding time windows with a duration of 5 sec. and an overlap of 2.5 sec.; i.e., the time windows extended from 10-15 sec., 12.5-17.5 sec., 15-20 sec., 17.5-22.5 sec., etc. These time-varying models provided a more detailed representation of how the modal parameters varied with time (and therefore with the intensity of the shaking). It is noted that the selection of a time window for a time-varying model involves a trade-off between: (a) the need to use as fine a time window as possible, in order to obtain a detailed indication of the variation of the modal properties over time; and (b) the need to use a time window that is sufficiently long so that the number of cycles of shaking within each window is sufficient to provide a reasonable estimate of the level of damping in each mode.

4.1.3.2 Rocking Base Model

For both the time-invariant and time-varying models, the input motions to MODE-ID consisted of the horizontal motions recorded at the base of the structure, as well as the average (i.e., translational component only) of the vertical base motions. The output motions were considered to be the horizontal motions measured at all of the instrument locations above the base of the structure, as well as both sets of vertical motion records measured at the base. We have termed this model a "rocking-base model", since the mode shapes identified by MODE-ID incorporated the effects of rocking rotations at the base of the building about its north-south axis.

It is noted that a second type of model could also have been used in which the input motions would have consisted of both of the vertical base motion records (including the translational and rocking components) as well as the horizontal base motion records, and the output motions would have consisted of the horizontal motion records measured at all instrument locations above the base. This model is termed a "fixed-base model", since the resulting mode shapes would not

exhibit any vertical translations or rocking rotations (about the structure's north-south axis); i.e., for this model, the effects of these horizontal, vertical, and rocking motions would be incorporated into the building's pseudostatic response rather than its dynamic (normal mode) component of response.

Although we have used both rocking base and fixed base models in past studies of recorded building motions (e.g., Werner, et. al., 1992a and 1992b), the rocking base model was viewed as being much more desirable for this particular application. This is because one objective of our system identification of the recorded motions at the parking structure was to estimate modal parameters that could be used to calibrate a finite element model of the structure which, in turn, would be used for detailed seismic analysis (see Chap. 5). Because this finite element model includes the effects of rocking about the structure's north-south axis due to soil-structure interaction, our calibration of the model should use modes of vibration (from the recorded motions) that also include these rocking effects. For this reason, our system identification efforts focused on the estimation of a rocking base model.

4.1.3.3 Mode Shapes

The three-dimensional mode shapes estimated for the parking structure's significant modes of vibration include the effects of horizontal translation in the north-south and east-west directions, torsional rotation (about a vertical axis), and rocking of the structure about its north-south axis. The effects of torsion along the height of the building were evaluated by visually comparing the differences in the mode shape amplitudes at the instrument locations along the east and west sides of the structure to the average translation represented by these mode shape amplitudes. The effects of rocking on the structural response in the east-west directions was estimated by computing an equivalent rigid body translational component of the mode shape amplitude at each instrumented floor due to rocking, i.e.

$$\Phi_{R,i,n} = (\Phi_{v2,n} - \Phi_{v5,n}) \times H_i / D_{2-5} \qquad (4\text{-}3)$$

where, for the n^{th} mode, $\phi_{R,i,n}$ is the mode-shape's east-west component of translation at the i^{th} floor due to rocking of the base, $\phi_{v2,n}$ and $\phi_{v5,n}$ are the mode shape's vertical component of translation at the locations of Channels 2 and 5 along the base of the structure, D_{2-5} is the distance between Channels 2 and 5, and H_i is the height of the i^{th} floor above the base.

The mode shapes estimated from the recorded motions were used to evaluate the seismic response characteristics of not only the overall parking structure, but also individual elements within the structure where instruments were located. This included the deformability of the roof diaphragm in the north-south direction, and the deformability of the roof parapet above the north wall, in a north-south direction.

4.1.3.4 Model Assessments

An important element of the system identification process is an evaluation of how well the various models of the parking structure that were identified from each set of recorded earthquake motions represent the structure's seismic response during the Northridge Earthquake. This assessment was based on (a) our use of past experience to evaluate whether the minimum value of $J(\theta)$ obtained for each model was sufficiently small to represent a good overall fit between the measured response of the structure and the computed model response; and (b) visual comparison of recorded and computed model acceleration time histories and their Fourier amplitude spectra, at selected locations in the structure.

As part of this model assessment, we also evaluated the relative contribution of each element of the model (i.e., the pseudostatic response and each identified mode of vibration) to the structure's seismic response. To accomplish this, we tabulated how much $J(\theta)$ decreased as the pseudostatic matrix and each identified mode were successively incorporated into the model.

4.2 RESULTS

4.2.1 Pseudostatic Component

As previously noted, a theoretical pseudostatic matrix for parking structure was developed, in which the i^{th} column of the matrix contained the rigid body displacements at each output measurement location due to a unit displacement at the location of the i^{th} input motion measurement. The resulting pseudostatic matrix for the rocking base model of the parking structure is shown in Figure 4-1. This matrix was incorporated into all time-invariant and time-varying models that were identified for the structure.

4.2.2 Dynamic Component --Time-Invariant Models

4.2.2.1 General Modal Characteristics and Comparisons with Recorded Motions

As noted in Section 4.1.3.1, time-invariant modal parameters were estimated by MODE-ID for the following time segments: (a) 10-15 sec., which corresponds to the initial buildup of the strength of the shaking; (b) 15-30 sec., during which the strongest shaking of the parking structure took place; (c) 30-40 sec., during which the shaking of the structure decayed to very low levels; and (d) 40-60 sec., when the structure was undergoing essentially free vibration under very low intensities of shaking. No parameter identification was carried out for the 0-10 sec. time segment because the motions of the parking structure were negligible within that segment.

The characteristics of the significant normal modes that were estimated for these various time segments are shown in Table 4-1 and in Figures 4-2 through 4-5. These show that, for each time segment, a total of six modes of vibration were identified. The general characteristics of the modes that were identified are comparable for each time segment, and are summarized below:

- *First North-South Mode.* Mode 1 corresponds to the first translational mode of vibration in the north-south direction. At each instrumented floor, the north-south translational components of the mode shape amplitudes along the east and west faces of the parking structure are comparable to each other, increase nearly linearly with increasing height above the ground floor, and are much larger that the east west translational components (which are essentially negligible). In-plane deformations of the roof diaphragm are relatively large for the 10-15 sec. time segment, and are somewhat smaller for the other time segments.

- *First East-West Mode.* Mode 2 is dominated by the east-west translational components of motion, which increase nearly linearly with increasing height above the ground floor. These east-west components are accompanied by north-south components at the east and west faces of the instrumented fourth floor and roof diaphragms that are nearly equal and opposite; this indicates that the mode contains some torsional rotations of the diaphragms, and only small translations in the north-south direction. These torsional rotations could be due to coupling with a closely-spaced torsional mode (Mode 3 below). The in-plane diaphragm deformation in this mode is small. As shown in Figures 4-2 through 4-5, rocking of the base of the parking structure about its north-south axis is an important contributor to the total east-west translations of the structure in this mode of vibration.

- *Torsional Mode.* The mode shape for Mode 3 features significant torsional rotations that are much larger than those in Mode 2, accompanied by only very small north-south translations. The mode also includes east-west translations that may be due to coupling with a closely-spaced east-west translational mode of the parking structure (Mode 2 above).

- *Second North-South Mode.* The mode shape for Mode 4 contains north-south translational components at the fourth floor that are of comparable magnitude but opposite sign to those at the roof. These north-south translations are accompanied by smaller east-west translations (that increase slightly with increasing height) and by very large in-plane deformations of the roof diaphragm.

- *Higher Modes.* Modes 5 and 6 are higher modes of vibration that were not strongly excited by the ground shaking; therefore, the modal parameter estimates for these modes are more uncertain than are the modal parameters estimates for the lower and more strongly excited modes. Mode 6 contains large in-plane roof diaphragm deformations, as characterized by a significant north-south translation at the center of the diaphragm that is of opposite sign to the north-south translation of the east and west faces of the roof. In Mode 5, the north-south translation at the center of the roof diaphragm is also large, but has the same sign as the north-south translations at the east and west sides of the roof.

4.2.2.2 Comparisons between Computed Model Motions and Recorded Motions

For each time segment, the time-invariant models comprised of the above six normal modes plus the pseudostatic matrix shown in Figure 4-1 led to an excellent fit between the computed model

motions and the recorded motions. This excellent fit is evidenced by: (a) the very low values of the measure-of-fit parameter, $J(\theta)$, which are shown in Table 4-1 to range from about 0.021-0.035 (where, from past experience, values of $J(\theta)$ of about 0.15 or less generally represent an excellent fit); and (b) very close visual comparisons of the time histories and Fourier amplitude spectra of the computed model motions and the recorded motions, as typified by the comparisons shown in Figures 4-6 and 4-7.

The relative contributions of each mode and the pseudostatic matrix to the fit between the recorded motions and the computed model motions is represented by the ΔJ values shown for each model element in Table 4-1. These relative ΔJ values show that, for each time segment, the greatest contributor to the reductions in $J(\theta)$ is the first north-south mode (Mode 1), followed by the pseudostatic matrix. However, these ΔJ values are a misleading representation of the contributions of the first east-west mode to this reduction in $J(\theta)$, because: (a) only two of the nine output response measurements for the rocking base model of the parking structure recorded motions in the east-west direction (at Channels 8 and 12); and (b) because of this disparity in the relative number of measurements in the north-south and east-west directions, and the fact that the computation of $J(\theta)$ and ΔJ are computed as a summation of the measure-of-fit contributions over all instrument locations, the ΔJ value computed for the first east-west mode will underestimate the actual contributions of that mode to the parking structure's seismic response in the east-west direction. In fact, despite the relatively low values of ΔJ for the first east-west mode, judgment suggests that this mode should be a dominant contributor to the parking structure's response in the east-west direction. This is confirmed by the finite element analysis results described in Chapter 6.

4.2.2.3 Variations in Modal Parameters between Different Time Segments

A first estimate of the degree to which nonlinear behavior contributed to the overall seismic response of the parking structure during the Northridge Earthquake can be obtained by correlating the relative strengths of the shaking within the different time windows with the variations in the natural period and damping ratio values between these windows. Such comparisons for the structure's first north-south mode and first east-west mode -- the structure's dominant modes of vibration -- are shown in Table 4-2 and are summarized below. It is noted that, with only a very few exceptions, similar comparisons are observed for the higher modes of vibration of the parking structure (see Table 4-1).

- For both predominant modes, the natural periods are longest and the damping ratios are largest for the 15-30 sec. time window where the earthquake shaking is strongest, as expected. However, the rather small differences between these natural period and damping ratio values among all of the various time windows suggests that the parking structure did not undergo significant nonlinear response during the Northridge Earthquake. Table 4-2 shows that, for both modes, the damping ratios ranged from about 3 percent of critical to slightly less that 5 percent of critical among the various time windows. The differences in natural periods between the various time windows were somewhat smaller; the period values range from 0.45-0.53 sec. for the first north-south mode, and from 0.38-0.42 sec. for the first east-west mode.

- The variations in natural period and damping ratio between the various time windows exhibit similar trends for the two modes. For both modes, the natural periods are consistently longer for the 15-30 sec. time window than for the 10-15 sec. window, and the damping ratios are consistently smaller. As the time proceeds from the 15-30 sec. window of strongest shaking to the 30-40 sec. window of decreased shaking, the natural periods for the two modes are shortened somewhat and the damping ratios are decreased. However, for both modes, the periods are still longer than those for the initial 10-15 sec. time segment, and the damping ratios are still slightly larger.

- In the 40-60 sec. time window of weak earthquake shaking, the natural periods for both modes -- as well as the damping ratio for the north-south mode -- are further decreased, but are still larger than the corresponding quantities for the initial 10-15 sec. window. However, the damping ratio for the first east-west mode inexplicably increases in the 40-60 sec. time window to a value that approaches the level of damping estimated for the 15-30 sec. window of strongest shaking. This trend may possibly be due to the relatively few instruments in the east-west direction, which would lead to a greater degree of uncertainty in the estimated parameters for the east-west mode. In addition, past experience has shown that the estimation of damping ratios from recorded motions in buildings is typically more uncertain than is the estimation of natural periods.

4.2.3 Dynamic Component --Time-Varying Models

As previously noted in Section 4.1.3.1, time-varying models were identified using overlapping sliding time windows with a duration of 5 sec. and an overlap of 2.5 sec.; i.e., the time windows extended from 10-15 sec., 12.5-17.5 sec., 15-20 sec., 17.5-22.5 sec., etc. The objective of these models was to provide a more detailed representation of how the modal parameters varied with time (and therefore with the intensity of the shaking). The following paragraphs address the natural period and damping ratio estimates from the time-varying models, and how they compare with the estimates from the time-invariant models.

4.2.3.1 Natural Periods

Figure 4-8 shows comparisons of the natural period estimates from the time-varying and time-invariant models, for the first north-south and first east-west modes of vibration of the parking structure. This figure shows that, for both modes, the time-varying models lead to natural period values that are refined estimates of the values from the time-invariant models, in that the variation in natural period within each time window considered for the time-invariant models are now provided. However, both sets of models lead to similar general trends regarding the variation of natural period of the two modes over time, and the values of the natural periods.

4.2.3.2 Damping Ratios

Comparisons of the damping ratio estimates for the two modes from the time-varying and time-invariant models are provided in Figure 4-9. This figure shows that the damping ratio variations

that are estimated by the time-varying model are much more erratic than the natural period variations.

It would seem that this erratic behavior of the damping estimates must be related in some way to the shorter duration of the individual time windows considered in the time-varying model estimates. We had estimated that the 5 sec. duration of the window used for this model would be sufficient for providing reasonable damping estimates, since this duration is approximately a factor of 10 or more longer than the natural periods for the two modes (leading to at least 10 cycles of shaking within each window.) However, the erratic damping estimates shown for the time-varying models in Figure 4-9 indicate that a longer duration of the time windows would have been advisable.

4.2.4 Parapet Response

To investigate the seismic response characteristics of the instrumented parapet along the north wall of the roof, MODE-ID was used to carry out separate estimation of the predominant mode of vibration of this parapet element. In this, the input motions were considered to be the recorded north-south motions at Channel 10 (on the roof diaphragm, near its mid-length), and the output motions were taken as the motions recorded on the top of the roof parapet (Channel 14). A single-mode model of the parapet was assumed.

The natural periods and damping ratios estimated for each time window of the time invarient models are shown in Table 4-3. This table shows that the natural period of the parapet differed only slightly between the various time windows (ranging from 0.068-0.071 sec.), whereas the damping ratio variations were somewhat greater (ranging from 5.2-8.6 percent of critical). The fit between the computed and recorded motions of the parapet was generally good, as shown by the relatively low values of $J(\theta)$ shown in Table 4-3 and the comparisons between the computed and recorded parapet motions shown in Figure 4-10.

TABLE 4-1
MODAL PARAMETERS FOR ROCKING-BASE AND TIME INVARIANT MODEL OF PARKING STRUCTURE

	Time Window 10 - 15 seconds - J = 0.035						Time Window 15 - 30 seconds - J = 0.026					
	Mode 1	*Mode 2*	*Mode 3*	*Mode 4*	*Mode 5*	*Mode 6*	*Mode 1*	*Mode 2*	*Mode 3*	*Mode 4*	*Mode 5*	*Mode 6*
	1 NS	*1 EW*	*TOR*	*2NS*	-	-	*1 NS*	*1 EW*	*TOR*	*2 NS*	-	-
Natural Period (sec)	0.45	0.38	0.33	0.17	0.13	0.11	0.53	0.42	0.38	0.18	0.15	0.12
Damping Ratio (% of critical)	3.1	3.3	3.4	4.3	3.1	2.1	4.8	4.6	4.2	5.0	4.4	1.7
NS - Chan 6 (4th flr, W wall)	0.215	-0.107	0.281	-0.158	0.223	0.313	0.233	-0.175	0.201	-0.213	0.282	0.160
NS - Chan 9 (roof, W wall)	0.504	-0.199	0.533	0.114	0.370	0.373	0.518	-0.366	0.425	0.126	0.522	0.438
NS - Chan 7 (4th flr, E wall)	0.226	0.076	-0.266	-0.140	0.243	0.118	0.237	0.145	-0.267	-0.165	0.130	0.156
NS Chan 11 (roof, E wall)	0.494	0.192	-0.587	0.115	0.370	0.618	0.498	0.331	-0.551	0.198	0.325	0.503
NS - Chan 10 (roof, diaphragm)	0.636	0.010	-0.048	0.960	0.747	-0.587	0.611	0.006	-0.109	0.932	0.570	-0.707
EW - Chan 8 (4th flr, N wall)	0.003	0.367	0.173	-0.016	0.127	0.120	-0.001	0.337	0.250	-0.011	-0.363	-0.026
EW - Chan 12 (roof, N wall)	-0.004	0.830	0.416	-0.081	-0.202	-0.062	-0.008	0.711	0.537	-0.057	-0.082	-0.063
Ver. Chan 1 (1st flr, N wall)	0.002	0.202	0.091	-0.006	0.037	0.047	-0.002	0.207	0.144	0.009	-0.175	-0.024
Ver. Chan 2 (1st flr, N wall)	-0.002	-0.202	-0.091	0.006	-0.037	-0.047	0.002	-0.207	-0.144	-0.009	0.175	0.024
ΔJ	0.5625	0.0468	0.0240	0.1296	0.0226	0.0093	0.6683	0.0796	0.0560	0.0364	0.0026	0.0049
ΔJ for Pseudostatic Matrix	0.1707						0.1256					

TABLE 4-1 (Continued)
MODAL PARAMETERS FOR ROCKING-BASE AND TIME INVARIANT MODEL OF PARKING STRUCTURE

	Time Window 30 - 4- seconds - J = 0.020						Time Window 40 - 60 seconds - J = 0.029					
	Mode 1	*Mode 2*	*Mode 3*	*Mode 4*	*Mode 5*	*Mode 6*	*Mode 1*	*Mode 2*	*Mode 3*	*Mode 4*	*Mode 5*	*Mode 6*
	1 NS	*1 EW*	*TOR*	*2NS*	-	-	*1 NS*	*1 EW*	*TOR*	*2 NS*	-	-
Natural Period (sec)	0.50	0.41	0.36	0.18	0.14	0.11	0.48	0.40	0.35	0.17	0.13	0.11
Damping Ratio (% of critical)	4.1	3.7	3.5	3.0	5.2	2.1	4.0	4.5	3.1	3.9	3.6	1.7
NS - Chan 6 (4th flr, W wall)	0.232	-0.130	0.173	-0.249	0.204	0.085	0.229	-0.149	0.272	-0.240	0.132	0.027
NS - Chan 9 (roof, W wall)	0.517	-0.293	0.388	0.168	0.350	0.556	0.504	-0.321	0.587	0.154	0.250	0.455
NS - Chan 7 (4th flr, E wall)	0.241	0.176	-0.252	-0.180	0.200	0.223	0.239	0.129	-0.268	-0.166	0.172	0.210
NS Chan 11 (roof, E wall)	0.497	0.393	-0.505	0.159	0.322	0.466	0.504	0.295	-0.552	0.161	0.324	0.461
NS - Chan 10 (roof, diaphragm)	0.611	0.081	-0.078	0.918	0.820	-0.645	0.619	0.012	-0.004	0.923	0.886	-0.730
EW - Chan 8 (4th flr, N wall)	0.000	0.348	0.284	-0.023	-0.050	-0.024	0.005	0.365	0.176	-0.043	-0.019	-0.057
EW - Chan 12 (roof, N wall)	-0.008	0.723	0.610	-0.091	-0.119	-0.034	0.003	0.750	0.399	-0.099	-0.022	-0.014
Ver. Chan 1 (1st flr, N wall)	-0.001	0.178	0.146	-0.007	-0.037	-0.009	0.003	0.194	0.090	-0.014	0.001	-0.009
Ver. Chan 2 (1st flr, N wall)	0.001	-0.178	-0.146	0.007	0.037	0.009	-0.003	-0.194	-0.090	0.0255	0.001	0.009
ΔJ	0.7814	0.0296	0.0353	0.0124	0.0061	0.0026	0.5484	0.1475	0.0366	0.0255	0.0017	0.0010
ΔJ for Pseudostatic Matrix	0.1122						0.2098					

TABLE 4-2
VARIATIONS IN NATURAL PERIODS AND DAMPING RATIOS OVER DIFFERENT TIME WINDOWS – TIME-INVARIANT MODEL

Time Window		First North-South Mode		First East-West Mode	
Duration (sec)	**Earthquake Motions**	**Natural Period (sec)**	**Damping Ratio (percent of critical)**	**Natural Period (sec)**	**Damping Ratio (percent of critical)**
10-15	Increases from very low levels of shaking to strong motion	0.45	3.1	0.38	3.3
15-30	Strongest motions	0.53	4.8	0.42	4.6
30-40	Decaying from strong shaking to small intensity levels	0.50	4.1	0.41	3.7
40-60	Very low levels of shaking	0.48	4.0	0.40	4.5

TABLE 4-3
MODAL PARAMETERS FOR ROOF PARAPET

Time Window (sec)	Natural Period (sec)	Damping Ratio %	Measure-of-fit Parameter J(θ)
10-15	0.071	6.0	0.1724
15-30	0.070	8.6	0.1011
30-40	0.069	5.2	0.0404
40-60	0.068	8.0	0.585

Note: Natural period and damping ratio values were estimated by MODE-ID, assuming a single-mode model. Input motions were the recorded earthquake motions at Channel 10 of the parking structure, and output motions were the recorded motions at Channel 14.

Los Angeles - 6-story Parking Structure
(CSMIP Station No. 24655)

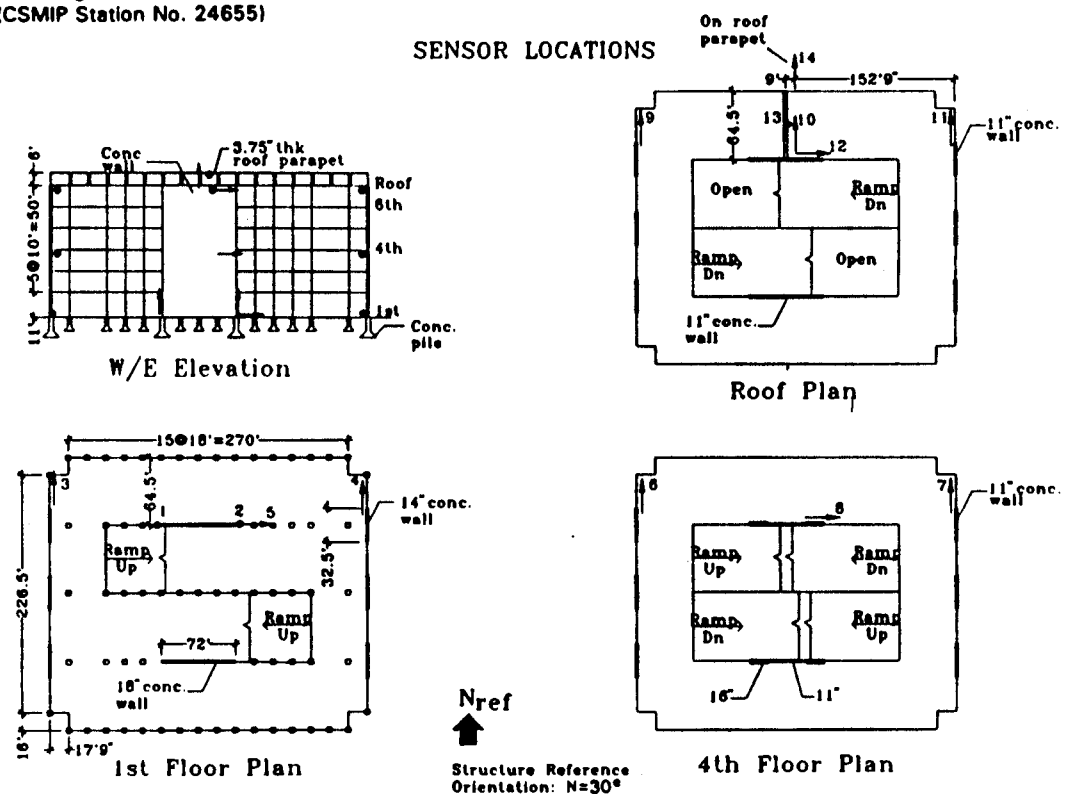

Output \ Input	3	4	5	$\bar{V}$
6	1	0	0	0
9	1	0	0	0
7	0	1	0	0
11	0	1	0	0
10	0.5	0.5	0	0
8	0	0	1	0
12	0	0	1	0
1	0	0	0	1
2	0	0	0	1

Input Channels: 3, 4, 5, $\bar{V}$

where $\bar{V} = (Ch1 + Ch2)/2$

Output Channels: 6, 9, 7, 11, 10, 8, 12, 1, 2

FIGURE 4-1
PSEUDOSTATIC MATRIX FOR ROCKING BASE MODEL OF PARKING STRUCTURE

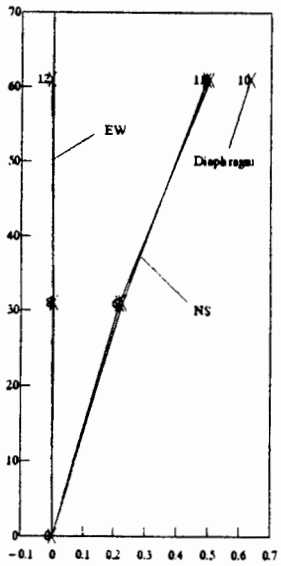

a) Mode 1: First North-South
(T=0.45 sec, ξ = 3.1 %)

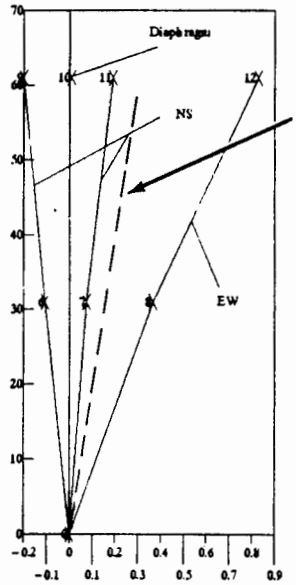

b) Mode 2: First East-West
(T=0.38 sec, ξ = 3.3 %)

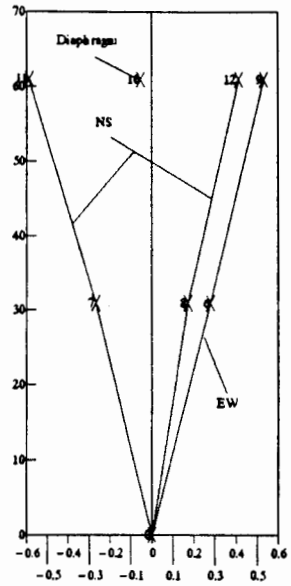

c) Mode 3: Torsional
(T=0.33 sec, ξ = 3.4 %)

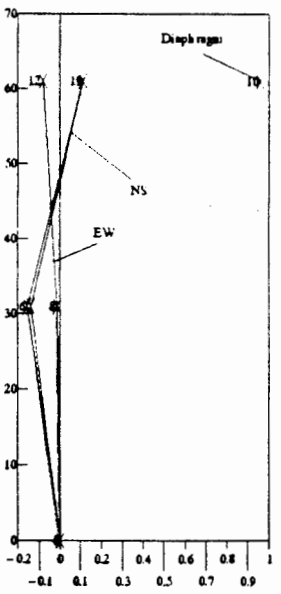

d) Mode 4: Second North-South
(T=0.17 sec, ξ = 4.3 %)

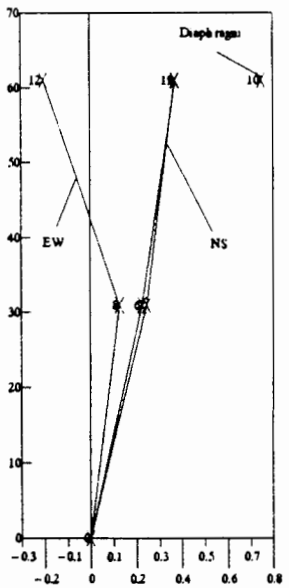

e) Mode 5: Higher Mode
(T=0.13 sec, ξ = 3.1 %)

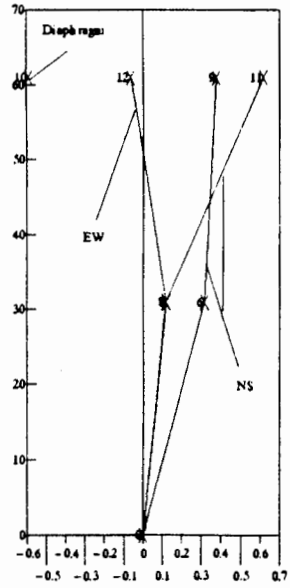

f) Mode 6: Higher Mode
(T=0.11 sec, ξ = 2.1 %)

FIGURE 4-2
THREE-DIMENSIONAL MODE SHAPES FOR TIME-INVARIANT ROCKING-BASE MODEL OF PARKING STRUCTURE, TIME SEGMENT = 10-15 SECONDS

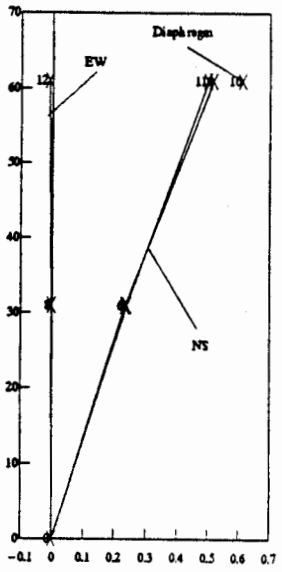

a) Mode 1: First North-South
(T=0.53 sec, ξ = 4.8 %)

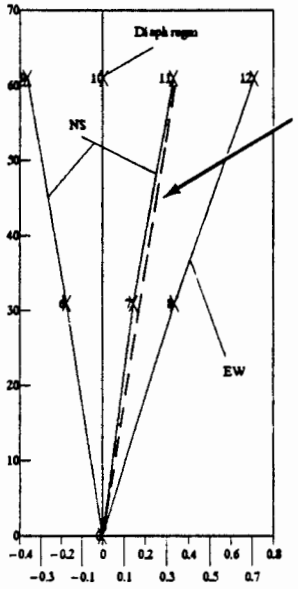

b) Mode 2: First East-West
(T=0.42 sec, ξ = 4.6 %)

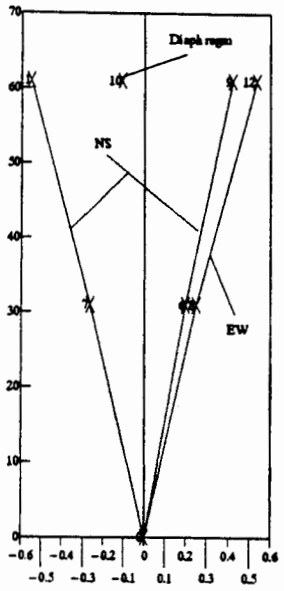

c) Mode 3: Torsional
(T=0.38 sec, ξ = 4.2 %)

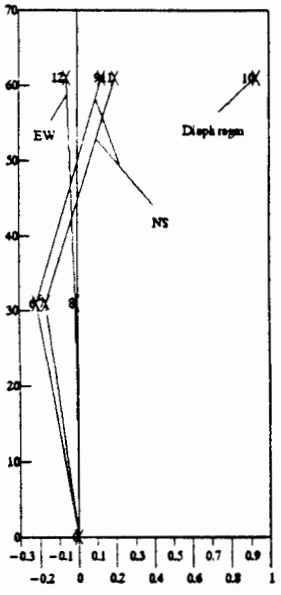

d) Mode 4: Second North-South
(T=0.18 sec, ξ = 5.0 %)

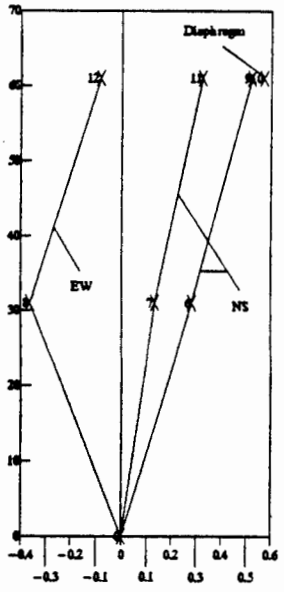

e) Mode 5: Higher Mode
(T=0.15 sec, ξ = 4.4 %)

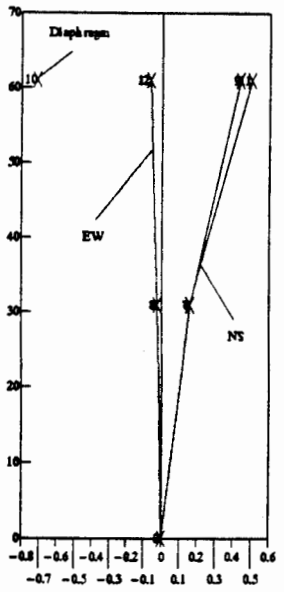

f) Mode 6: Higher Mode
(T=0.12 sec, ξ = 1.7 %)

FIGURE 4-3
THREE-DIMENSIONAL MODE SHAPES FOR TIME-INVARIANT ROCKING-BASE MODEL OF PARKING STRUCTURE, TIME SEGMENT = 15-30 SECONDS

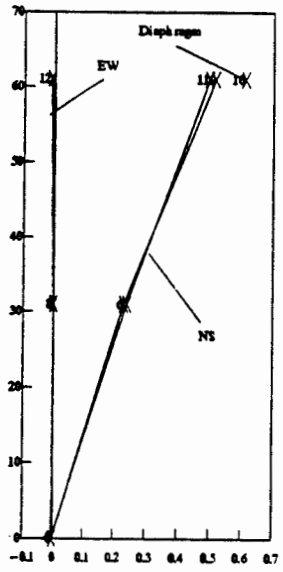

a) Mode 1: First North-South
(T=0.50 sec, ξ = 4.1 %)

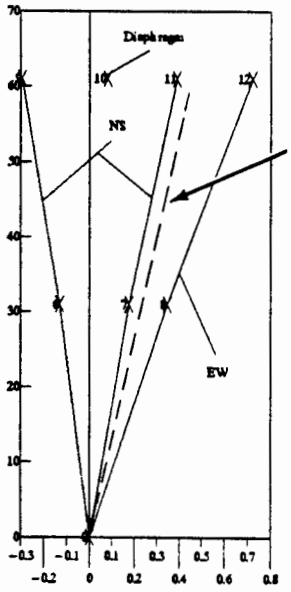

b) Mode 2: First East-West
(T=0.41 sec, ξ = 3.7 %)

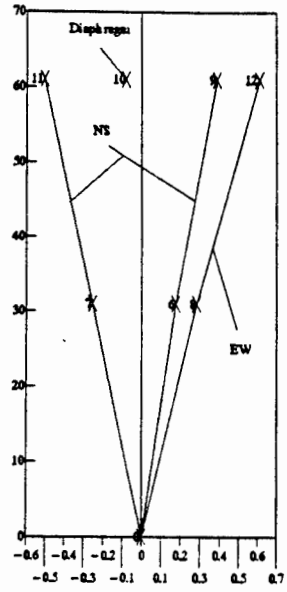

c) Mode 3: Torsional
(T=0.36 sec, ξ = 3.0 %)

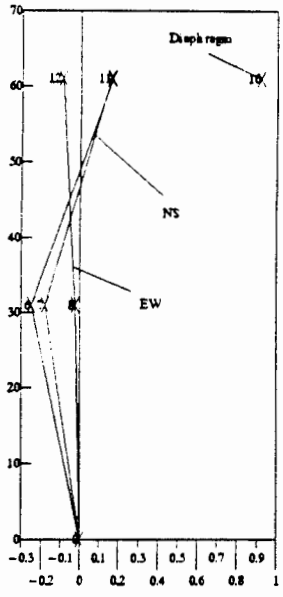

d) Mode 4: Second North-South
(T=0.18 sec, ξ = 3.0 %)

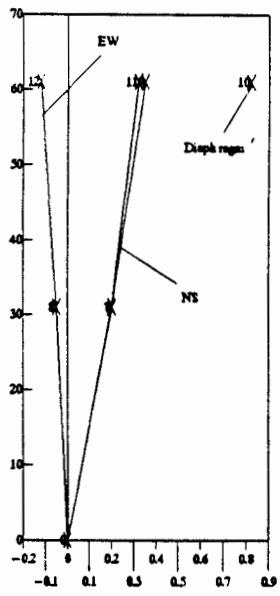

e) Mode 5: Higher Mode
(T=0.14 sec, ξ = 5.2 %)

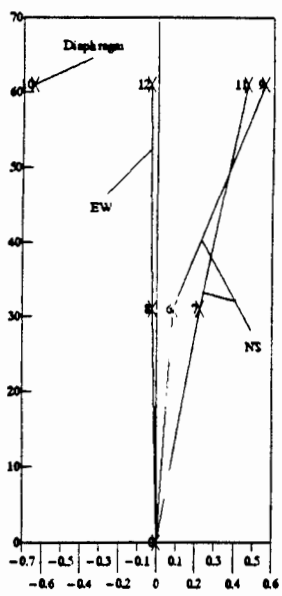

f) Mode 6: Higher Mode
(T=0.11 sec, ξ = 2.1 %)

FIGURE 4-4
THREE-DIMENSIONAL MODE SHAPES FOR TIME-INVARIANT ROCKING-BASE MODEL OF PARKING STRUCTURE, TIME SEGMENT = 30-40 SECONDS

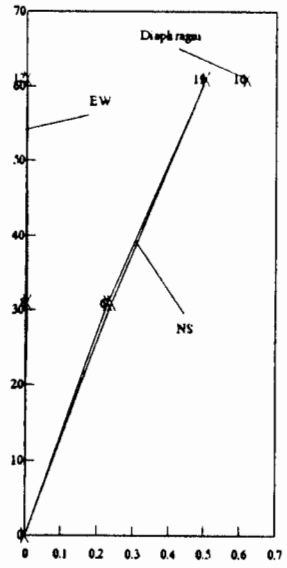

a) Mode 1: First North-South
(T=0.48 sec, ξ = 4.0 %)

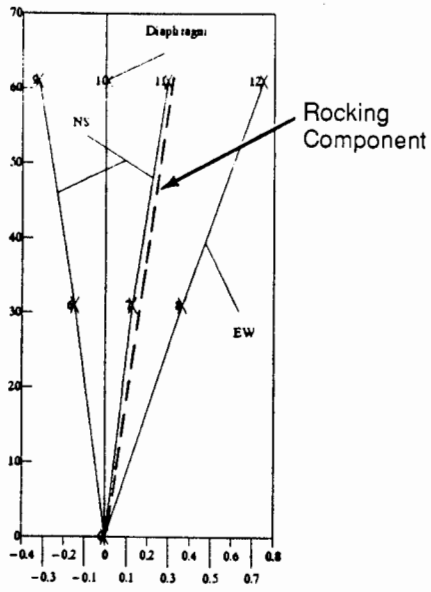

b) Mode 2: First East-West
(T=0.40 sec, ξ = 4.5 %)

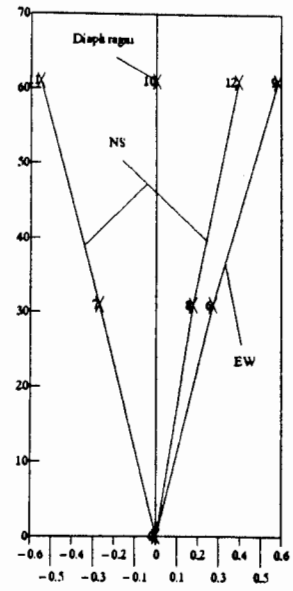

c) Mode 3: Torsional
(T=0.35 sec, ξ = 3.1 %)

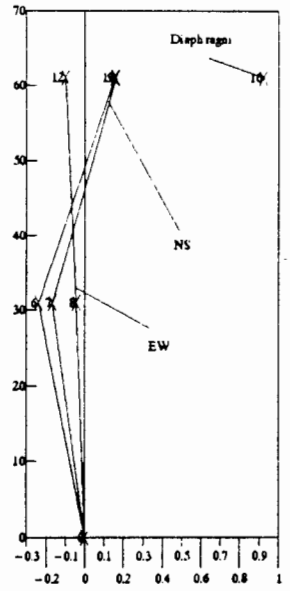

d) Mode 4: Second North-South
(T=0.17 sec, ξ = 3.9 %)

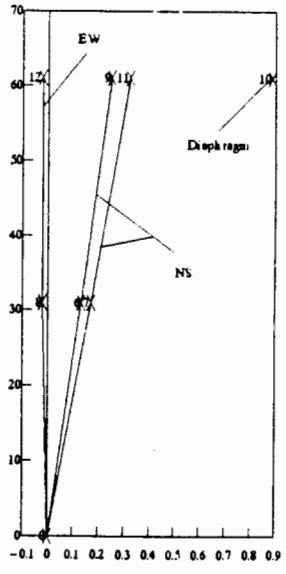

e) Mode 5: Higher Mode
(T=0.13 sec, ξ = 3.6 %)

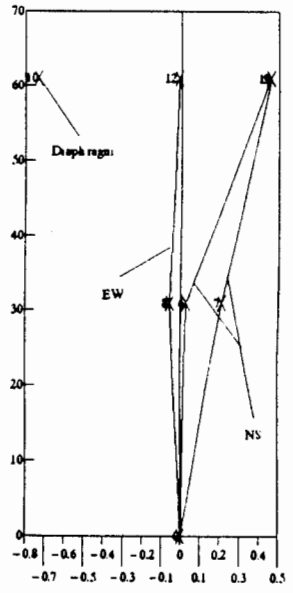

f) Mode 6: Higher Mode
(T=0.11 sec, ξ = 1.7 %)

FIGURE 4-5
THREE-DIMENSIONAL MODE SHAPES FOR TIME-INVARIANT ROCKING-BASE MODEL OF PARKING STRUCTURE, TIME SEGMENT = 40-60 SECONDS

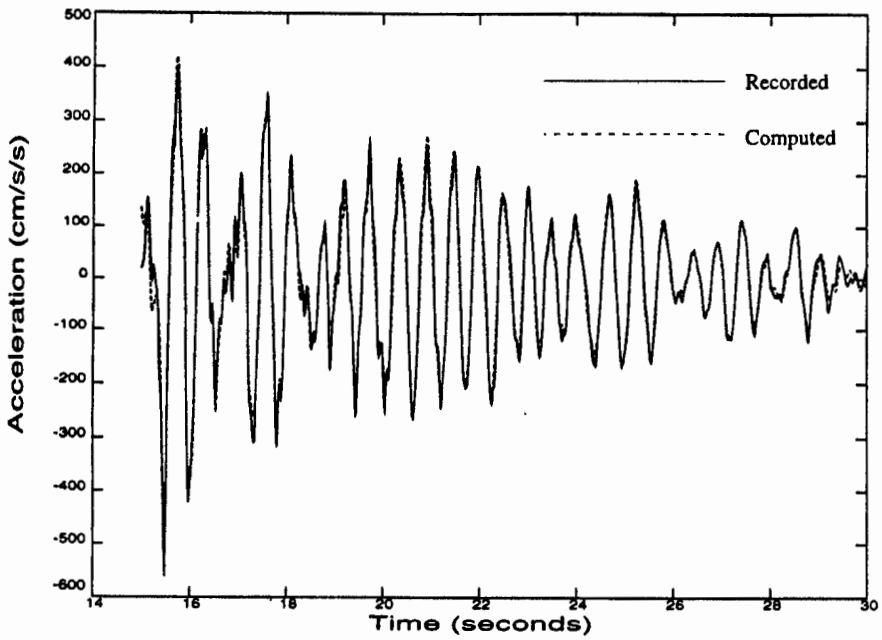

a) Acceleration Time Histories

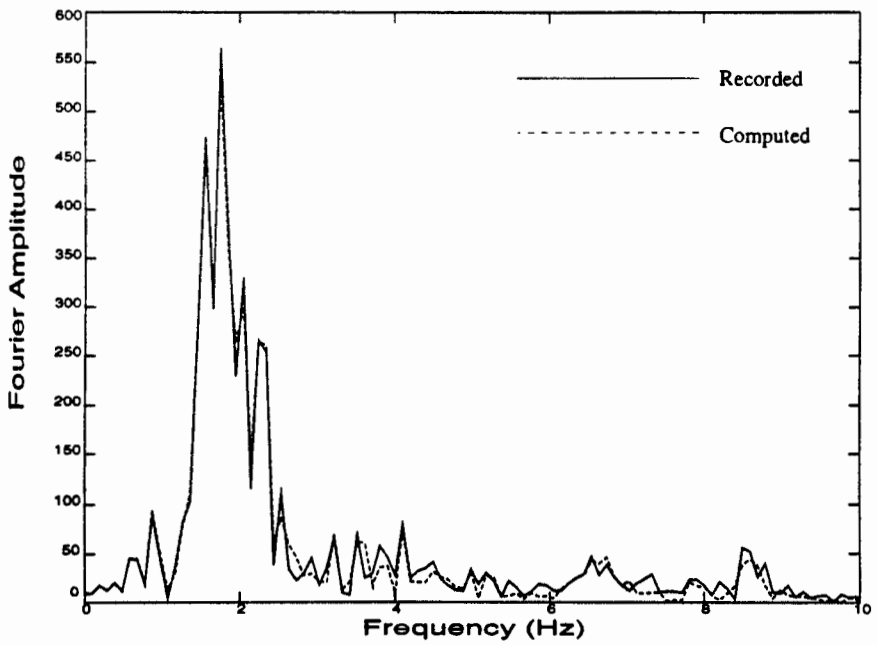

b) Fourier Amplitude Spectra

FIGURE 4-6
COMPARISONS BETWEEN RECORDED MOTIONS OF PARKING STRUCTURE AND COMPUTED MODEL MOTIONS OF TIME-INVARIANT ROCKING-BASE MODEL: CHANNEL 9 (ROOF NORTH-SOUTH), TIME SEGMENT = 15-30 SECONDS

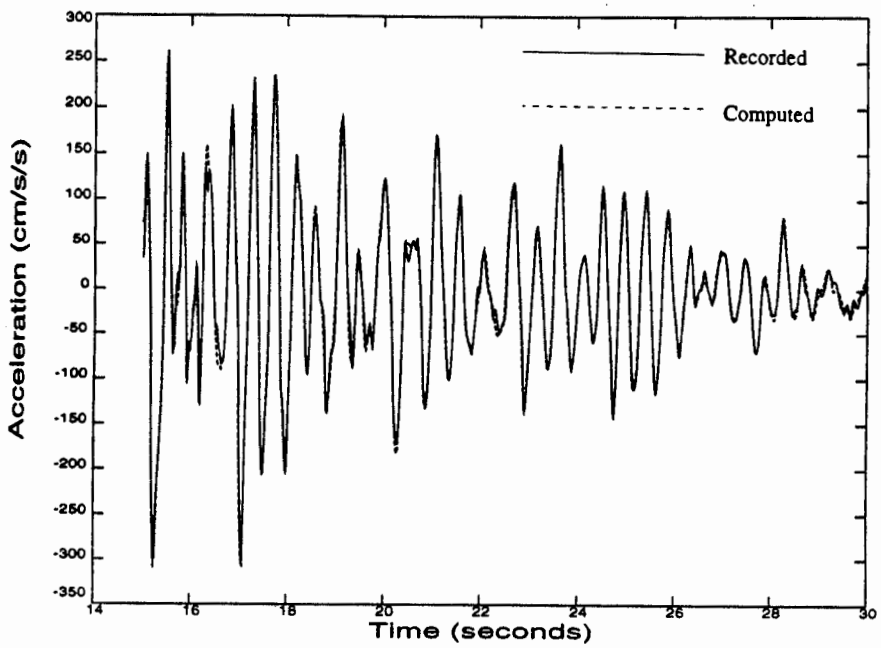

a) Acceleration Time Histories

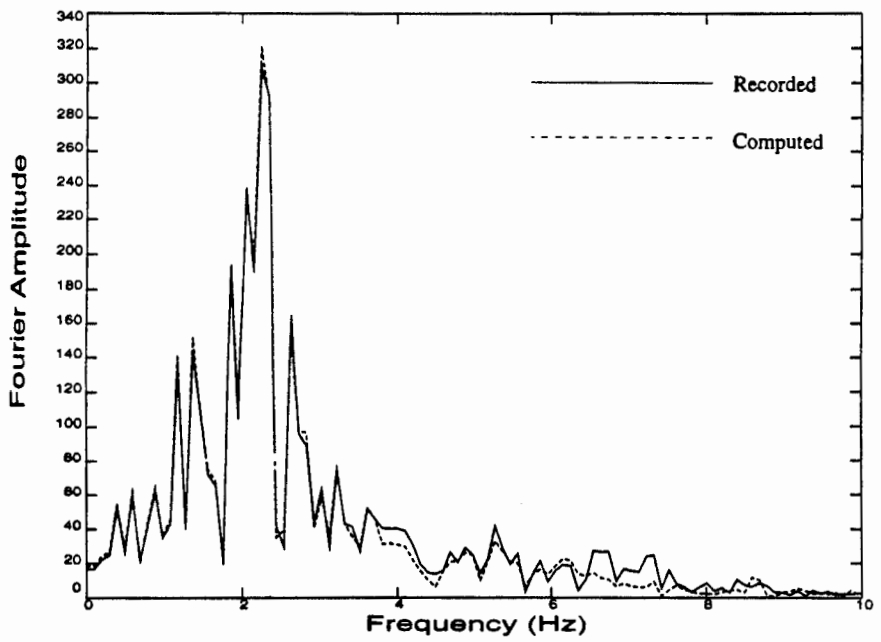

b) Fourier Amplitude Spectra

FIGURE 4-7
COMPARISONS BETWEEN RECORDED MOTIONS OF PARKING STRUCTURE AND COMPUTED MODEL MOTIONS OF TIME-INVARIANT ROCKING-BASE MODEL: CHANNEL 12 (ROOF EAST-WEST), TIME SEGMENT = 15-30 SECONDS

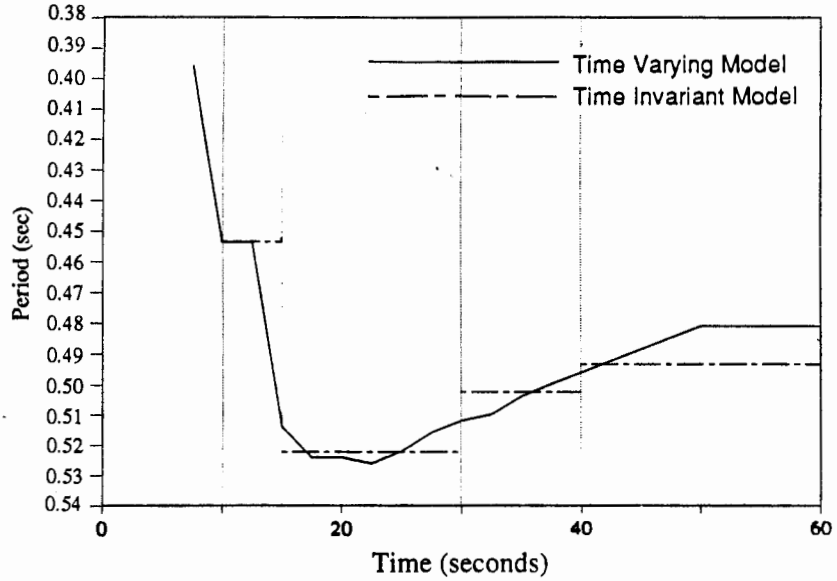

a) Mode 1: First North-South

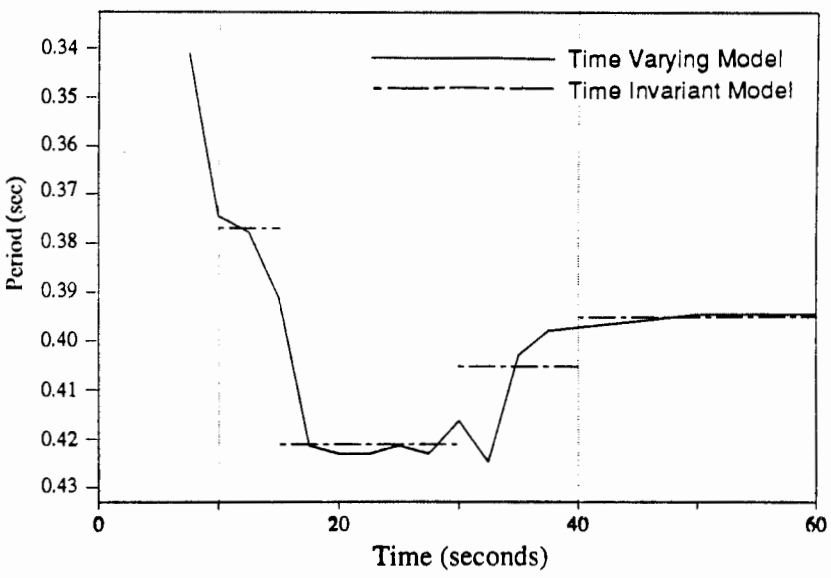

b) Mode 2: First East-West

FIGURE 4-8

VARIATION OF NATURAL PERIODS OF PARKING STRUCTURE OVER TIME

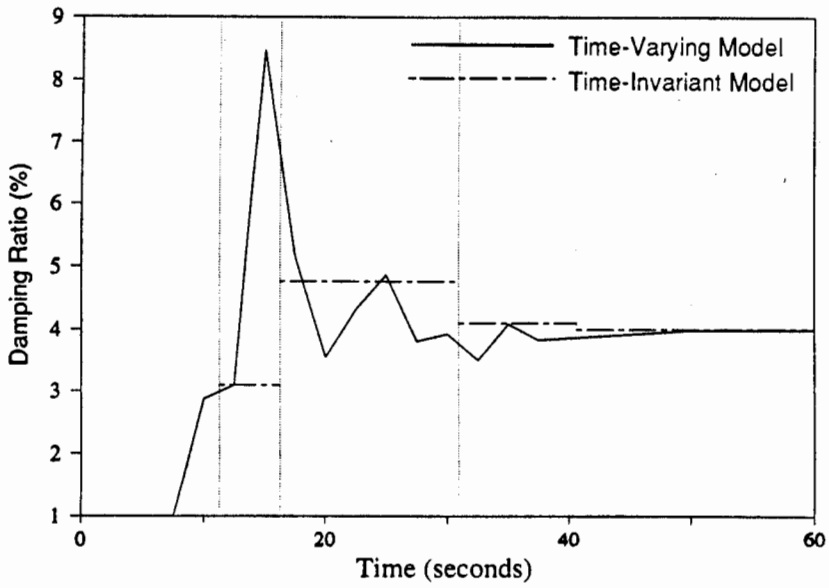

a) Mode 1: First North-South

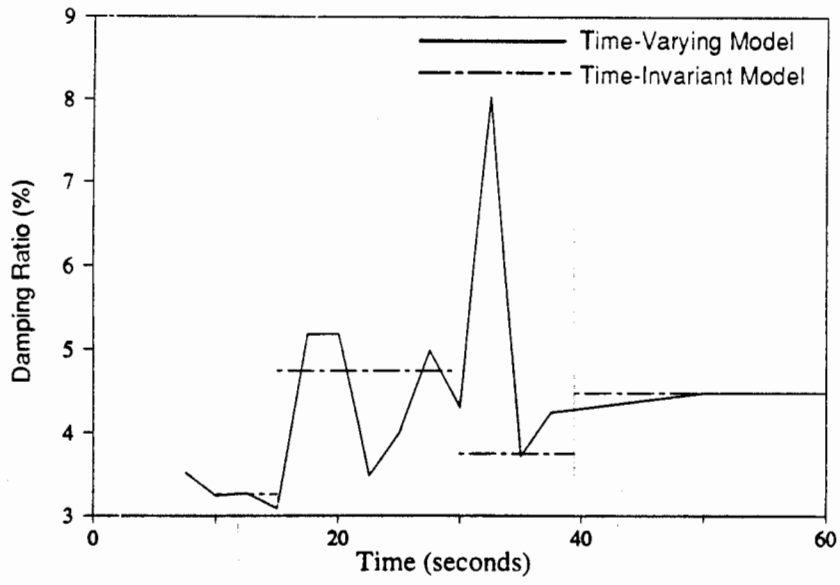

b) Mode 2: First East-West

FIGURE 4-9
VARIATION OF DAMPING RATIOS OF PARKING STRUCTURE OVER TIME

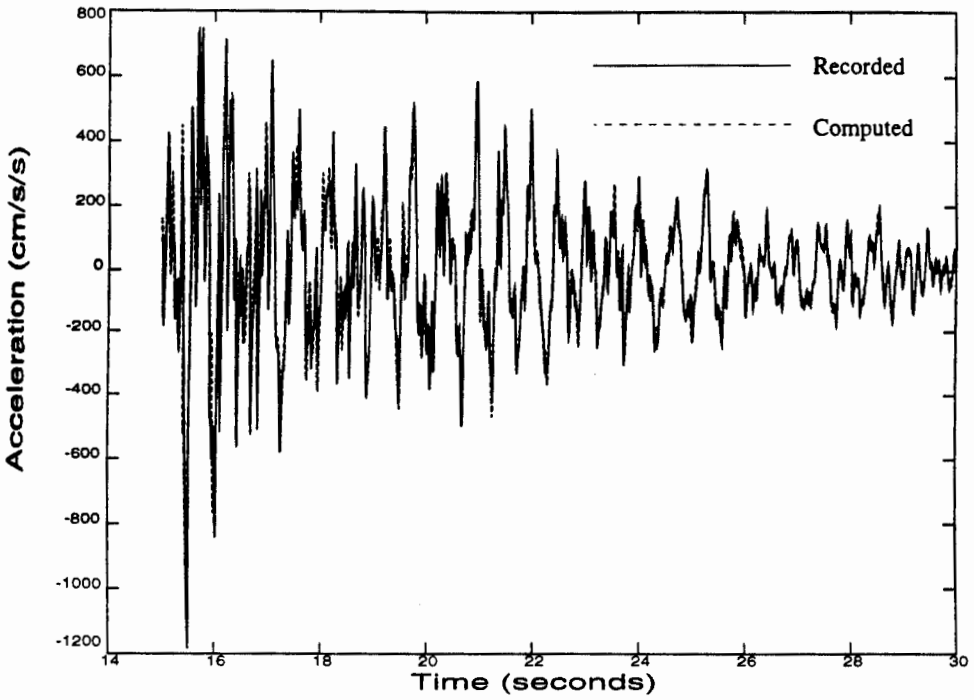

a) Acceleration Time History

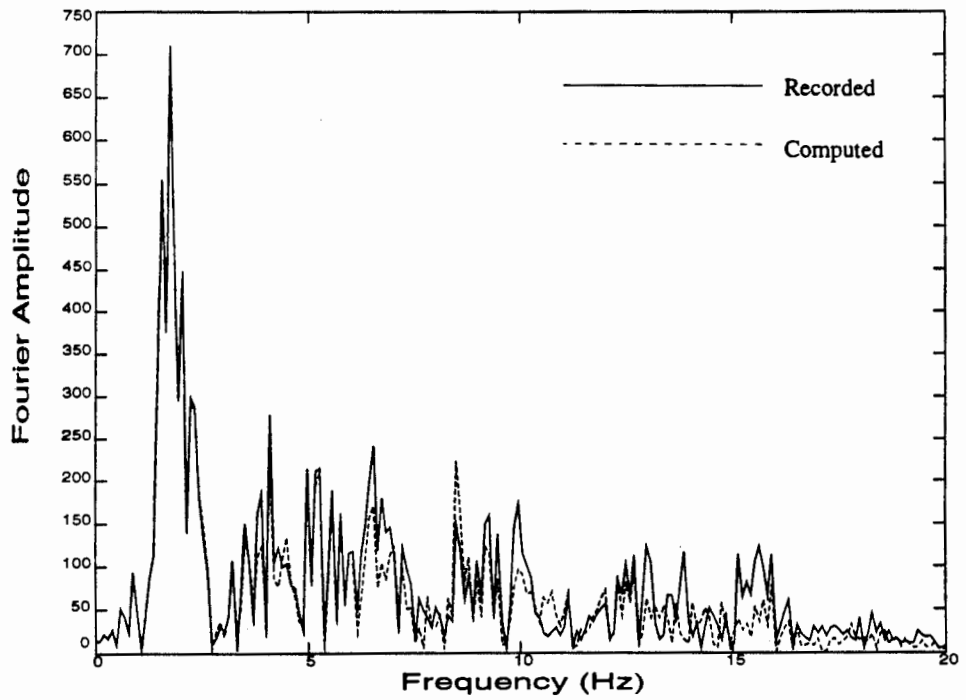

b) Fourier Amplitude Spectra

FIGURE 4-10
COMPARISON BETWEEN RECORDED PARAPET MOTIONS AND COMPUTED MODEL MOTIONS FROM SINGLE MODE MODE-ID MODEL (TIME WINDOW = 15-30 SECONDS)

5.0 FINITE ELEMENTS COMPUTER MODELS

5.1 OBJECTIVE AND SCOPE

Several detailed finite elements computer models were developed to study the dynamic behavior of the parking structure under consideration. Since the Northridge earthquake did not result in noticeable damage to the structure, only linear models were considered using the SAP90 general finite element computer program. The models were calibrated against the structure's recorded motions, through comparison of the computed model motions and the recorded motions and check of the modal parameters of the finite element model against those identified by MODE-ID from the strong motion records (Chapter 4).

Once the finite element models were calibrated and checked in this way they were used to carry out detailed analysis of the structure's dynamic response to the recorded base motions. The resullts of these analyses were used to:

(a) Compare seismic forces, drifts, and other response characteristis using the Uniform Building Code (UBC94) load distribution vs. those obtained from the dynamic response spectrum analysis using the code spectrum curve and the recorded site-specific response spectrum curves as input to the analysis.

(b) Evaluate the adequacy of the current modeling techniques for parking structures and recommend procedures for improvement of these techniques.

5.2 MODEL DESCRIPTION

Figure #5.1 shows the three-dimensional (3-D) plot of the finite element model that was developed for the parking structure. Partial views of the 3-D model that show east and west walls and ramps, are shown in Figures #5.2 and #5.3. The general characteristics of the models are as follows:

- The model was quite large, with 2309 nodes (resulting in 13,399 equations of motion) and 4896 beam-column (line) and shell elements.

- The shear walls were modeled with shell elements. These walls were supported on soil springs with a coefficient of subgrade reaction of 300 1b/in/in, in order to incorporate soil-structure interaction.

- All ramps were modeled using shell elements. Uncracked and cracked diaphragms were considered. Cracked diaphragms were modeled using a reduction of elastic modulus (E) equal to 60% of the value of the small-strain elastic modulus.

- Coupling beams between the east and west walls were modeled using cracked and uncracked section properties. The computer runs with cracked properties used a reduced elastic modulus equal to 60% E.

- Columns were attached to the sloped diaphragm; Hinged conditions were used at the base of the columns.

- The first computed 25 modes of vibration were considered in the analysis, producing over 99% mass participation.

- The damping ratio was assumed to be 5% of critical damping for all modes.

- The walls of the masonry service rooms at the lower level of the parking structure were modeled with shell elements.

- The inertia of the parking structure was modeled as concentrated masses that were lumped at the nodes of the finite element model. Only the dead weight of the structure was represented (It is noted that the structure was almost vacant during the Northridge earthquake).

- The masses of the stairwell towers were lumped at the corner nodes of the structure. The parapets and architectural veneers were not considered as structural elements, but their masses were considered based on a tributary area distribution.

5.3 INPUT MOTIONS

The computer models were subjected to horizontal input motions in the north-south and east-west directions in the form of 5-percent damped response spectra. Along the north-south direction, these input motions corresponded to the average of the spectra of the recorded base motions of Channels # 3 and Channel # 4 (see Figure 5.4a). Along the east-west direction, a response spectrum curve recorded at channel # 5 was considered as shown in Figure 5.4 (b). Due to the absence of free-field vertical acceleration records, no ground shaking was considered in the vertical direction.

In addition to the response spectrum analyses, transient analyes were performed using the recorded time-history motions in both directions. The standard mode superposition method and the Ritz vectors algorithm are used in SAP90 program to solve the dynamic equilibrium equations of motions for the complete structure.

5.4 NORMAL MODES OF VIBRATION

Table 5.1 shows the resulting eigen values, frequencies, and mass participation, for the model with cracked diaphragms. The following observations were made:

- The first fundamental mode is a lateral mode along the Y direction (North-South). It provides approximately 75% of the mass participation in the north-south direction. The fourth mode is a double curvature mode in the same direction, and provides for over 8% of the mass participation at this direction

- The second fundamental mode is a lateral mode along the X direction (East-West). It provides approximately 77% of the mass participation in the east-west direction. The fifth mode is a double curvature mode in the same direction, and provides for over 8% of the mass participation at this direction.

- The third mode is a pure torsional mode. The sixth mode is a double torsional mode.

- The first 12 modes provides over 90% of the mass participation in both directions. The first 19 modes provides over 95% of the mass participation in both directions. The first 25 modes provides over 99% of the mass participation in both directions.

Figures 5.5 (a), 5.5 (b), 5.5 (c) show the first, second, and third mode of vibration. Table 5.2 compares between the period of the vibrations of the first six fundamental modes obtained from Mode-ID, and Runs #1, and #2. It is clear from this table that the cracked diaphragm model (Run #2) provides better correlation with the results obtained from Mode-ID method, particularly for the modes sensitive to in-plane diaphragm motion (i.e. Mode 1 and Mode 4 which correspond to the modes in the North-South direction).

Figure 5.6 show a comparison between the shapes of the fundamental modes in both directions. It is shown that the first fundamental modes in the North-South and East-West directions are almost linear. The Second order modes are typical double curvature modes. This result compares very well with the results obtained from the Mode-ID method.

A comparison between the maximum recorded acceleration, at the locations of Channel #6 through Channel #12, is shown in Table 5.3. In general good results were obtained from the finite elements models. The computed time history records (signatures) are plotted vs. the recorded time-history results (Figure 5.7 (a) through Figure 5.7 (g)). The comparison is given for the time window between 15 seconds and 30 seconds, which is the time duration of the dominant ground motion. It is indicated that a reasonable fit between the computed and the recorded spectra curves were obtained.

Figures 5.7(a) through 5.7(g) illustrate that excellent agreement is obtained for the building's frequencies, but there is indication of overshooting of the amplitudes at some cycles. This suggests that larger damping ratio than those obtained from the Mode-ID method would give better fit. It is also indicated that the computed response along the east-west direction is more accurate than the response obtained along the north-south direction.

Table 5.1 Eigen Values, Frequencies, and Mass Participation results.

E I G E N V A L U E S A N D F R E Q U E N C I E S

MODE NUMBER	EIGENVALUE (RAD/SEC)**2	CIRCULAR FREQ (RAD/SEC)	FREQUENCY (CYCLES/SEC)	PERIOD (SEC)
1	0.141522E+03	0.118963E+02	1.893357	0.528162
2	0.196933E+03	0.140333E+02	2.233467	0.447734
3	0.255362E+03	0.159801E+02	2.543306	0.393189
4	0.116786E+04	0.341740E+02	5.438967	0.183858
5	0.176740E+04	0.420405E+02	6.690954	0.149456
6	0.207629E+04	0.455663E+02	7.252100	0.137891
7	0.268395E+04	0.518069E+02	8.245321	0.121281
8	0.276340E+04	0.525681E+02	8.366473	0.119525
9	0.284001E+04	0.532918E+02	8.481650	0.117902
10	0.303825E+04	0.551203E+02	8.772672	0.113990
11	0.383522E+04	0.619292E+02	9.856336	0.101458
12	0.394371E+04	0.627990E+02	9.994769	0.100052
13	0.427561E+04	0.653881E+02	10.406842	0.096091
14	0.482534E+04	0.694647E+02	11.055645	0.090452
15	0.573340E+04	0.757192E+02	12.051089	0.082980
16	0.629613E+04	0.793481E+02	12.628648	0.079185
17	0.702192E+04	0.837969E+02	13.336693	0.074981
18	0.733675E+04	0.856548E+02	13.632392	0.073355
19	0.952885E+04	0.976158E+02	15.536044	0.064366
20	0.116611E+05	0.107987E+03	17.186627	0.058185
21	0.133571E+05	0.115573E+03	18.394027	0.054365
22	0.202255E+05	0.142216E+03	22.634455	0.044180
23	0.253714E+05	0.159284E+03	25.350819	0.039446
24	0.513714E+05	0.226653E+03	36.072874	0.027722
25	0.556125E+05	0.235823E+03	37.532408	0.026644

P A R T I C I P A T I N G M A S S - (percent)

MODE	X-DIR	Y-DIR	Z-DIR	X-SUM	Y-SUM	Z-SUM
1	0.234	75.149	0.000	0.234	75.149	0.000
2	77.032	0.184	0.000	77.266	75.333	0.000
3	0.039	0.006	0.000	77.305	75.339	0.000
4	0.139	8.549	0.000	77.444	83.888	0.000
5	8.191	0.931	0.000	85.635	84.818	0.000
6	2.575	2.460	0.000	88.210	87.278	0.000
7	1.458	0.014	0.000	89.668	87.292	0.000
8	1.367	0.056	0.000	91.035	87.347	0.000
9	2.652	0.152	0.000	93.687	87.499	0.000
10	0.159	0.235	0.000	93.846	87.734	0.000
11	0.002	0.411	0.000	93.848	88.146	0.000
12	0.264	1.733	0.000	94.112	89.878	0.000
13	1.249	0.252	0.000	95.361	90.131	0.000
14	0.190	0.009	0.000	95.551	90.140	0.000
15	0.122	0.265	0.000	95.673	90.404	0.000
16	0.439	0.111	0.000	96.111	90.516	0.000
17	0.105	2.661	0.000	96.216	93.177	0.000
18	0.282	0.285	0.000	96.498	93.462	0.000
19	0.006	1.581	0.000	96.505	95.044	0.000
20	0.618	0.020	0.000	97.123	95.064	0.000
21	0.020	1.715	0.000	97.143	96.779	0.000
22	1.118	0.000	0.000	98.260	96.780	0.000
23	0.026	0.594	0.000	98.286	97.373	0.000
24	0.562	0.877	0.000	98.849	98.250	0.000
25	0.331	1.141	0.000	99.179	99.391	0.000

Table 5.2
Fundamental Periods (Sec.)

Case	Fundamental Periods (Sec.)					
	Mode 1	Mode 2	Mode 3	Mode 4	Mode 5	Mode 6
Mode ID (Time Window 15-30 Secs.)	0.530	0.420	0.380	0.180	0.150	0.120
Finite Element Model	0.517	0.430	0.389	0.157	0.128	0.120
Finite Element Model with Cracked Diaphragm	0.528	0.447	0.393	0.183	0.150	0.137

* First mode is lateral in N-S direction
* Second mode is lateral in E-W direction
* Third mode is Torsional
* Fourth, fifth, and sixth modes are one degree higher order of first, second and third modes, repectively.

TABLE 5.3
Comparison Between Maximum Recorded Acceleration and Computed Acceleration

Channel #	Chann #6	Chann #7	Chann #8	Chann #9	Chann #10	Chann #11	Chann #12
Max. Recorded Acceleration (g)	0.32	0.34	0.22	0.58	0.84	0.55	0.31
Max. Computed Acceleration (g)	0.334	0.34	0.196	0.583	0.79	0.598	0.389
Max. Computed Acceleration (g) with Flexible Diaphragm	0.327	0.34	0.20	0.60	0.90	0.61	0.368

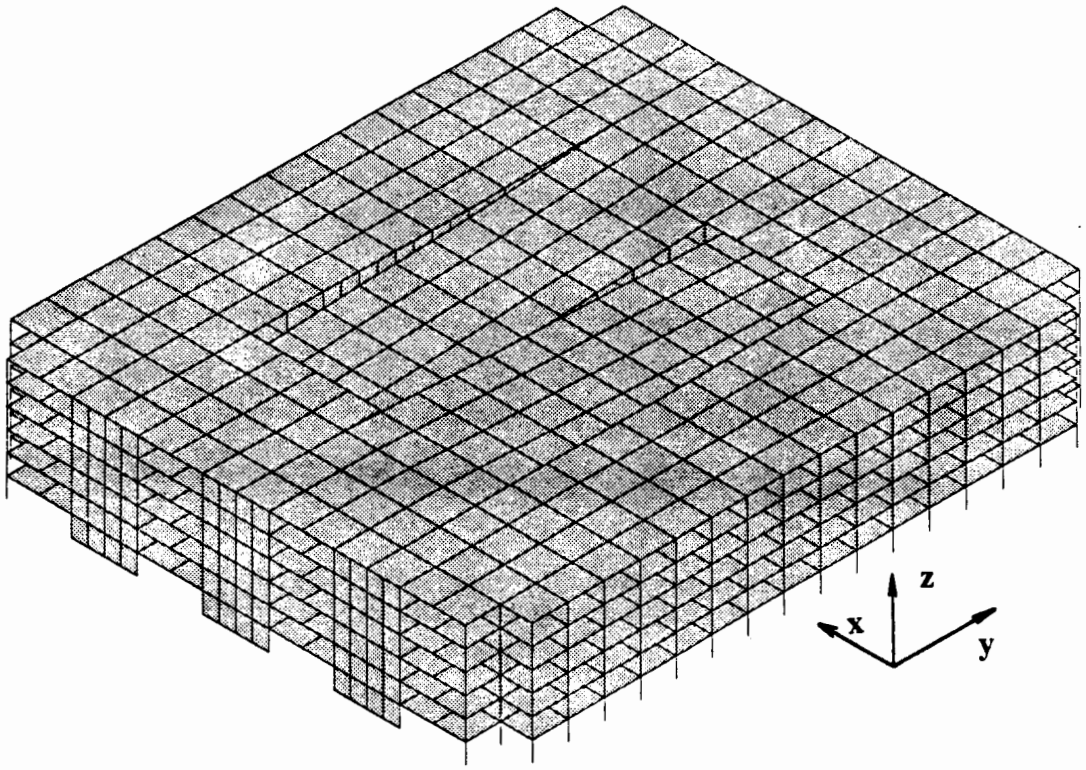

Figure 5.1 (a) **3-D Finite Elements Model Showing Shell Elements**

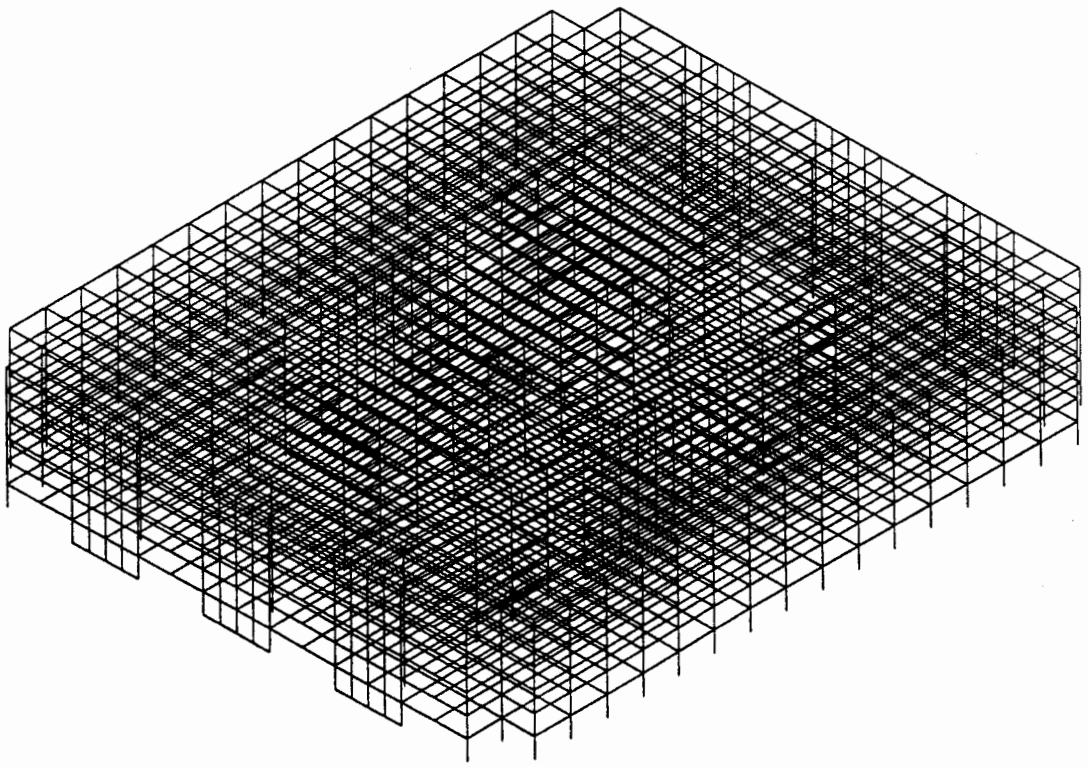

Figure 5.1 (b) **3-D Finite Elements Model Showing Line Elements**

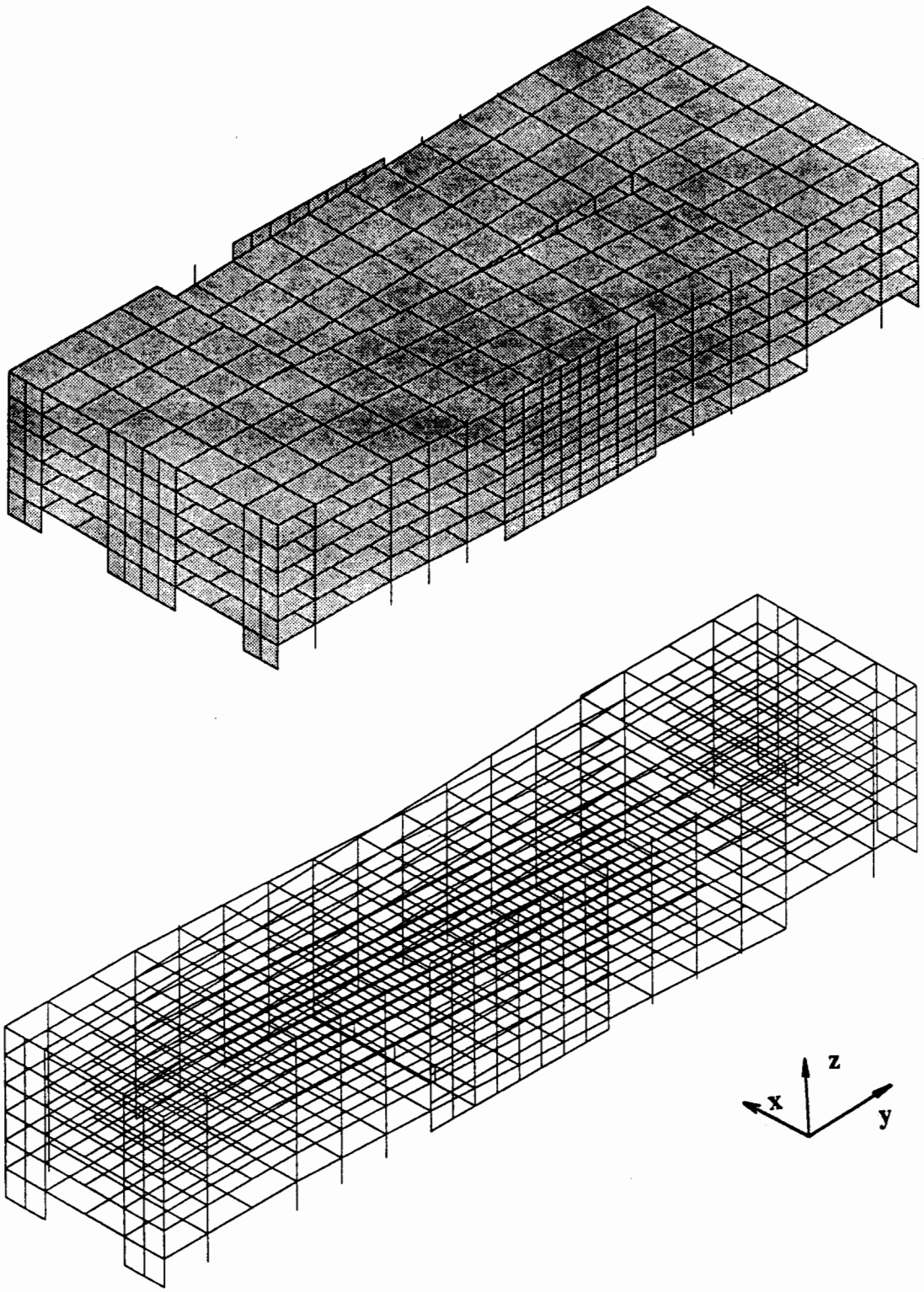

Figure 5.2 **Partial View of the 3-D Finite Elements Model Showing East-West Walls and Ramps (shell elements are shown above, line elements are shown below).**

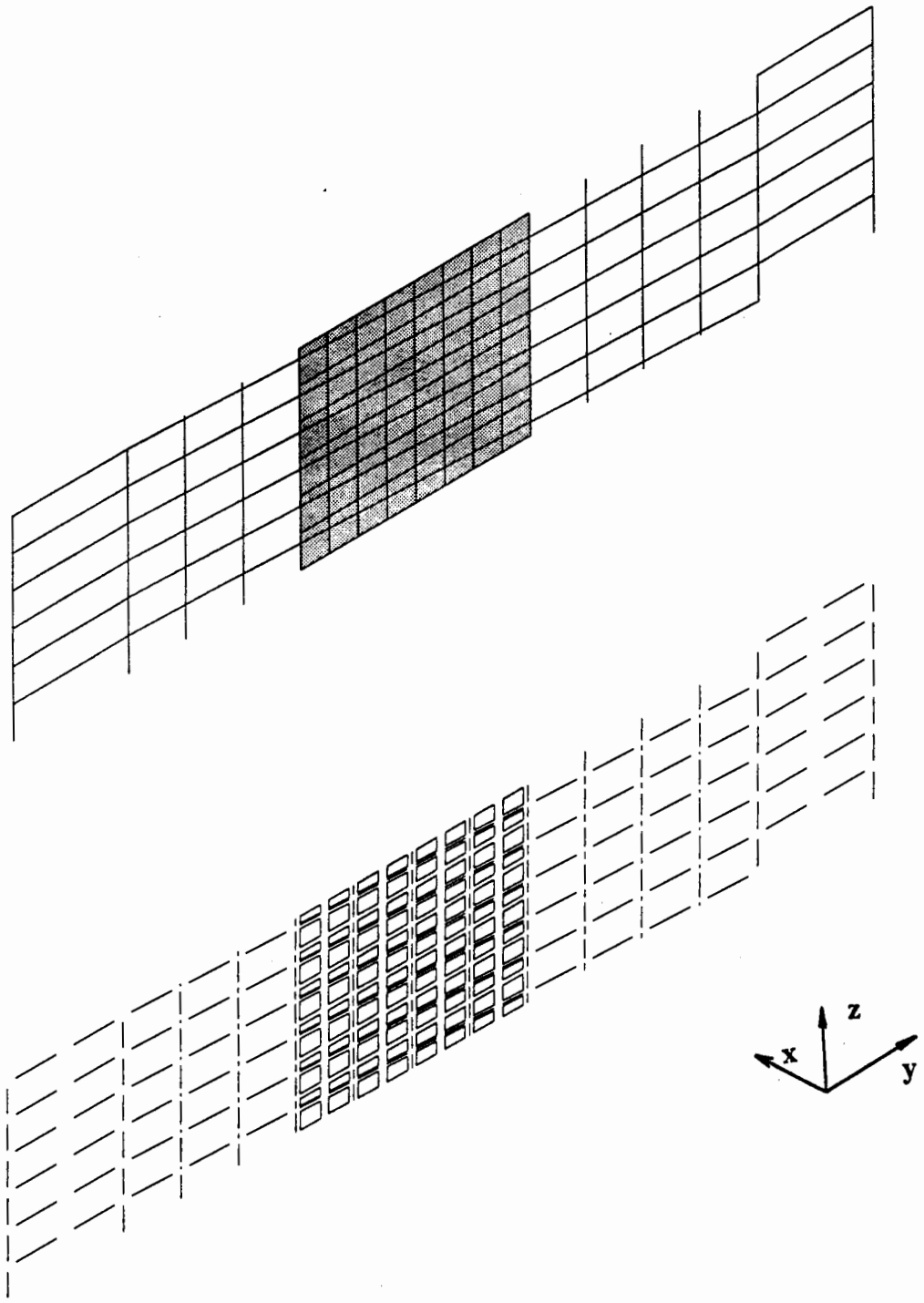

Figure 5.3 **Section showing the modeling of East-West Wall and Ramps (shell and line elements are shown above, shrunk elements are shown below).**

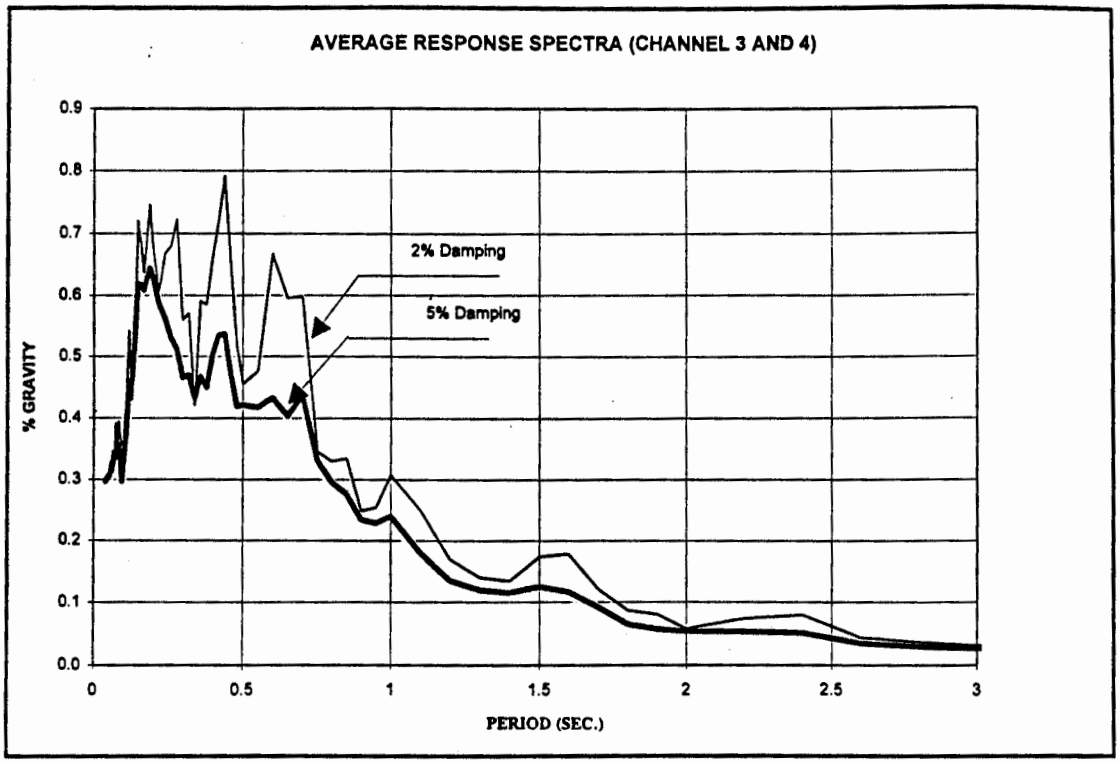

Figure 5.4 (a) **Input ground response spectrum acting in the North-South direction**

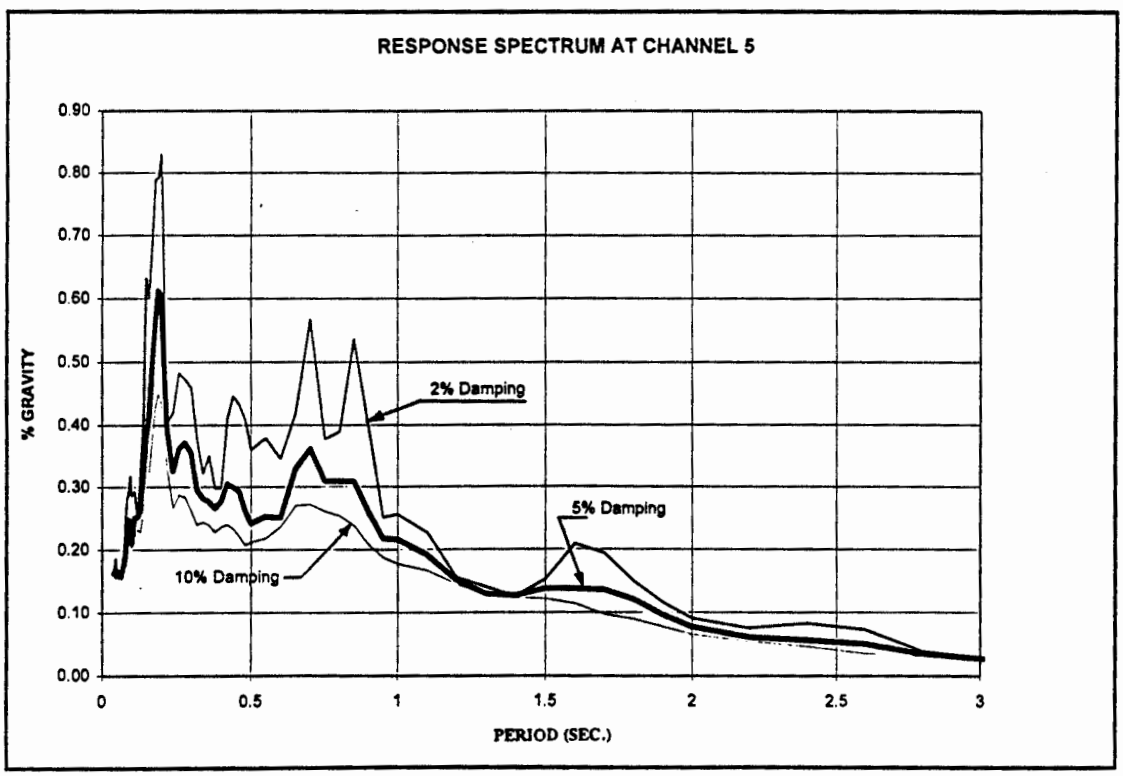

Figure 5.4 (b) **Input ground response spectrum acting in the East-West direction**

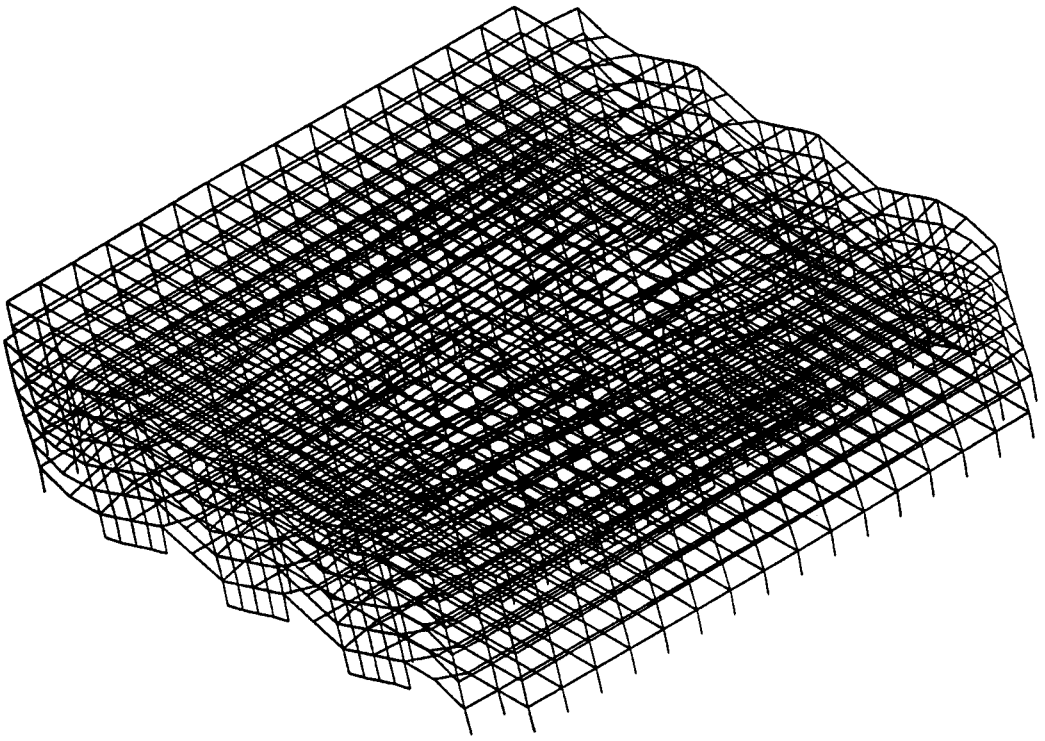

Figure 5.5 (a) First fundamental mode shape acting in the Y direction (North-South).

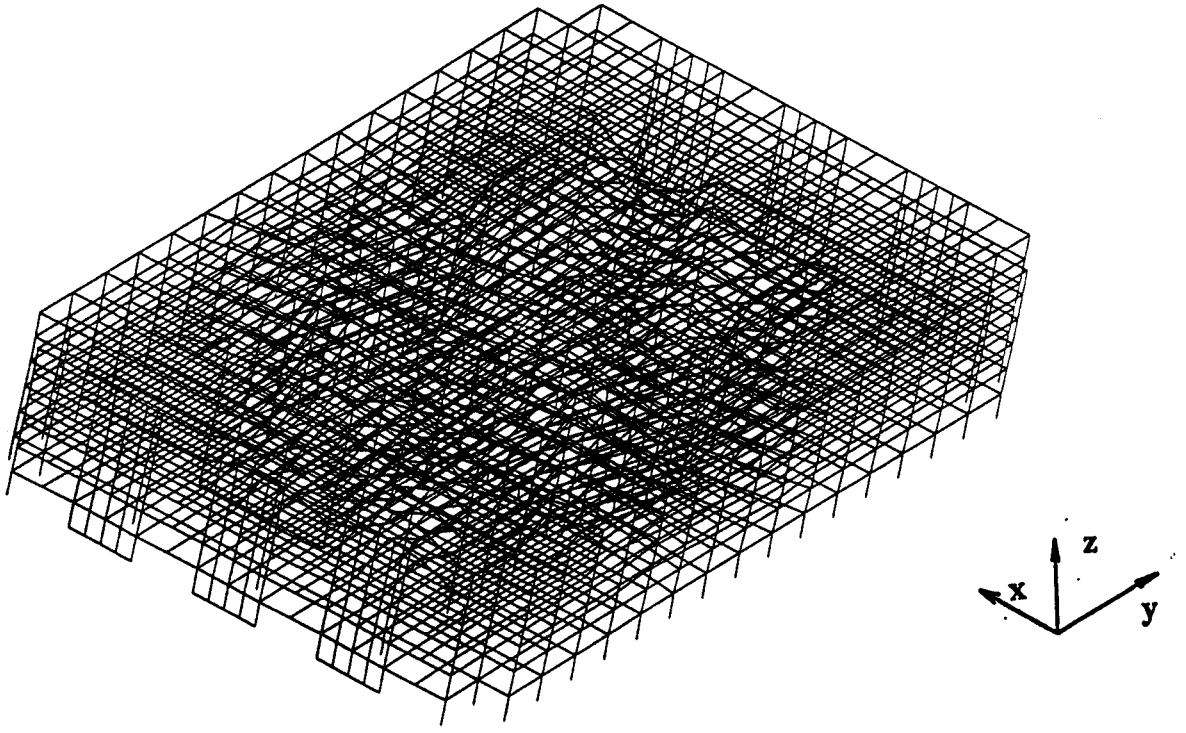

Figure 5.5 (b) Second fundamental mode shape acting in the X direction (East-West).

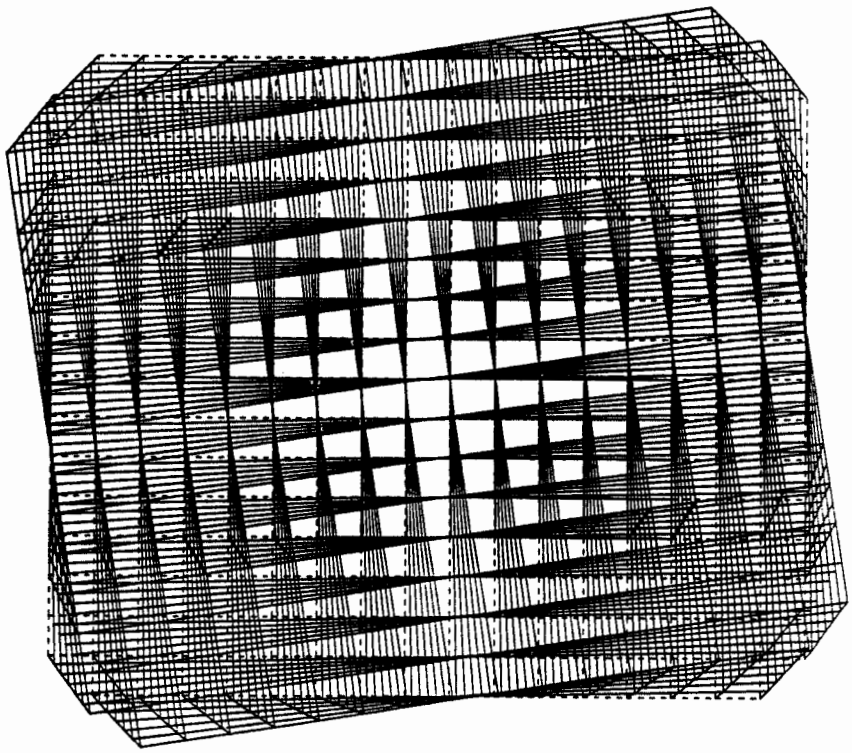

Figure 5.5 (c) **Torsional Mode Shape (Plan view).**

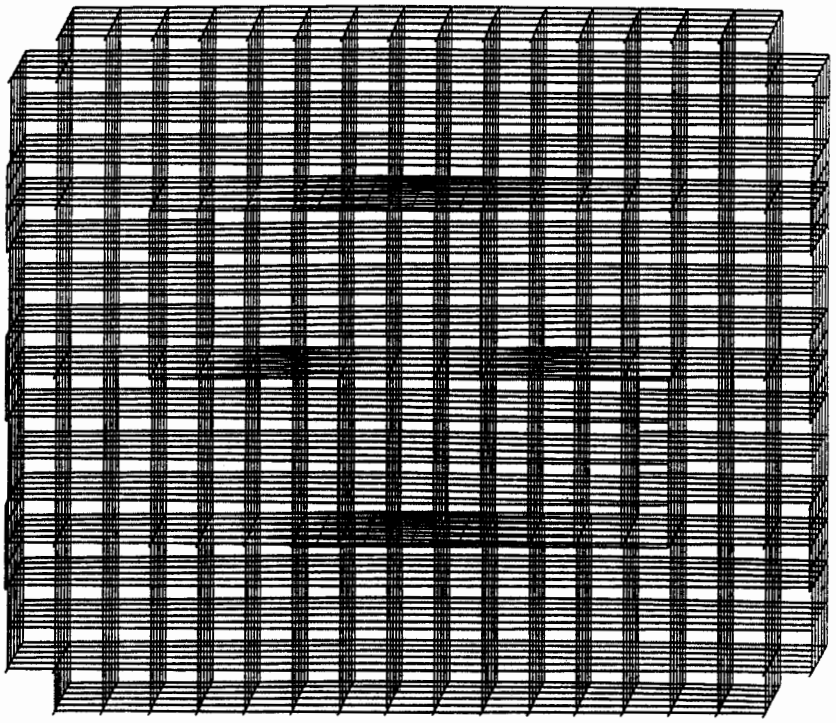

Figure 5.5 (d) **Results of Lateral Displacements using Site Specific Response Spectrum.**

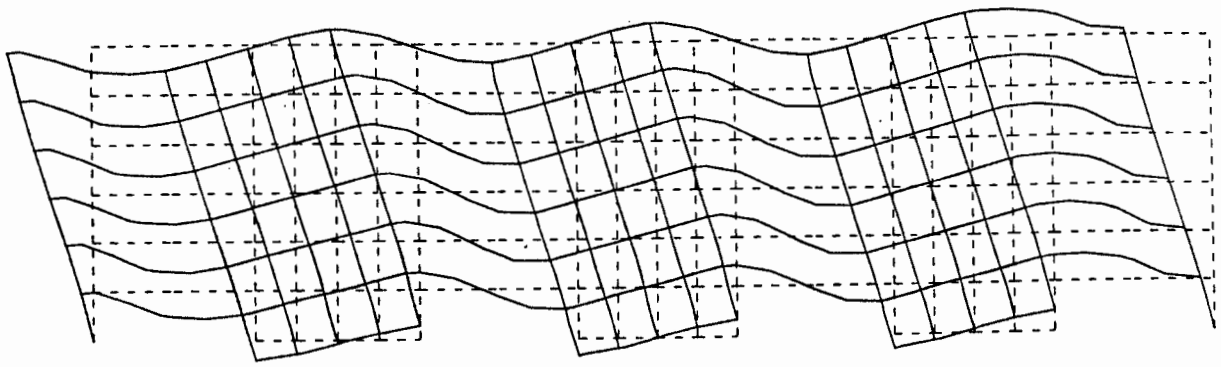

Mode #1

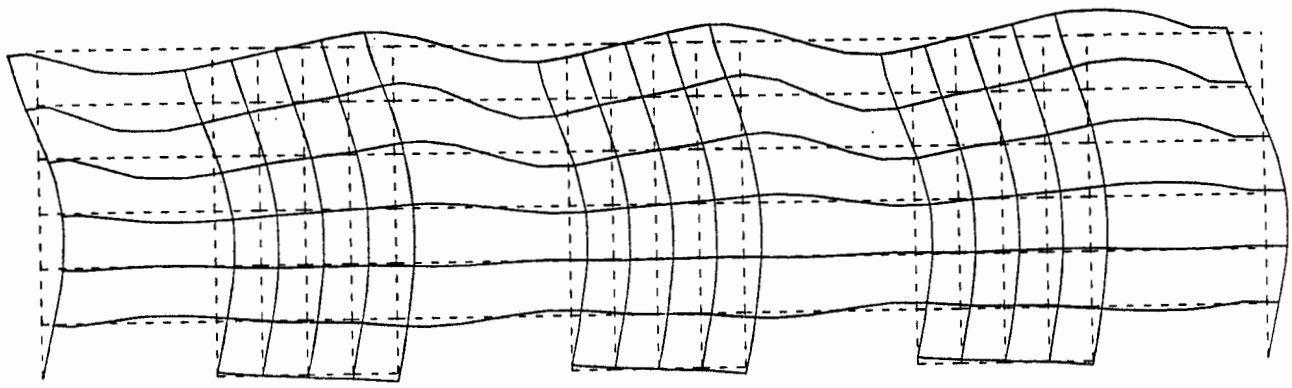

Mode #4

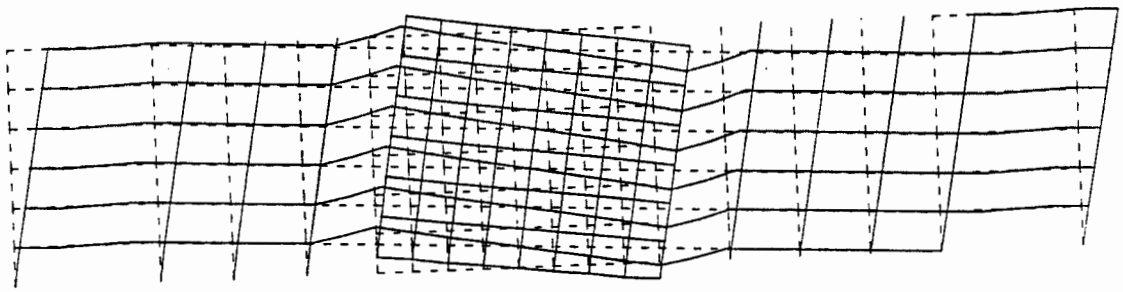

Mode #2

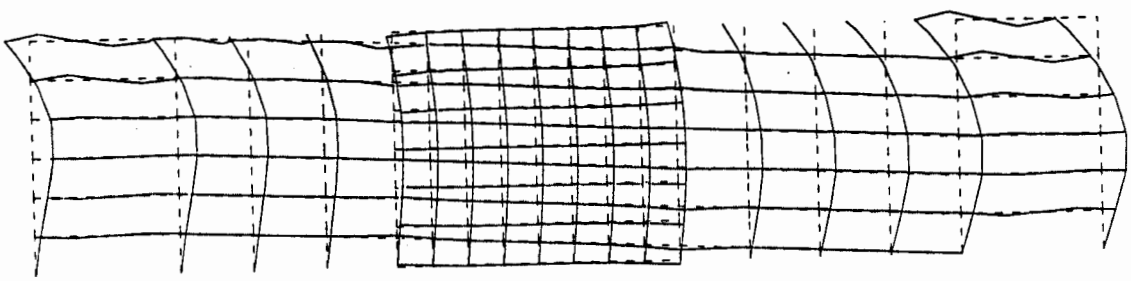

Mode #5

Figure 5.6 Comparison Between the Shape of the Fundamental Modes.

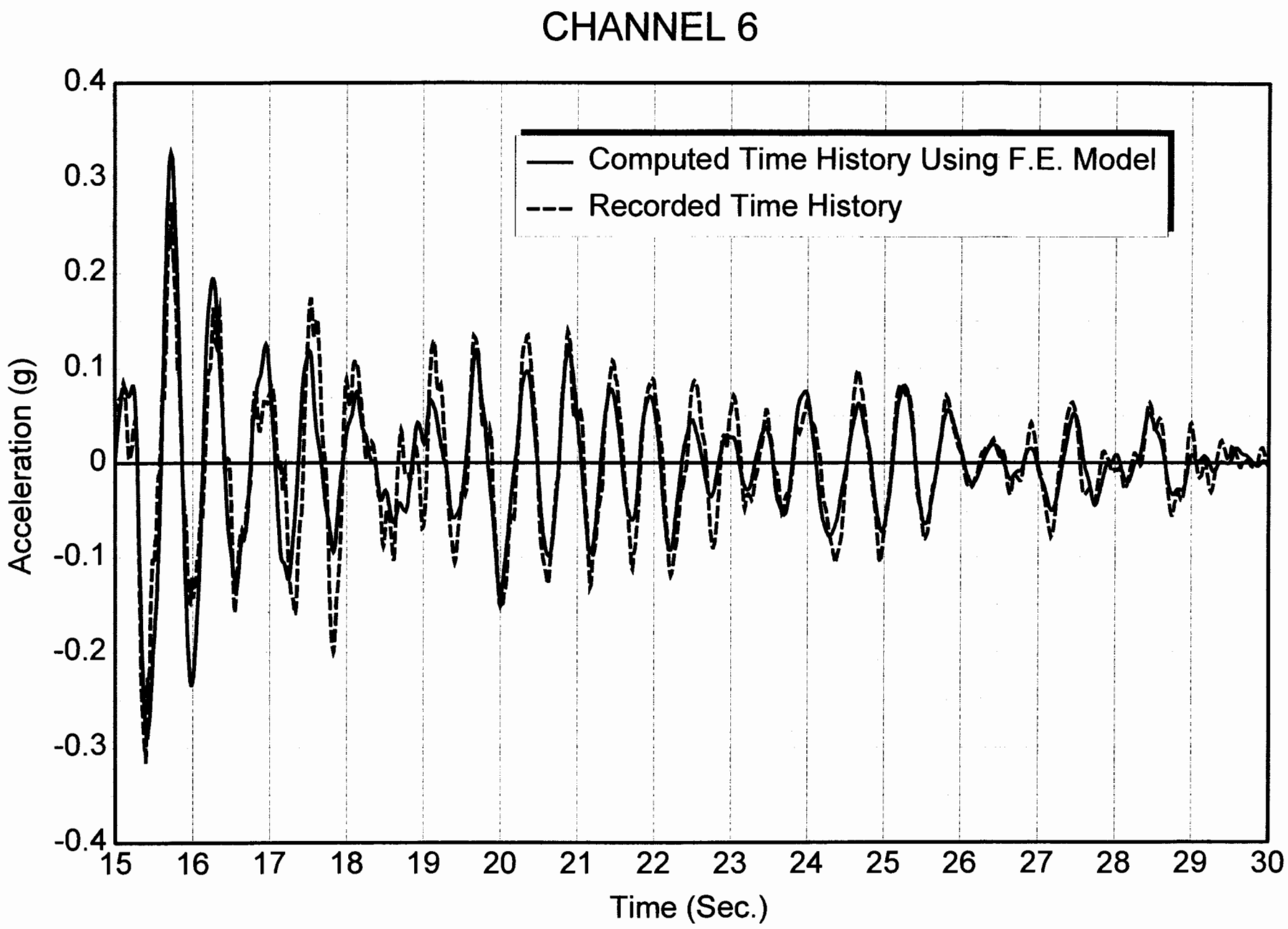

Figure 5.7(a) Computed vs. Recorded Acceleration Time History for Channel # 6

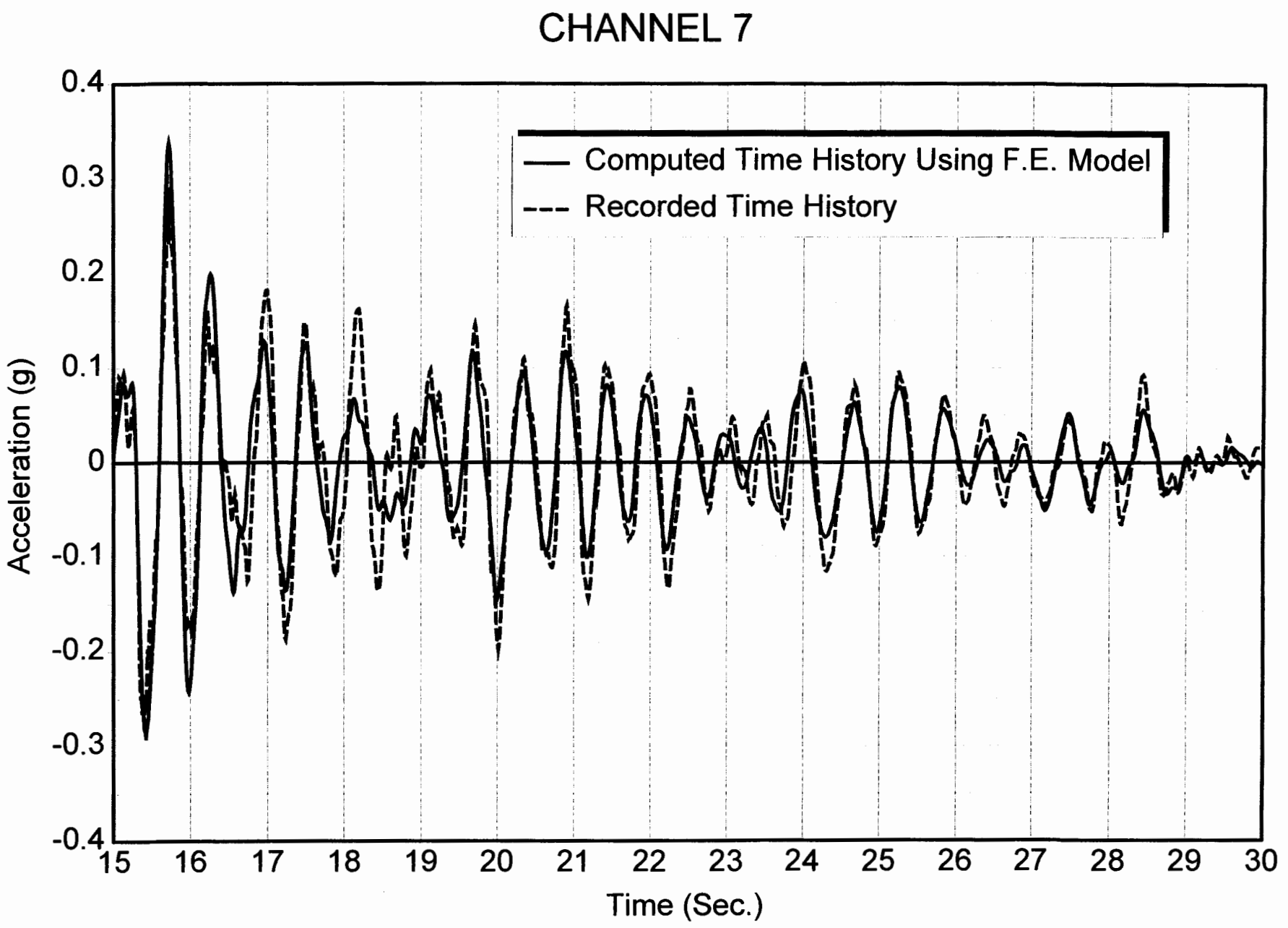

Figure 5.7(b) Computed vs. Recorded Acceleration Time History for Channel # 7

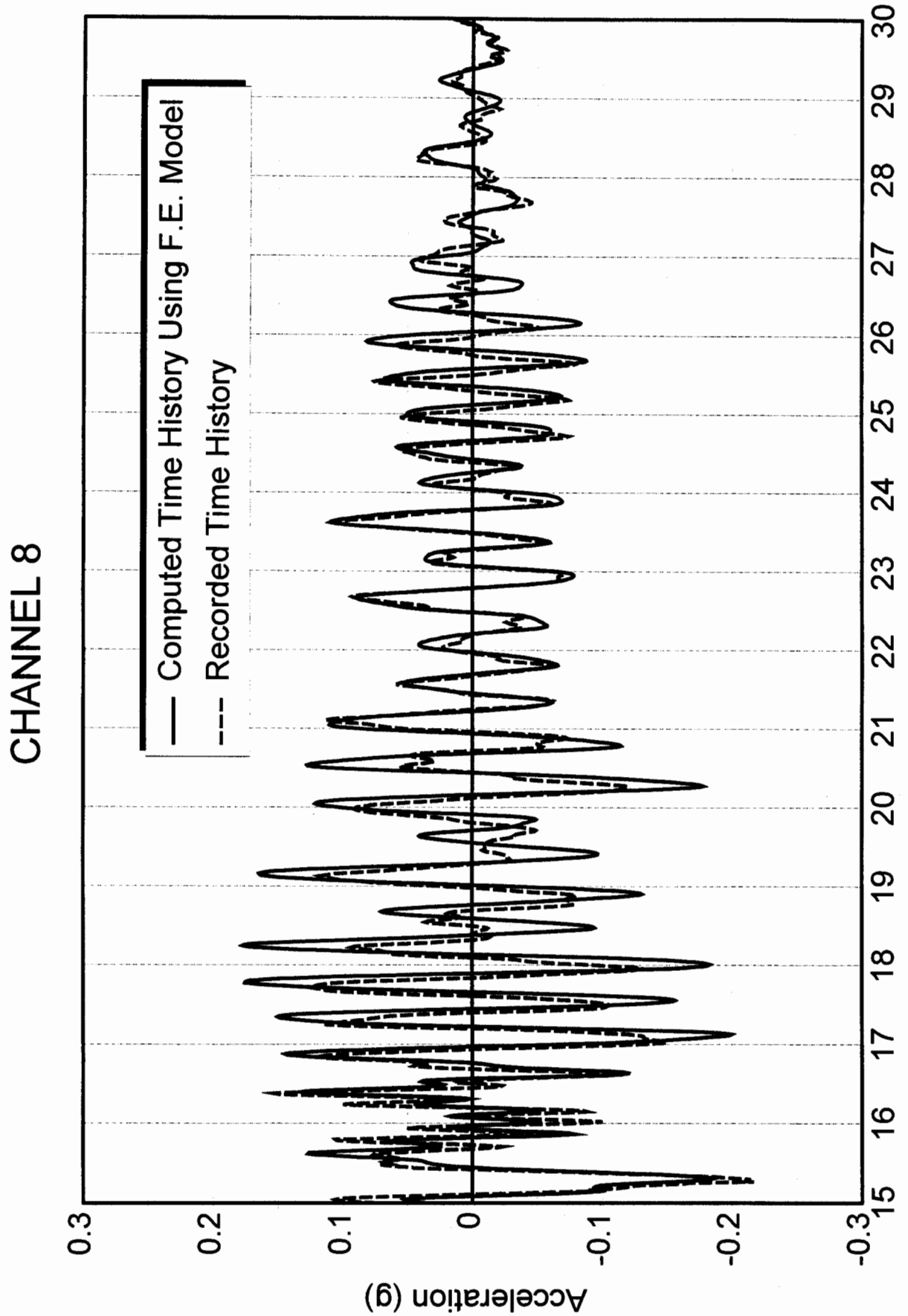

Figure 5.7(c) Computed vs. Recorded Acceleration Time History for Channel # 8

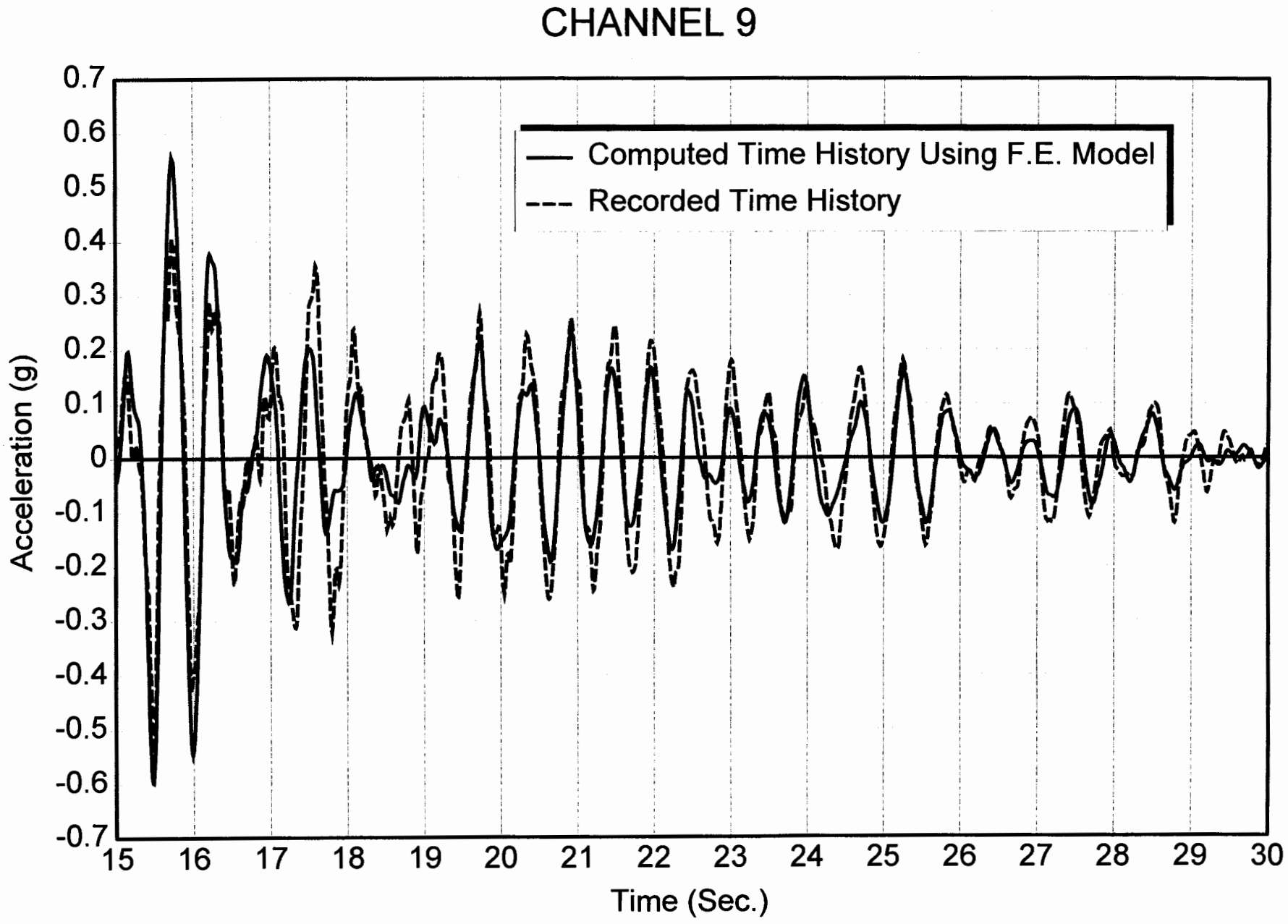

Figure 5.7(d) Computed vs. Recorded Acceleration Time History for Channel # 9

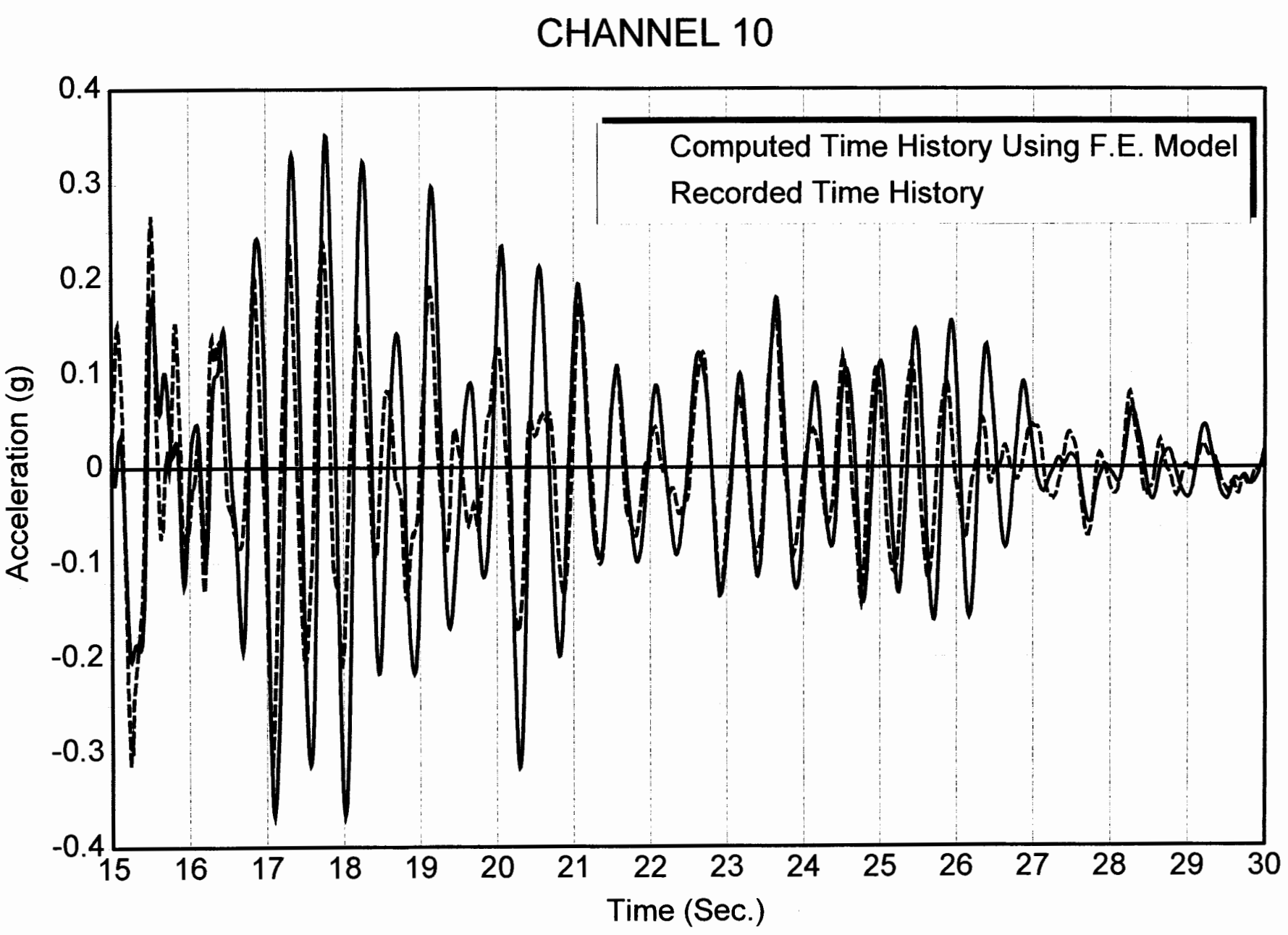

Figure 5.7(e) Computed vs. Recorded Acceleration Time History for Channel # 10

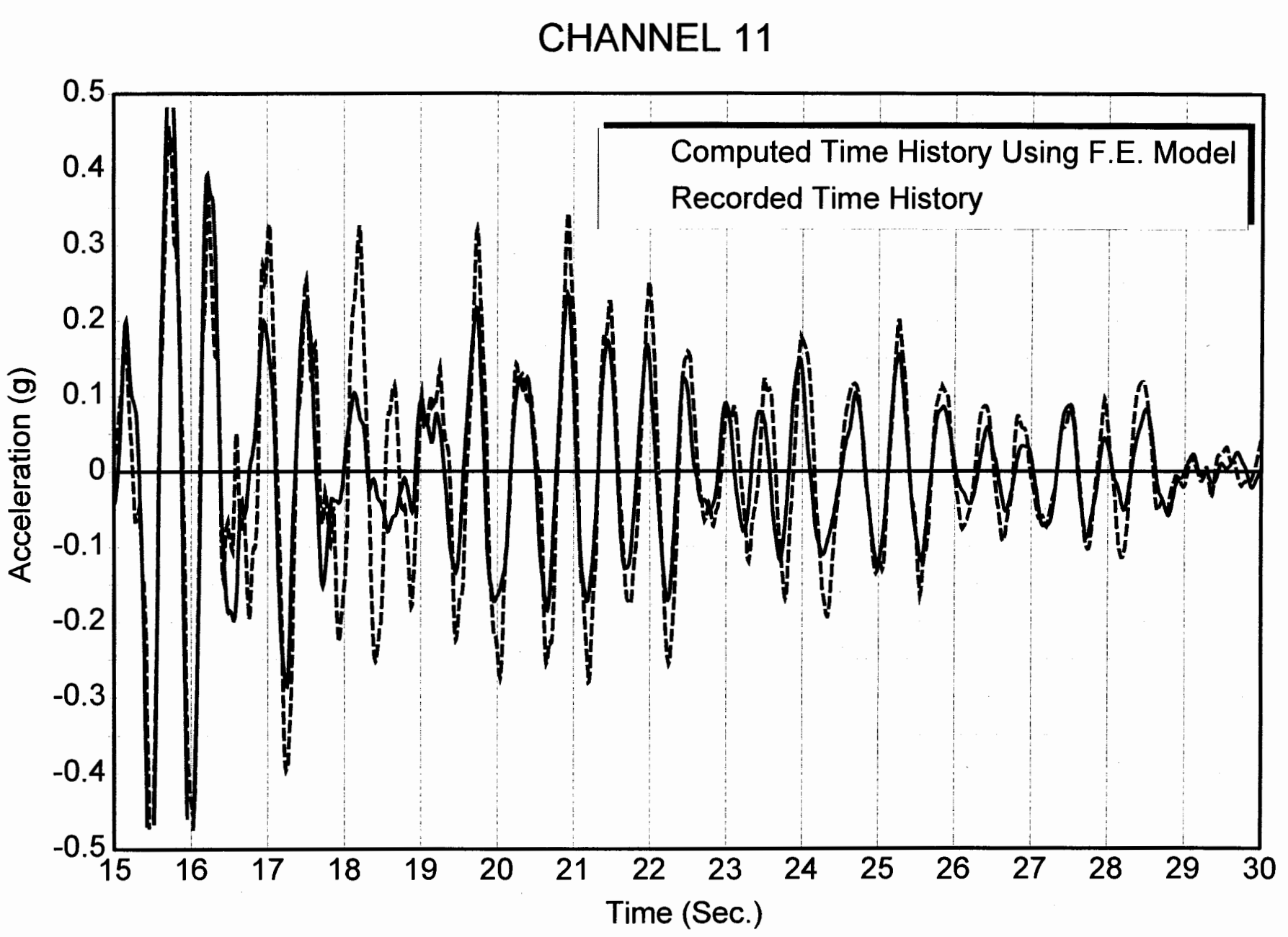

Figure 5.7(f) Computed vs. Recorded Acceleration Time History for Channel # 11

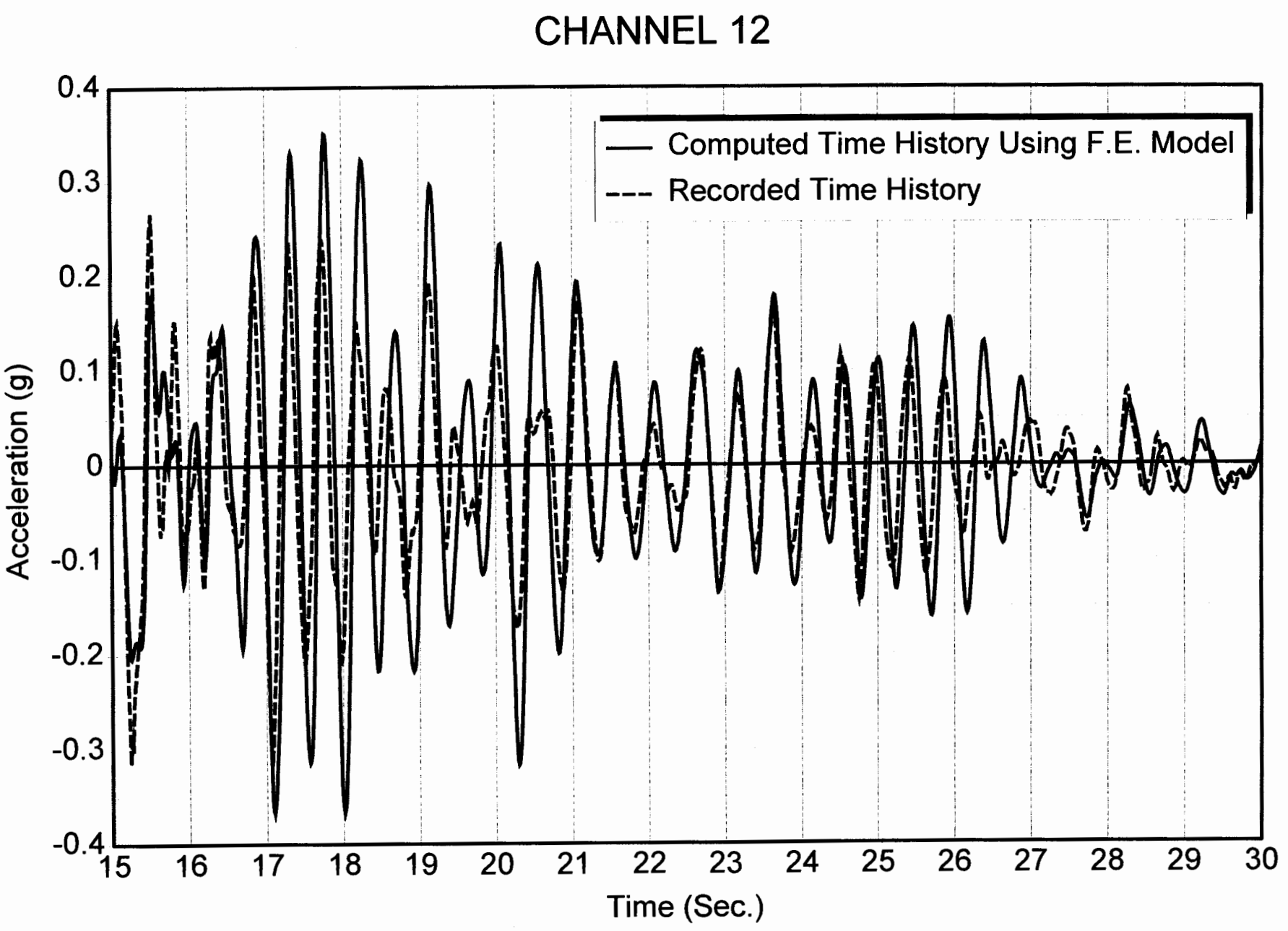

Figure 5.7(g) Computed vs. Recorded Acceleration Time History for Channel # 12

6.0 ASSESSMENT OF THE STRUCTURAL BEHAVIOR AND COMPARISON WITH SEISMIC DESIGN PROVISIONS.

6.1 ANALYSIS CASES

In order to assess the structural behavior and to compare between the predicted and recorded response and the code provisions, four computer runs were performed as follows.

Run #1

The finite element model was subjected to the recorded ground response curves corresponding to 5% damping. Along the north-south direction, a response spectrum curve corresponding to the average of Channel # 3 and Channel # 4 was considered. This curve is shown in Figure #5.4 (a). Along the east-west direction, a response spectrum curve recorded at channel #5 was considered as shown in Figure #5.4 (b). Due to the absence of free-field vertical acceleration records, no ground shaking was considered in the vertical direction. Uncracked section properties were used in this run.

Run #2

This run is similar to Run #1, except that cracked sections were used for the diaphragms and the coupling beams of the shear walls. The cracked section properties were assumed to have an elastic modulus equal to 60% of the small-strain elastic modulus (E).

Run #3

In addition to the recorded ground shaking, the model was also subjected to the UBC94 response spectrum curve for Zone 4. This curve corresponds to 0.4 peak ground acceleration, with a peak spectrum acceleration of 1.0 g. The objective of this analysis is to provide a comparison between response spectrum code results and the Northridge recorded values.

Run #4

The computer results were also compared with the results obtained from the UBC94 Code equivalent static lateral loads. In the regard, R_w of 8 was considered. All lumped nodal weights were scaled down based on to the code triangular distribution, according to the nodes' height from the ground. A spread sheet for the code results using fundamental periods obtained from the computer model is shown in Appendix C..

6.2 SEISMIC BASE SHEAR

Table #6.1 shows the results of the seismic base shear obtained for the 4 cases defined above. The following observation were made:

- The code seismic shears are larger along the east-west direction than the north-south direction (13.2% g compared to 11.7% g). However, the finite element results using UBC code spectrum indicate different distribution (99% g along the North-South direction, and

77% along the East-West direction). It is shown that the base shear obtained from the code response spectrum curve, and the recorded ground motion are 8.46 and 5.88 times the code base shear, respectively. These factors correspond to the ductility which is required to be supplied by the structural elements of the Garage.

- The results using the recorded ground motion are much smaller than the results using the UBC94 response spectrum. Along the North-South directions the base shear is only 0.43 of the base shear obtained using code spectrum. This factor is only 0.29 along the East-West direction.

6.3 SEISMIC DEFORMATIONS

Figure #5.5 (d) shows the typical 3-D deflected shape of the parking structure when subjected to the recorded ground motions in both lateral directions. Figures #6.1 and #6.2 show the deformed shape and the shear stress contours of the North-South walls and the East-West walls, respectively. These figures show that the computed deformed shapes of the walls increase almost linearly over the height of the structure.

Table #6.2 provides a comparison between the seismic lateral displacement in the parking structure at different levels. Table #6.3 provides the maximum diaphragm displacements at the middle of the span of the diaphragm at the sixth level, along the North-South direction.

The following observations were made:

(1) The inter-story drift based on the finite element results is approximately 0.2%, and did not result in noticeable damage to the nonstructural elements such as the exterior veneer or the stair towers.

(2) Although the ground motion did not result in noticeable damage, the maximum deflection obtained from Run #1 is approximately 2.85 times the code deflection. This indicates that possibly, at a higher level of ground shaking, the ratio may exceed the value recommended by the current provisions of the code which is based on the $3(R_w/8)$ factor. Therefore, an increase of this factor to reflect the nonlinear response of the structure at higher levels of ground shaking is recommended.

(3) The finite element model indicates that the north-south deflection at the mid-span of the diaphragm is approximately 10% higher than the deflection at the end shear walls. The finite element model with cracked diaphragms leads to a mid-span diaphragm deflection that is 16 percent higher than the deflection of the end walls

6.4 SEISMIC STRUCTURAL FORCE

Table #6.4 provides the computed seismic shear and moment demands at typical North-South and East-West reinforced concrete shear walls. This table shows that the recorded motions produced shear and flexural seismic demands that less than the capacity of the walls. This explains the

absence of hair line shear cracks in these walls. In addition, there was no indication of any overstressing at the location of the construction joints at the third level (where Phase II construction started).

However, Table 6.5 indicates that the shear walls experienced noticeable uplift. Maximum uplift forces of 2225 kips and 1763 kips in the E-W walls and N-S walls, exceeded the estimated 1210 kips uplift resistance forces. This resisting force is based on the yield values of the steel reinforcement at the connection between the walls and the drilled caissons (Drawing #7), in addition to the resisting concrete weight of the tributary area of the structure. The capacity of the caisson itself against uplift is estimated at 1250 to 1500 kips, which includes the concrete weight, the caisson weight, the soil weight, and the soil surface friction. The resulting upward displacements along the E-W and N-S directions, are 0.31" and 0.29", respectively. It is noted that the code uplift forces are less than the uplift resistance forces, indicating that code stress checks will not predict this uplift behavior.

The computer modeling of this nonlinear uplift behavior was greatly simplified in this investigation by using linear spring elements under the base of the walls. Therefore, no separation between the walls and the foundation was permitted (i.e, only linear model was considered). However, the results from a fixed based computer model (i.e. no uplift is allowed), showed a much stiffer model (approximately 40% stiffer). No significant reduction of forces was observed between this stiff model, and the model which allows for soil flexibility. According to the shape of the input recorded response spectrum, there is not reduction of the spectrum acceleration due to period elongation within this time range (i.e. 0.4 to 0.6 seconds).

Figure 6.3 shows the shear stress contours at the roof of the parking structure. The maximum seismic shear and moment demands at this roof are given in Table 6.5. Finite element models using recorded ground motions, indicated that the roof will be overstressed in flexural with a D/C ratio exceeding 2.0. This indicates that the top roof will experience flexural cracking, and provides more flexible response. As mentioned earlier, the computer model with cracked sections, resulted in a more flexible response, with a slight increase in the seismic forces.

One emergency measure, which was enforced by the City of Los Angeles after the Northridge earthquake, is to use shear strength reduction factor of 0.6 instead of 0.9 for the design of chords and collector members of the diaphragms. For this particular parking structure, no damage was observed in chord steel area. However, it is noted that this parking structure was not exposed to the upper limit ground shaking which is expected in down town Los Angeles.

A stress check was performed to assess the seismic behavior of the short columns. It is noted that along grid lines (B), (C), and (D) short columns were created due to the sloped ramps configuration. The result of this investigation, which is shown in Table 6.7 for some critical short columns, indicated that the column's seismic shear demand forces due to the recorded input motions did not exceed their ultimate strength capacity, i.e., the demand/capacity ratio less than 1.0. Table 6.7 also indicates that higher levels of seismic shaking, due to the UBC response spectrum, will result in overstressing of these columns with demand/capacity ratio of approximately 2.5. This may be critical and could result in shear failure of these nonductile

columns. Typical column details (Drawing # 5 and #6), show limited tie reinforcements of #3 @ 12" o.c. New code provisions for gravity columns require minimum ties of #4 @ 6" o.c.

Another stress check was performed to examine the upper coupling beams connecting the N-S shear walls (See Table 6.8). It is shown that these beams were overstressed using both the UBC equivalent static forces, and the response spectrum analysis using the recorded response spectrum curves. The shear D/C is 2.84 and the flexural D/C is 1.94. The proposed ATC-33 (75% draft, Table 6-15) recommends the use of limiting D/C ratios for shear and flexure as 1.0 and 2.0, respectively, for immediate occupancy performance. Higher limiting D/C values of 2.0 and 4.0 are allowed for behavior based on life-safety based performance.

One important assessment for this particular parking structure, is to study the integrity of the connections between the precast concrete columns and the floor slab. It was observed that the details shown in Drawing # 6, is prone to excessive stressing that may lead to local failure at the connection (Porush, et. al, 1995). Table 6.9 provides the results of the stress check of some of the critical connections. D/C ratios up to 2.18 were obtained using the finite element model with recorded ground motion. However, no indication of overstressing was found during the site review. It is also indicated in Table 6.9 that D/C ratios up to 5.25 can be obtained at some of these connections, when using the Code response spectrum. It is highly questionable that these connections will sustain such large demands without experiencing excessive damage. Failure of these connections may lead to the separation of the columns from the slab, which may result in columns' instability (Porush, et. al, 1995).

6.5 RESPONSE OF VERTICAL VIBRATION OF THE ROOF GIRDER

In order to measure the vertical acceleration at the top level of the parking structure, one of the sensors was installed at the middle of the 65-foot long upper girder along grid # 9 (Station #13). This sensor, which is shown in Photo # 11, produced 0.52 g maximum acceleration during the Northridge earthquake. The generated response spectra curves are depicted in Figure 3.3, for 2%, 5%, and 10% damping ratios. As shown, the local fundamental period of the beam is approximately 0.27 seconds. The maximum spectral acceleration is 5.3 g, 3.4 g, and 2.15 g, corresponding to 2%, 5%, and 10% damping ratios, respectively.

A two-dimensional computer model was prepared to model the vertical response of the top girder. The computer model includes 392 nodes and 396 line elements. Girders located on the second level through the top level were considered in the model, and the floor masses were lumped at closely spaced nodal points. 2% damping was considered in the finite element model; full section properties were also considered. The model was subjected to the recorded vertical acceleration at the base columns.

Twenty (20) modes were extracted with the first mode (estimated as 0.29 seconds). A list of the fundamental periods is shown in Table 6.10. Figures 6.4 includes the finite element computer model and first five mode shapes of the model. A comparison between the recorded response spectrum and the computed response spectra curves is shown in Figure 6.5.

The following observations were made:

(1) For large span girders (65 ft long), effective floor vertical acceleration in the middle of the girder can be significant (up to 3.5 times the peak ground vertical acceleration). This large acceleration produces significant vertical loading that should be included in the design. Both the increase and the decrease of the total loads action on the girder should be considered. It is noted that the decrease of the effective vertical loading on prestressed beams can lead to shear overstressing at the end of the beams (Hilmy, et. al, 1994).

(2) The acceleration of the nonstructural elements that may be attached at the middle of the long span girder (e.g. piping, etc) with fundamental periods between 0.20 to 0.40 seconds, can be significant. However, equipment with fundamental periods exceeding 0.7 seconds will have much a smaller acceleration regardless the damping ratio considered.

(3) It appears that 2% damping is a realistic damping level in the vertical direction of the parking structure.

(4) In the parking structure considered, the linear finite element model can accurately model the vertical response of the long span girders. Two-dimensional finite elements (using line elements and lumped masses) were used. Masses were calculated using tributary areas.

(5) The current building codes do not provide simplified formulas to consider the effect of the vertical acceleration on the floor girders or beams. It appears that guidelines to consider such an effect are required. One design approach would be to increase or decrease the gravity loads acting on the beam with 2.5 times the peak ground vertical acceleration (in %g) times the gravity loads.

(6) There was only one sensor to measure floor vertical acceleration in this parking structure. We recommend the installation of additional sensors to measure the vertical response of one of the coupling beams between the north-south shear walls.

6.6 RESPONSE OF THE ROOF PARAPET

In order to measure the out-of-plane acceleration at the roof parapet of the parking structure an accelerometer (channel # 14) had been installed at the top of the roof parapet at the intersection of Grid line (E) and Grid line (9). This accelerometer, which is shown in Photo # 12, recorded very strong shaking (with a peak acceleration of 1.21 g).

The results of the analysis, using channel # 10 (diaphragm) as an input motion, is summarized in Table 6.11. The analysis indicated that the fundamental period of vibration averaged 0.07 seconds, with damping ratios varying from 5.2% to 8.6%.

A three-dimensional computer model was developed to model the interaction between the parapet and the parking structure. Ten line elements were used to model the parapet. Other line elements were used to model the vertical beam and edge beams. Lumped masses were used at the nodes of

the parapet elements. Uncracked sections were used for section properties. During this investigation an Eigen values analysis was used, followed by a transient analysis using Channel # 10 record as an input motion; 5% damping was considered.

Figures # 6.6 show the mode shapes of the parapet. The result of the finite element analysis indicated that the first and second mode shapes provide for over 99% of the mass participation (78.6% and 21.3%, respectively). The first fundamental period is 0.079 seconds, and the second mode is 0.016 seconds, as shown in Table 6.11.

The computed time history of the parapet acceleration is shown in Figure #6.7. This Figure shows also a comparison between the recorded and generated linear time history for the out-of-plane top acceleration. It is shown that an excellent prediction of the behavior can be obtained using the analytical model. The curves show almost the same frequencies and amplitudes.

According to the UBC94, the total design lateral seismic force (F_p) shall be determined from the following formula:

$$F_p = ZI_pC_pW_p \qquad \text{(UBC94 eq. 30-1)}$$

Using: $Z = 0.40$
$I_p = 1.00$
$C_p = 2.00$ for unbraced (cantilevered) parapets.

Therefore $F_p = 0.40 \times 1.00 \times 2.00\ W_p = 0.80\ W_p$

The design lateral forces determined using the above formula shall be used to design members and connections which transfer these forces to the seismic-resisting systems.

Using ultimate strength design for reinforced concrete, code seismic forces should be increased with 1.4 factor:

Therefore: $F_p = 1.4 \times 0.80\ W_p = 1.12\ W_p$

Using 4.75" reinforced concrete parapet (6.00' high):

$$M_{demand} = 1.12\ (0.145 \times 4.75/12\ ) \times 6.0 \times 6.0/2 = 1.157\ \text{k.ft /ft}$$

With vertical reinforcements as one middle layer of # 4 @ 12" o.c.
The ultimate capacity with $\phi = 0.9$:

$$M_{capacity} = 1.496\ \text{k.ft /ft}$$

Therefore: $M_{demand} < M_{capacity}$ O.K.

Since the maximum recorded acceleration of the parapet is 1.21 g and the maximum roof acceleration is 0.84 g, the maximum relative acceleration between the top of the parapet and the base of the parapet = 1.21 - 0.84 = 0.37 g

By scaling this acceleration by the ratio of the code peak ground acceleration (0.4g) and the maximum recorded peak ground acceleration in the direction of the parapet (0.29 g):

The maximum expected relative acceleration

= 0.37 x 0.4/0.29 = 0.51 g << 1.12 g (as required by code)

This shows that in this building the design of the parapet, based on the code formula, is conservative and should produce satisfactory results. Moreover, it is noted that the flexural response of the reinforced concrete parapet is ductile, which allows for energy dissipation at the nonlinear range when M_{demand} exceeds $M_{capacity}$.

Table 6.1
Seismic Base Shear in the Parking Structure

Case	N-S Direction E-W Direction		E-W Direction	
	V (Kips)	% G	V (Kips)	% G
Finite Element Analysis Using Recorded Motions (uncracked Diaphragm)	18,567	43%	9,940	23%
Finite Element Analysis Using Recorded Motions (cracked Diaphragm)	19,187	44%	10.356	24%
Finite Element Analysis UBC Spectra at Zone 4	44,084	99%	33,100	77%
Code Equivalent Static (UBC 94) with Rw = 8	5,052	11.7%	5,705	13.2%

Table 6.2
Seismic Lateral Displacement in the Parking Structures

Case	F.E. analysis with recorded motion		F.E. analysis with cracked diaphragm		F.E. analysis with UBC Spectrum		Code Static Rw=8	
Level	N-S wall	E-W wall	N-S wall	E-W wall	N-S wall	E-W wall	N-S wall	E-W wall
Roof	1.43"	0.74"	1.45"	0.84"	3.40"	2.63"	0.50"	0.39"
6th	1.21"	0.62"	1.23"	0.70"	2.90"	2.23"	0.43"	0.31"
5th	0.97"	0.50"	0.98"	0.56"	2.31"	1.81"	0.34"	0.24"
4th	0.71"	0.37"	0.72"	0.42	1.71"	1.36"	0.25"	0.18"
3rd	0.46"	0.24"	0.46"	0.28"	1.10"	0.90"	0.17"	0.11"
2nd	0.21"	0.12"	0.21"	0.14"	0.52"	0.45"	0.08"	0.04"

Table 6.3
Maximum Diaphragm Displacements (N-S)

Case	F.E. analysis with recorded motion	F.E. analysis with cracked model	F.E. analysis with UBC Spectra	Code Static Rw=8
Roof	1.581"	1.663"	3.78"	0.56"

Table 6.4
Maximum Seismic Shear and Moment Demands on Typical N-S and E-W Walls

Wall	N-S wall				E-W wall			
Case	Seismic Shear		Seismic Moment		Seismic Shear		Seismic Moment	
	V (kips)	D/C	M (k.ft)	D/C	V (kips)	D/C	M (k.ft)	D/C
Finite Element Analysis Using recorded Motion	2244	0.96 *	59,160	0.69	5110	0.73	208,334	0.56
Finite Element Analysis Using UBC Spectra	5328	2.28 *	142,604	1.65	16586	2.36	676,211	1.80
Code Equivalent Static Rw = 8	842	0.84 **	36,585	0.595	2852	0.95	123,940	0.33

* Using $\phi = 1$

** Using $\phi = 0.6$ and factored load.

Table 6.5
Maximum Seismic Uplift Forces and Displacements

Wall	**N-S middle wall**		**E-W wall**	
Case	**Uplift force**	**Uplift disp.**	**Uplift force**	**Uplift disp.**
Finite Element Analysis Using recorded Motion	**1763 kips**	**0.29"**	**2225 kips**	**0.31"**
Finite Element Analysis Using UBC Spectra	**4230 kips**	**0.68"**	**7444 kips**	**1.05"**
Code Equivalent Static Rw = 8	**627 kips**	**0.10"**	**1143 kips**	**0.16"**

Note: Uplift forces in this table do not include reduction due to gravity loads

Table 6.6
Maximum Seismic Force in Ramps at Roof (N-S direction)

Forces	Shear (Kips)		Moment (Kips)	
Case	V (Kips)	D/C	M (K.FT)	D/C
Finite Element Analysis Using recorded Motion	**278**	**0.527**	**13,700**	**2.04**
Finite Element Analysis Using UBC Spectra	**690**	**1.30**	**34,004**	**5.07**
Code Equivalent Static Rw = 8	**139**	**0.60**	**6,270**	**0.94**

Table 6.7
Maximum Shear Forces At Selected Short Column At Ramps

Forces	Col #1	Col #2	Col #3	Col #4	Col #5	Col #6	D/Cmax
Finite Element Analysis Using recorded Motion	43	99	103	75	87	88	0.96 *
Finite Element Analysis Using UBC Spectra	118	242	248	148	262	253	2.46 *
Code Equivalent Static Rw = 8	10.4	28.1	35	25	26	25	0.55**

Col. # 1: at Grid (7) and (C) between 1st North Ramp and 2nd South Ramp.
Col. # 2: at Grid (7) and (C) between 2nd North Ramp and 3rd South Ramp.
Col. # 3: at Grid (8) and (C) between 1st North Ramp and 2nd South Ramp.
Col. # 4: at Grid (8) and (C) between 5th North Ramp and 5th South Ramp.
Col. # 5: at Grid (6) and (B) between 5th Ramp and 5th Level.
Col. # 6: at Grid (6) and (B) between 4th Ramp and 4th Level.
*ϕ = 1.0
*ϕ = 0.85 and use of factored loads

Table 6.8
Maximum Forces At Upper Coupling Beam (N-S Direction)

Forces	Shear (Kips)		Moment (k.ft)	
Case	V	D/C	M	D/C
Finite Element Analysis Using recorded Motion	347	2.84	5,615	1.94
Finite Element Analysis Using UBC Spectra	834	6.83	13,468	4.67
Code Equivalent Static Rw = 8	123	1.66	1,979	1.07

Table 6.9
Maximum Pull Forces At Selected Column-Slab Connections

Forces	Conn. # 1		Conn. # 2		Conn. # 3		Conn. # 4	
Case	P (kips)	D/C	P (kips)	D/C	P (kips)	D/C	P (kips)	D/C
Finite Element Analysis Using recorded Motion	116	2.18	91	1.72	76	1.43	73	1.37
Finite Element Analysis Using UBC Spectra	278	5.25	219	4.13	227	4.28	217	4.09
Code Equivalent Static Rw = 8	35	1.03	31	0.91	40	1.18	38	1.12

Connection # 1: For Column at Grid (7) and (C) @ 2nd Level South Ramp.
Connection # 2: For Column at Grid (8) and (C) @ 2nd Level South Ramp.
Connection # 3: For Column at Grid (6) and (B) @ 5th Level.
Connection # 4: For Column at Grid (6) and (B) @ 4th Level .

E I G E N V A L U E S A N D F R E Q U E N C I E S

MODE NUMBER	EIGENVALUE (RAD/SEC)**2	CIRCULAR FREQ (RAD/SEC)	FREQUENCY (CYCLES/SEC)	PERIOD (SEC)
1	0.454723E+03	0.213242E+02	3.393859	0.294650
2	0.534704E+03	0.231237E+02	3.680245	0.271721
3	0.557257E+03	0.236063E+02	3.757058	0.266166
4	0.583246E+03	0.241505E+02	3.843669	0.260168
5	0.608926E+03	0.246764E+02	3.927374	0.254623
6	0.619426E+03	0.248883E+02	3.961093	0.252456
7	0.284368E+04	0.533262E+02	8.487123	0.117826
8	0.336823E+04	0.580364E+02	9.236785	0.108263
9	0.398290E+04	0.631102E+02	10.044301	0.099559
10	0.444267E+04	0.666534E+02	10.608212	0.094267
11	0.469810E+04	0.685427E+02	10.908911	0.091668
12	0.481531E+04	0.693924E+02	11.044150	0.090546
13	0.130090E+05	0.114057E+03	18.152748	0.055088
14	0.191820E+05	0.138499E+03	22.042828	0.045366
15	0.202293E+05	0.142230E+03	22.636558	0.044176
16	0.247616E+05	0.157358E+03	25.044355	0.039929
17	0.337719E+05	0.183771E+03	29.248117	0.034190
18	0.683223E+05	0.261385E+03	41.600776	0.024038
19	0.139317E+06	0.373252E+03	59.404855	0.016834
20	0.342684E+06	0.585392E+03	93.168026	0.010733

P A R T I C I P A T I N G M A S S - (percent)

MODE	X-DIR	Y-DIR	Z-DIR	X-SUM	Y-SUM	Z-SUM
1	0.000	0.000	13.469	0.000	0.000	13.469
2	0.000	0.000	3.843	0.000	0.000	17.312
3	0.000	0.000	0.054	0.000	0.000	17.366
4	0.000	0.000	29.183	0.000	0.000	46.550
5	0.000	0.000	15.257	0.000	0.000	61.807
6	0.000	0.000	15.266	0.000	0.000	77.073
7	0.000	0.000	0.017	0.000	0.000	77.090
8	0.000	0.000	0.001	0.000	0.000	77.091
9	0.000	0.000	0.003	0.000	0.000	77.094
10	0.000	0.000	0.000	0.000	0.000	77.094
11	0.000	0.000	0.001	0.000	0.000	77.095
12	0.000	0.000	0.000	0.000	0.000	77.095
13	0.000	0.000	13.262	0.000	0.000	90.357
14	0.000	0.000	1.123	0.000	0.000	91.480
15	0.000	0.000	0.759	0.000	0.000	92.239
16	0.000	0.000	0.005	0.000	0.000	92.244
17	0.000	0.000	0.167	0.000	0.000	92.411
18	0.000	0.000	2.343	0.000	0.000	94.754
19	0.000	0.000	1.498	0.000	0.000	96.252
20	0.000	0.000	2.594	0.000	0.000	98.846

Table 6.10: Eigen Values, Frequencies, and Participating Mass (F.E. Model of Roof Beam)

EIGENVALUES AND FREQUENCIES

MODE NUMBER	EIGENVALUE (RAD/SEC)**2	CIRCULAR FREQ (RAD/SEC)	FREQUENCY (CYCLES/SEC)	PERIOD (SEC)
1	0.630629E+04	0.794122E+02	12.638839	0.079121
2	0.142608E+06	0.377635E+03	60.102461	0.016638
3	0.605830E+07	0.246136E+04	391.737976	0.002553
4	0.450032E+08	0.670845E+04	1067.682372	0.000937
5	0.173746E+09	0.131813E+05	2097.863016	0.000477
6	0.478713E+09	0.218795E+05	3482.230803	0.000287
7	0.107615E+10	0.328047E+05	5221.026061	0.000192
8	0.210603E+10	0.458915E+05	7303.865555	0.000137
9	0.372498E+10	0.610326E+05	9713.637041	0.000103
10	0.660408E+10	0.812655E+05	12933.806607	0.000077

PARTICIPATING MASS - (percent)

MODE	X-DIR	Y-DIR	Z-DIR	X-SUM	Y-SUM	Z-SUM
1	78.663	0.000	0.000	78.663	0.000	0.000
2	21.327	0.000	0.000	99.990	0.000	0.000
3	0.010	0.000	0.000	100.000	0.000	0.000
4	0.000	0.000	0.000	100.000	0.000	0.000
5	0.000	0.000	0.000	100.000	0.000	0.000
6	0.000	0.000	0.000	100.000	0.000	0.000
7	0.000	0.000	0.000	100.000	0.000	0.000
8	0.000	0.000	0.000	100.000	0.000	0.000
9	0.000	0.000	0.000	100.000	0.000	0.000
10	0.000	0.000	0.000	100.000	0.000	0.000

Table 6.11: Eigen Values, Frequencies, and Participating Mass (F.E. Model of Roof Parapet)

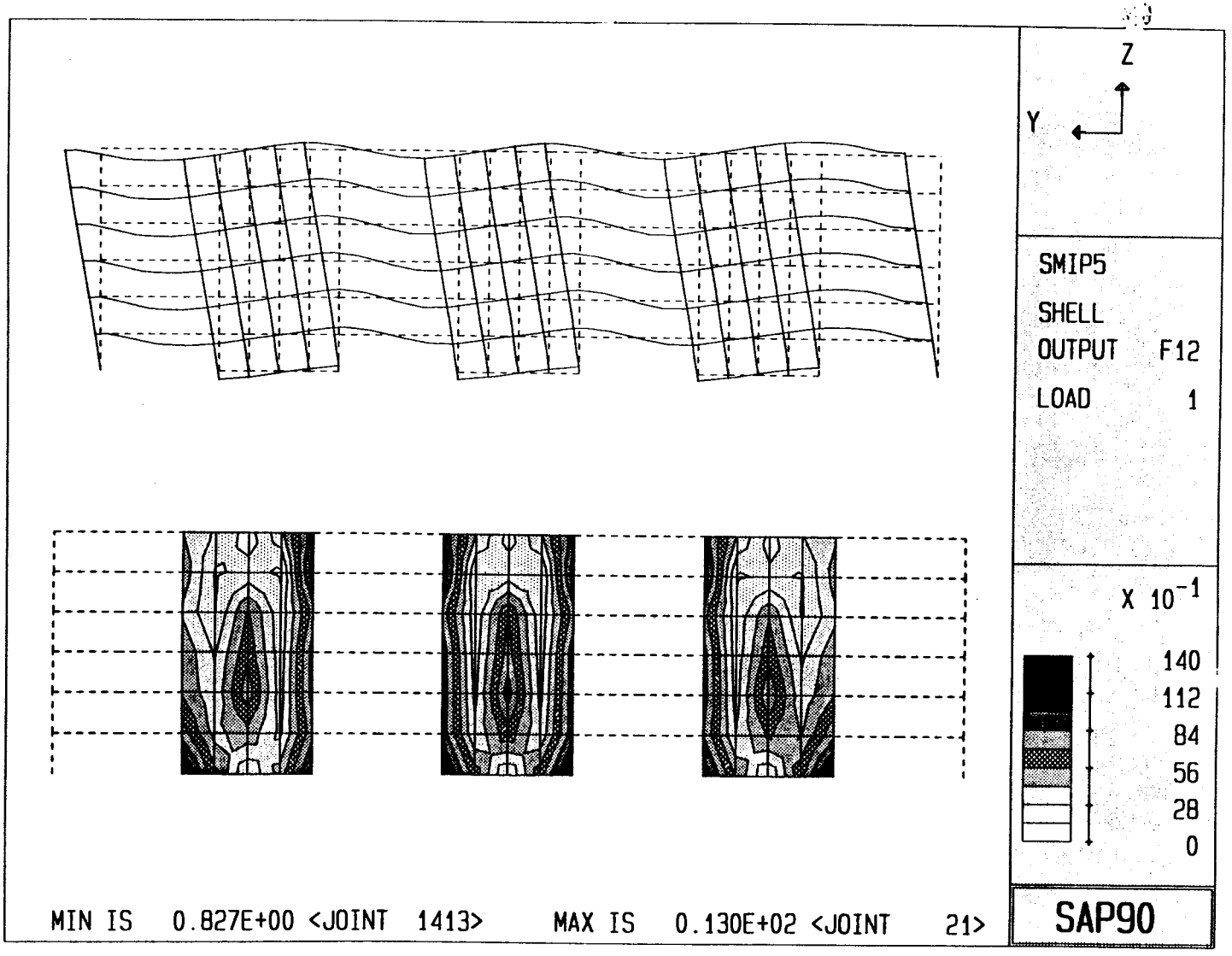

Figure 6.1: Deflected Shape and Shear Stress Contour of the North-South Walls
(Finite Elemet Model with Unraced Sections. Signs of deformation is based on first fundamental mode shape in this direction)

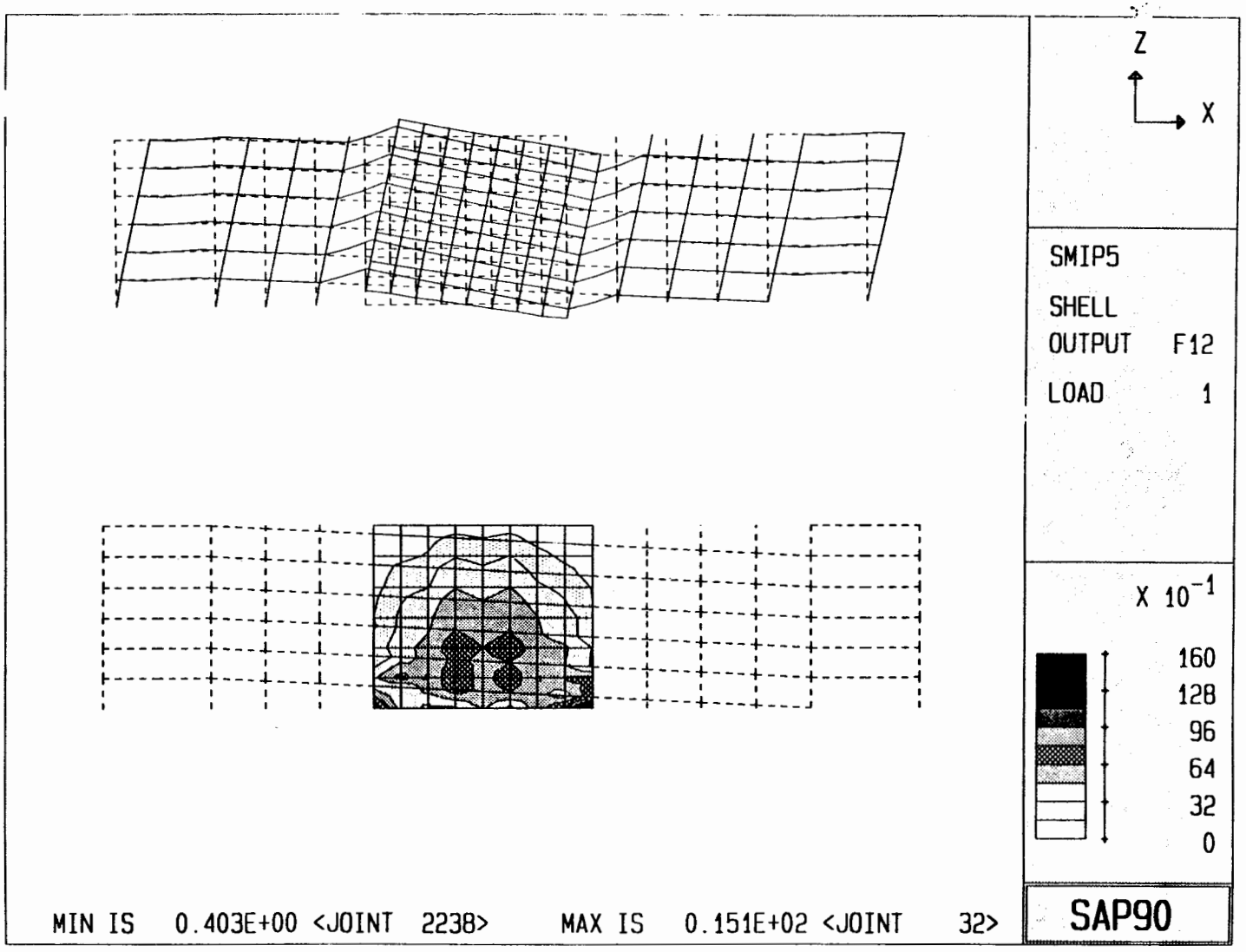

Figure 6.2: Deflected Shape and Shear Stress Contour of the East-West Walls
(Finite Elemet Model with Unraced Sections. Signs of deformation is based on first fundamental mode shape in this direction)

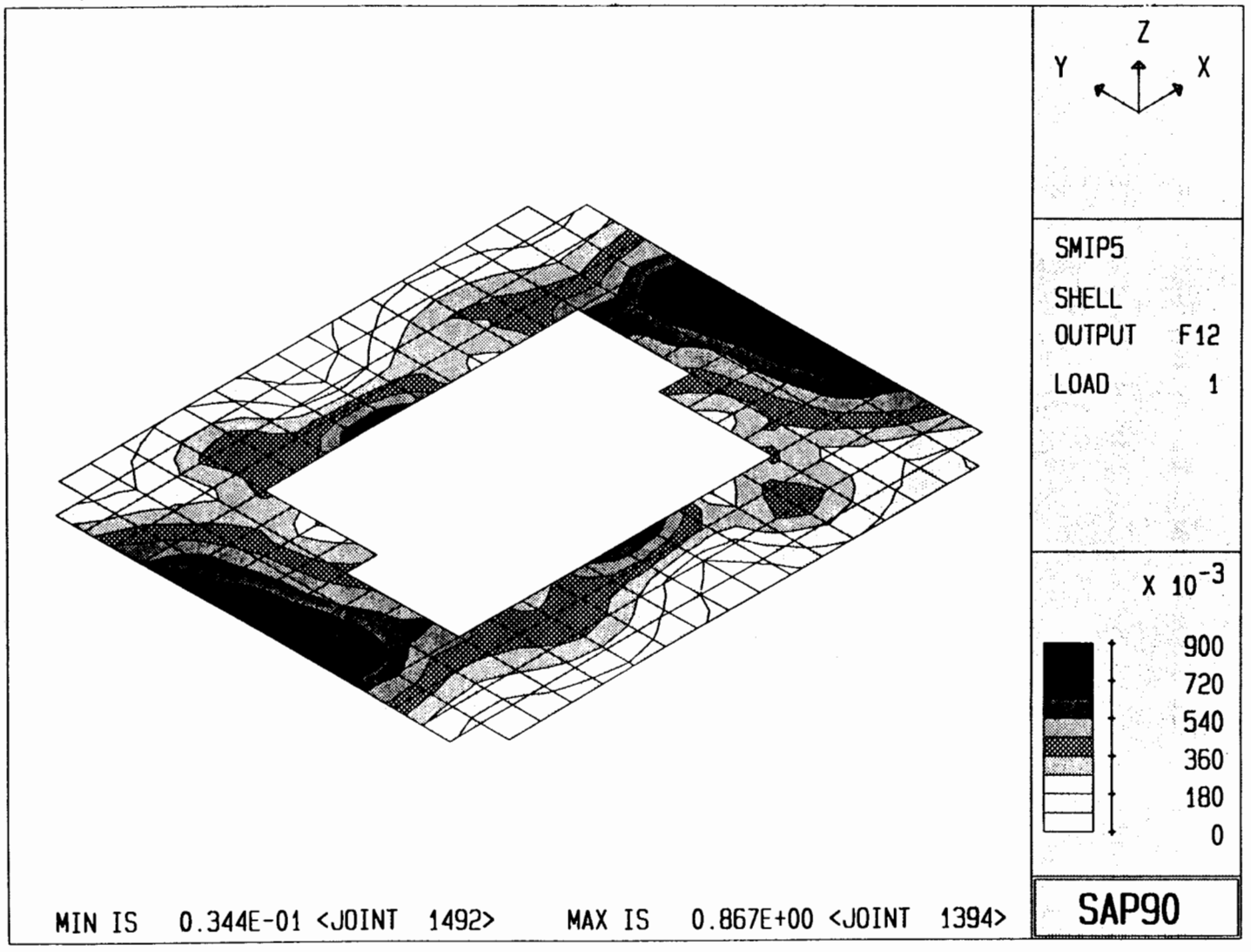

Figure 6.3: Shear Stress Contours at the Top Roof

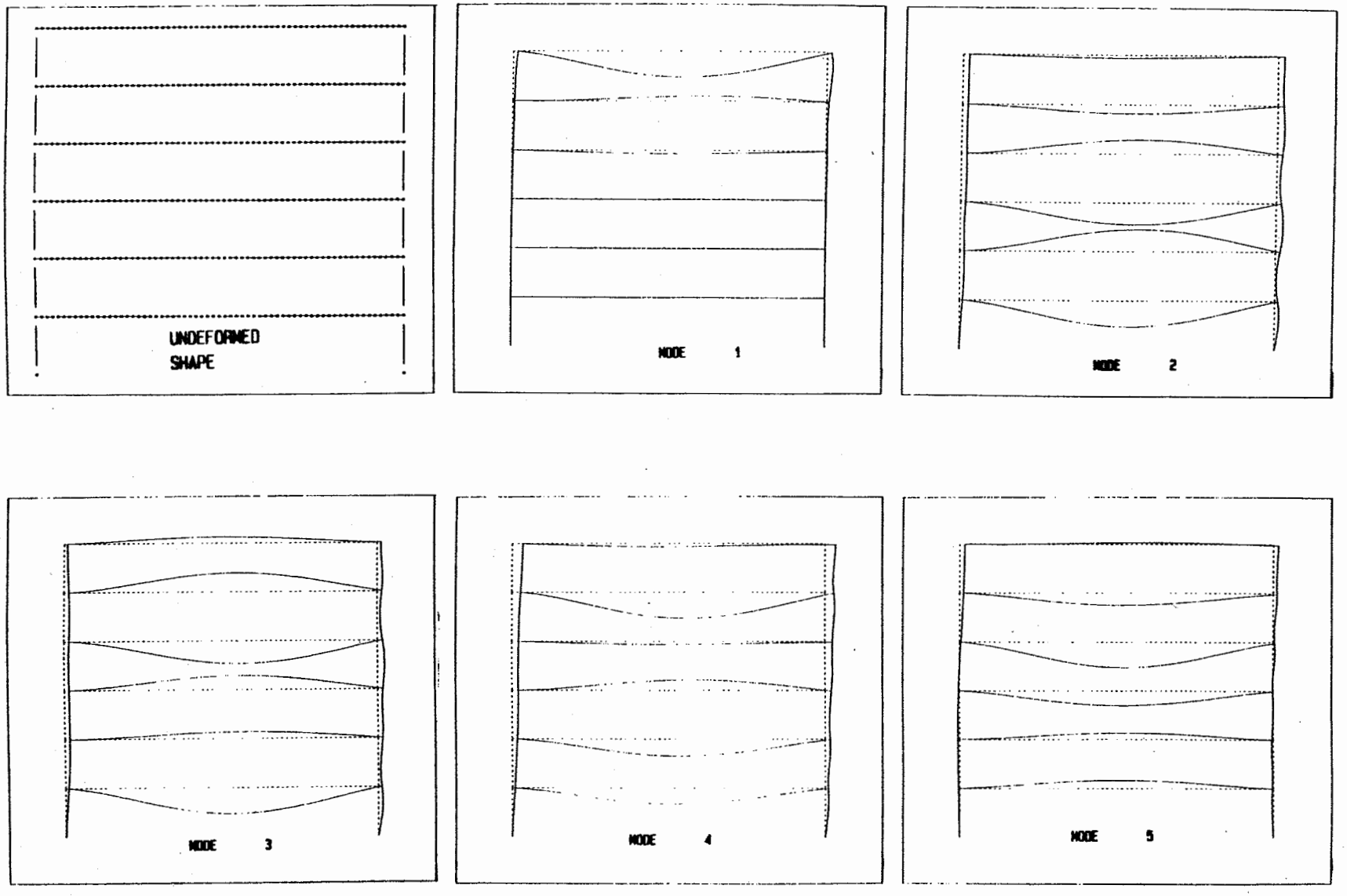

Figure 6.4: **Finite Element Computer Model and Mode Shapes (Study of the Vertical Vibration of the Roof Beam).**

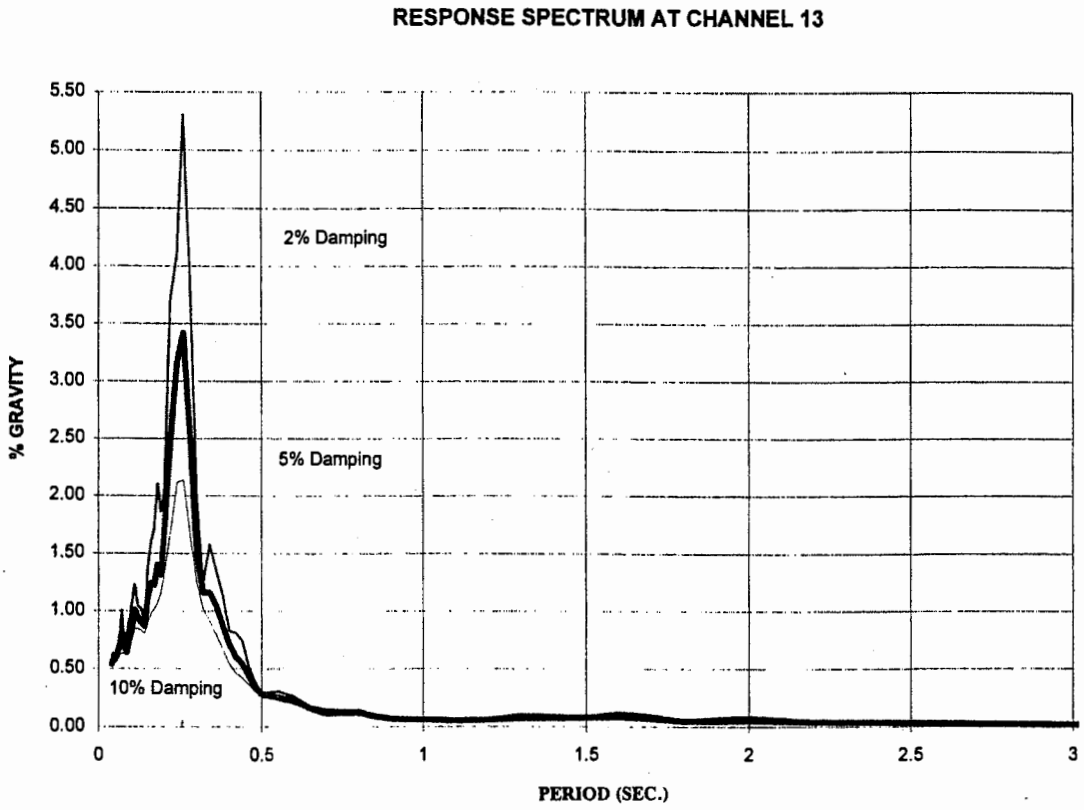

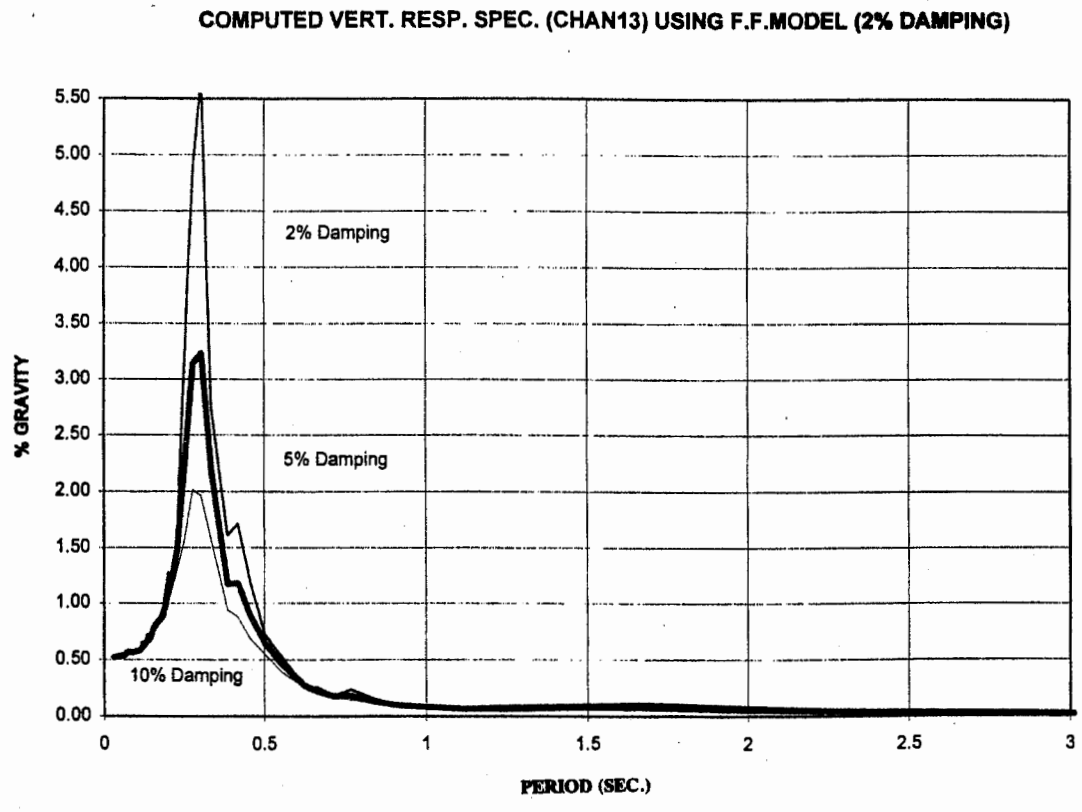

Figure 6.5 Comparison Between the Recorded and the Computed Response Spectra Curves at Channel # 13.

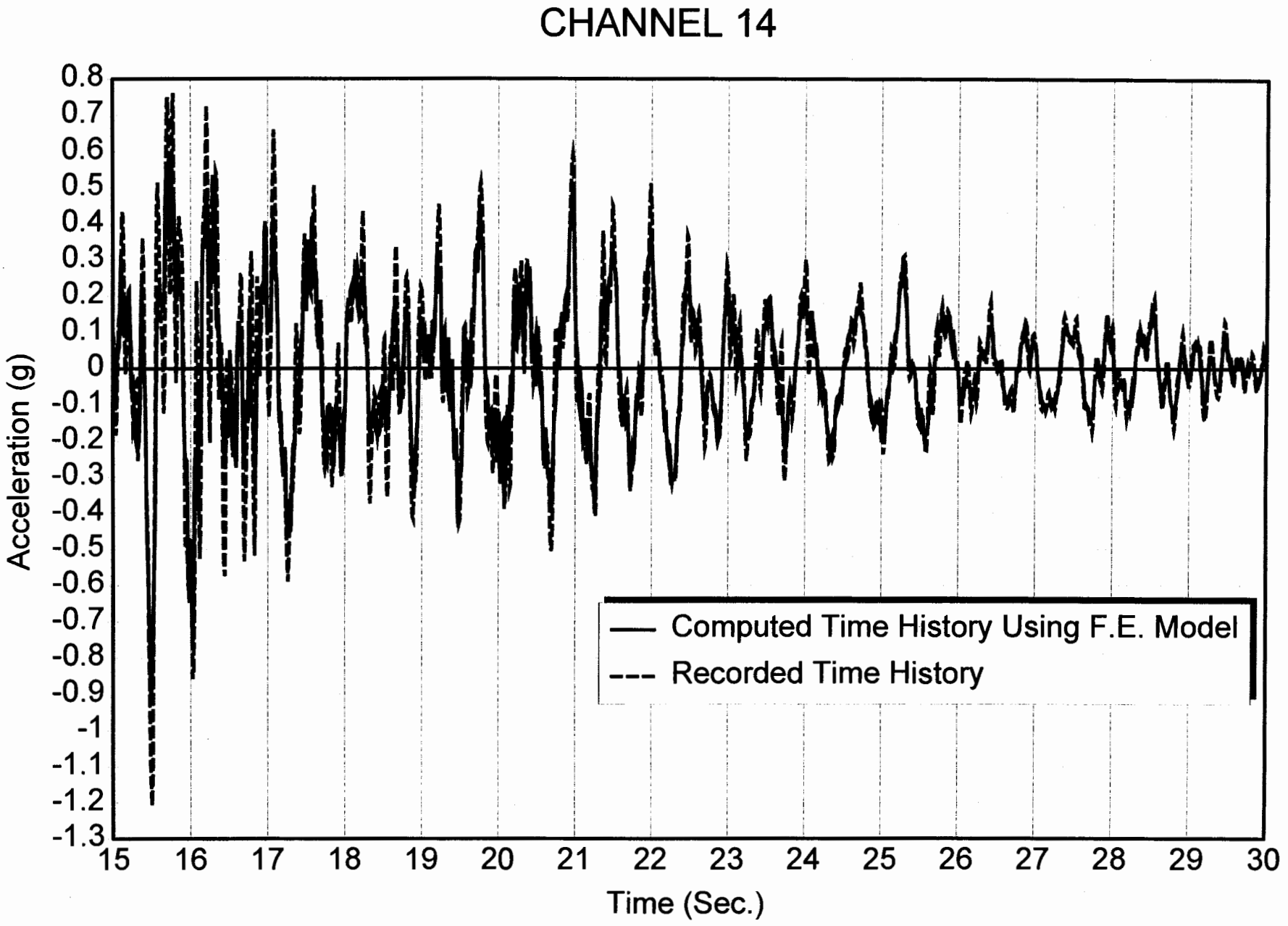

Figure 6.7 Computed vs. Recorded Acceleration Time History for the Parapet.

7.0 COMPARISON OF THE STRUCTURAL BEHAVIOR WITH THE RESPONSE OF SIMILAR PARKING STRUCTURES.

The parking structure examined in this report was the first parking structure to be instrumented under the CDMG strong motion instrumentation program. The structure did not suffer from major damage during the January 17, 1994 Northridge earthquake. However, during this earthquake, nine other parking structures at heavily used shopping centers, hospitals, and colleges either partially or completely collapsed. Four of those structures were built between 1986 and 1992, and the others were built between 1965 and 1982. Damaged or severely cracked columns, beams, and shear walls prompted building inspectors to close at least 26 other parking structures in the San Fernando Valley, Glendale, Santa Monica and west Los Angeles.

Many of the structural features of the parking structure examined in this report, can be found in other parking structures which were damaged during the Northridge earthquake. Moreover, the analytical investigation performed on this parking structure indicated that the structure would have suffered serious damage, had the Northridge ground shaking lasted longer or reached the acceleration level expected during an upper limit seismic event, which may occure at this site (i.e and event with 10% probability of occurrence in 50 years).

It is noted that this parking structure was constructed in two phases. The first phase utilized precast concrete columns attached to the cast-in-place concrete through coil inserts as shown in Drawing #6. The current investigation showed that these connections are prone to damage in case of severe ground shaking.

In this section, several of the important structural deficiencies found in this parking structure are examined and compared with similar features in other parking structures which experienced damage during the Northridge earthquake.

7.1 LACK OF COMPATIBILITY BETWEEN THE GRAVITY SYSTEM AND THE LATERAL RESISTING SYSTEM

Under the current provisions of the design codes, it is possible to separate the structural systems into two separate systems. The first system is the gravity system which supports the dead and live loads of the structure. The second system is the lateral laod resisting system which provides the required lateral resistance against seismic and wind loads. During a seismic event, the gravity system should be able to sustain a minimum level of lateral deformation that is imposed on the structure. This requirement is addressed in almost all seismic design codes. For instance, the Uniform Building Code (UBC 1994) emphasis the need for deformation compatibility between the two structural systems. UBC Sec. 1613.2.4 states that "all framing elements not required by design to be part of the lateral force-resisting system shall be investigated and shown to be adequate for vertical load-carrying capacity when displaced $3(R_w/8)$ times the displacements resulting from the required lateral forces. P-Δ effects on such elements shall be accounted for..."

In many cases, particularly in old parking structures, these requirements were overlooked or misunderstood. Nevertheless, at least one new parking structure that was designed based on the compatibility approach of the current code, was damaged. As a result, the code approach, particularly the value of $3(R_w/8)$, has been criticized and questioned. The emergency measures implemented by the City of Los Angeles, after the Northridge earthquake call for the use of cracked sections in calculating the lateral displacements. Other recent design trends is to use $\frac{1}{2}R_w$ instead $3(R_w/8)$. As shown in Chapter 6, the analytical study performed for this parking structure indicated that higher displacement levels more than the ones obtained the $3(R_w/8)\Delta$ may be expected during strong ground shaking.

Several parking structures were damaged during the Northridge earthquake, as a result of the lack of compatibility between the gravity system and the lateral resisting system. Examples include the southwest parking structure located at the Northridge Fashion Center, and the Kaiser permanenta Garage at West Los Angeles. The parking structure at The Cal State University at Northridge (CSUN), which was studied by the first author (Ref.), experienced similar behavior. The main lateral resisting system of this structure consists of three levels of exterior precast ductile moment frames. The gravity load consists of cast-in-place slab supported by precast beams and columns; the interior columns did not have ductile details, and could not sustain the large seismic deformations caused by the earthquake. Damage included failure to the column-slab connections, and smashing at the base of the columns. Photo #7.1 shows the sequence of failure that was triggered by the damage of the interior columns.

7.2 DAMAGE TO COLUMNS WITH NON-DUCTILE DETAILS, AND DAMAGE TO SHORT COLUMNS

One major deficiency found in parking structures damaged during the Northridge earthquake is the lack of adequate ductile details of the structural elements. In particular, the concrete columns in old parking structures did not have enough confinement; stirrups with small diameters and large spacing are often used. In addition, the existence of rebar with a small splice length are often found in gravity columns designed during the 1960's and 1970's.

Interior column details of the parking structure under study varies from #3 @ 12" o.c. to #4 @ 12" o.c. The current ACI-318 has new provisions for the minimum confinement of gravity columns. It has been also proposed by the City of Los Angeles to use a minimum of #4 @ 6" o.c. along the entire height of the gravity columns.

Examples of poor performance of non-ductile frames columns during the Northridge earthquake include the Northridge Fashion Center East Garage, where the interior circular columns experienced permanent rotation beyond repair (Photo #7.2).

As in many existing parking structure, the parking structure under study includes interior short columns along the sides of the ramps. The architectural configuration of the sloped ramps result in a small effective length of the columns. The shear demands for a short column increase significantly and may cause loss of columns' instability to resist vertical loads. The analytical investigation

(Section 6) shows that some of these short columns reached nonlinear stress range. However, no noticeable damage was observed.

The Glendale Fashion Square parking structure provides an example of the seismic risk caused by short columns. This structure was designed in the 1960's with short columns at all three levels. Some of the columns have #3 stirrups spaced approximately 8" o.c. and therefore, the columns were not able to resist the magnified shear forces developed at the columns. This resulted in the massive failure of the short columns at the lower level of the structure (Photo #7.3).

7.3 FAILURE OF PRECAST CONNECTIONS

Inadequate detailing of the connections of the precast structural elements was one of the main causes of damage observed in the precast concrete parking structures during the Northridge earthquake. One major deficiency was observed in the CSUN parking structure (Porush et. al , 1995), where the coil inserts connecting the precast columns to the cast-in-place concrete slab were damaged and resulted in a separation of the columns from the slabs leading to the column instability. Similar details of these inserts exist in the parking structure under study. Current code provisions require increasing the seismic demands on these precast connections. However, a thorough analysis is needed to obtain an accurate estimate of the seismic demands on these connections. This analysis was typically overlooked in old designs. For instance, the current investigation shows that the details given in Drawing # 6 are overstressed in some locations with D/C ratios more than 5.0. These capacity of these connections are highly questionable to sustain such demands.

The code provisions for "Ties and continuity", stated in UBC 94, Section 1631.2.5 , require that "All parts of a structure shall be interconnected and the connections shall be capable of transmitting the seismic force induced by the parts being connected. As a minimum, any smaller portion of the building shall be tied to the remainder of the building with elements having at least a strength to resist Z/3 times the weight of the smaller portion. A positive connection for resisting a horizontal force acting parallel to the member shall be provided for each beam, girder or truss. This force shall not be less than Z/5 times the dead plus live load."

For fasteners of exterior elements, UBC 94, Section 1613.2.4.2 item 5, requires that all fasteners in the connecting system such as bolts, inserts, welds and dowels to be designed for four times the forces determined by the formula $F_p = ZI_pC_p W_p$.

Based on the current investigation, it is recommended that the current requirements of precast connections, particularly the ones playing significant role in connecting the main parts of the structure (such as the coil inserts between precast columns and slabs), should be carefully revised. The objective is obtain an accurate definition of the seismic demands on these important joints, and develop a rational assessment of their ductilities. It is noted that in the case of CSUN parking structure, the damage to the column-floor connections was observed within three different modes of failure. The first mode is the failure of the welds between the coil hoops and the rebars. The second mode is the rupture of the steel rods. The third mode is the spalling of concrete around the inserts embedded in the columns. During a strong ground shaking, a similar behavior could occur in the parking structure examined in this report.

7.4 DAMAGE CAUSED BY VERTICAL ACCELERATION

The Northridge earthquake resulted in some of the highest values of vertical acceleration ever recorded in Southern California. Some records show values of peak ground accelerations that exceeded the value of gravity near the epicenter of the earthquake. Parking structures, with long-span beams (spanning over 60 feet), are particularly sensitive to vertical acceleration, due to magnified bow string vertical forces. Post-tensioned beams may be vulnerable to both upward and downward movements due to high shear stresses that may be developed at the beams' ends. Columns may also experience high axial demands.

The study of the vertical vibrations of the upper roof beam of the subject parking structure is given in Section 6.4. It was shown that the effective floor vertical acceleration in the middle of the girder, which is 65 ft long, can be significant (up to 3.5 times the peak ground vertical acceleration). It appears that 2% damping ratio is a resonable estimate for damping in the vertical direction of the parking structure.

The current building codes do not provide comprehensive formulas to consider the effect of the vertical acceleration on the floor girders or beams. Section 1628.10 of UBC 94 regarding "Vertical Component" states that for zone 3 and 4 "horizontal cantilever components shall be designed for a net upward force of 0.5 Z W_p. In addition to all other applicable load combinations, horizontal prestressed components shall be designed using not more than 50 percent of the dead load for the gravity load alone or in combination with the lateral force effects."

It appears that more rational guidelines to consider the effect of vertical acceleration are required. One design approach discussed recently within the engineering community is to increase or decrease the loading acting on long-span prestressed concrete beams by (2.5) times the ratio of the peak ground vertical acceleration (in %g) times the acting gravity loads on the beam.

Photo 7.4 shows the damage at one end of the post-tensioned precast double tees beams in the east parking structure in the Northridge Fashion Square (Engelkirk, et. al, 1994). This damage was contributed to the lack of ductility and the increased shear demands caused by vertical accelerations.

7.5 MODES OF FAILURE OF SHEAR WALLS

Several modes of failure of shear walls have been identified in the parking structures which were damaged during the Northridge earthquake (Hilmy, et. al, 1994). These failure modes include shear cracking of the shear walls, failure to wall-slab interface, failure to boundary elements, and foundation uplift.

The parking structure under consideration experienced rocking of the shear walls in both the East-West and the North-South shear walls. As a result, a period elongation of the structure was recorded within the time window of 15 seconds to 30 seconds of the main shock of the earthquake. Computer models described in Section 6.3 of this report indicated that D/C up to 1.8 was developed during the

Northridge earthquake, without showing noticeable damage. The resulting upward displacements along the East-West and North-South directions are 0.31" and 0.29", respectively.

It is noted that the resulting uplift forces based on the reduced equivalent static UBC code approach are much less than the predicted seismic forces during a strong ground shaking. In many cases, an uplift displacement may not be even obtained when the UBC code formula is used. The final summation of the Dead and Live loads (acting downward) and the reduced seismic forces (acting upward) may not result in a net upward movement of the foundation.

One significant damage to parking structures due to shear wall's uplift is shown in Photo #7.5. The parking structure is located in the Sherman Oaks Fashion center mall. The significant rocking of the walls led to damage to the connecting concrete beams. This damage was beyond repair and the structure was demolished following the Northridge earthquake.

7.6 FAILURE TO DIAPHRAGMS, COLLECTORS AND CHORD MEMBERS

Many of the parking structures include sloped ramps with large span-depth ratio. These ramps, when acting as diaphragm may experience large in-plane deformation. In this case, rigid diaphragm assumption may not lead to accurate results. In the parking structure under consideration, moderate in-plane deformations at the top roof were developed. Stress-check of the results indicated that the diaphragms, particularly at upper levels, reached the nonlinear range. Accordingly, cracked section with reduced elastic modules (i.e. 60% of E), resulted in more accurate dynamic characteristics.

Furthermore, structural connectors are required to transfer seismic loads from the parking decks to the shear walls. More reinforcements are typically needed to provide chord reinforcements of diaphragms. In many cases, force transfer in diaphragms may be critical, particularly in precast concrete parking structures. Some of these structures consist of precast concrete double tees beams, covered with only 2" lightweight concrete topping.

One example of a collector failure is shown at the Glendale Civic Center parking structure (Photo #7.6). For this structure, cast-in-place shear walls provided the primary lateral resisting system. Precast concrete beams were separated from adjacent shear walls and could not transfer the required drag forces. Instead the seismic forces transferred through the chord reinforcements embedded in the slab topping, which first yielded in tension, and then buckled in compression thought the topping at the subsequent compressive cycles. This behavior defies the common assumption of rigid diaphragms typically used in design.

The current provisions enforced by the City of Los Angeles after the Northridge earthquake, requires that "for concrete diaphragm chords and collector members, the reinforcement shall be spaced not closer than the $3d_b$ or 1 ½ inches and the concrete cover shall be no less than 2 ½ d_b or 2 inches. The shear strength-reduction factor shall be 0.6 instead of 0.9 for the design of chords and collector members for the diaphragms"

Photo #7.1 Sequence of Failure of the CSUN Parking Structure.

Photo #7.2 Damage to Nonductile Circular Columns at the Northridge Fashion Center East Garage.

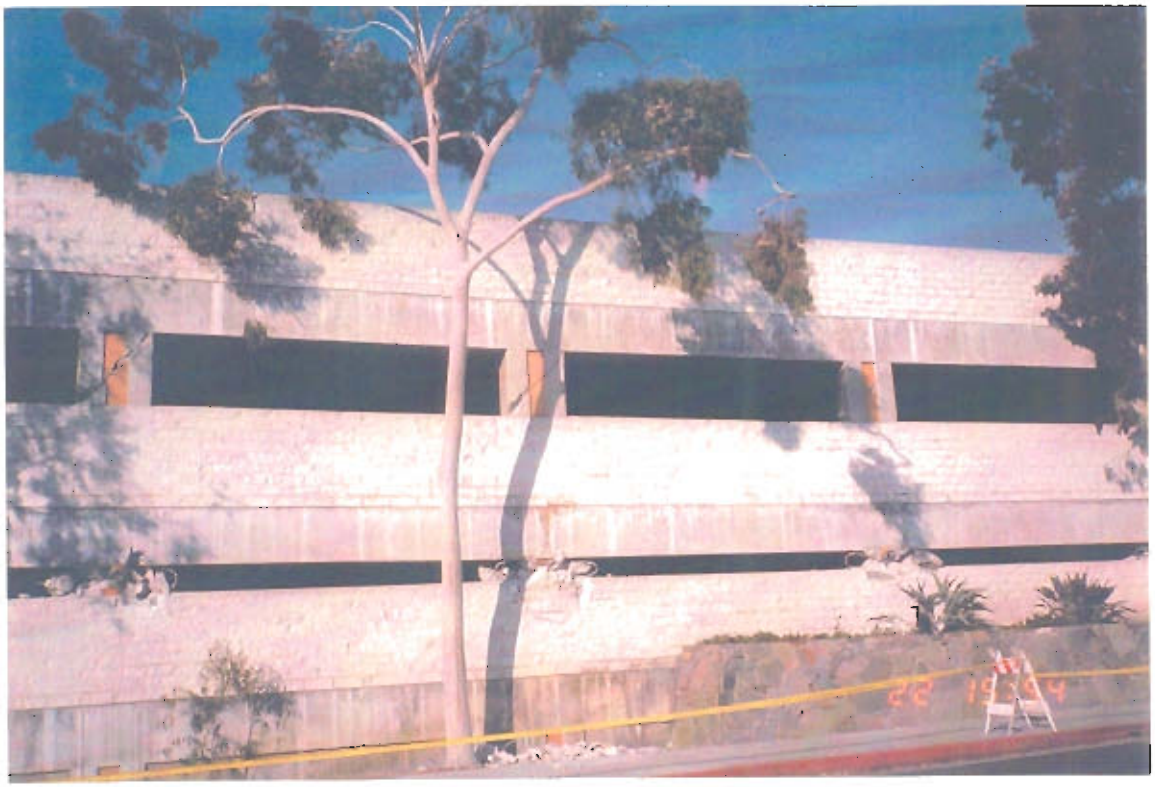

Photo #7.3 Failure of Short Columns at the Glendale Fashion Square Parking Structure.

Photo #7.4 Shear cracks at the ends of the post-tensioned double tees beam at the east parking structure in the Northridge Fashion Square.

Photo #7.5 Damage due to Rocking of Shear Walls (Sherman Oaks Fashion Center Mall).

Photo #7.6 Damage to Chord Steel Reinforcements (Glendale Civic Center Parking Structure)

8.0 CONCLUDING REMARKS

8.1 ASSESSMENT OF THE RESULTS

The parking structure studied in this report is the first parking structure from which significant strong-motion data has been obtained during January 17, 1994 Northridge earthquake. It is approximately 31 km from the epicenter of the earthquake. It was instrumented with a series of 14 strong motion accelerometers whose locations along the first floor, fourth floor, and roof . This instrumentation system has been designed to measure horizontal translations in two orthogonal directions and torsional rotations of each of these instrumented floors, first floor vertical translations and rocking rotations about the north-south axis, in-plane roof diaphragm deformations in the north-south direction, and bending deformations of the parapet on the north side of the roof. In addition, a single vertical accelerometer is located on the roof.

The peak horizontal accelerations recorded during the Northridge Earthquake in the north-south and east-west directions consisted of base accelerations of 0.29 g and 0.15 g respectively, which are smaller that the expected upper level event at the site (i.e. 10% probability of occurrence in the next 50 years). Preliminary inspection of all of the structure's recorded motions indicated noticeable rocking of the structure about its north-south axis, prominent in-plane deformations of the roof diaphragm, and relatively small torsional rotations. Nonlinearity of the structure does not appear to be significant as the cycles of floor accelerations do not appear to widen substantially with increasing time. Therefore, the recorded motions can be predictive of the parking structure behavior as it experiences significant material Nonlinearity.

A well-established system identification procedure, MODE-ID, was used to estimate a model of the parking structure such that the computed motions of the model represented a best fit in a least-squares sense to the structure's recorded earthquake motions. This model consisted of: (a) a theoretical pseudostatic matrix (whose elements were calculated directly based on the assumption that the base of the structure is ridge and were, therefore, not estimated by MODE-ID); and (b) the natural periods, mode shapes, and damping ratios of the structure's significant modes of vibration that were excited during the Northridge earthquake (which were estimated by the MODE-ID procedure). As indicated below, these modal parameters were subsequently used to calibrate a detailed finite element model of the parking structure and its elements and connections. Time-invariant and time-varying modal parameters were estimated, in order to indicate the degre of nonlinearity of the structure's response to the earthquake motions.

The system identification resulted in models whose computed motions compared very closely to the parking structure's recorded earthquake motions. The model parameters that were estimated showed that: (a) the structure's response was dominated by its first north-south and first east-west translational modes of vibration in its two principal directions, together with its pseudostatic response component; (b) rocking of the structure about its base was an important contributor to its east-west translational response (and possibly to its north-south response as well, although rocking in the north-south direction was not explicitly measured by the current array of strong motion instruments at the structure); (c) higher modes of vibration that did not contribute strongly to the

total structural response but were nevertheless identified by MODE-ID included a torsional mode (that was closely spaced with the structure's first east-west mode) and a second north-south translational mode of vibration; and (d) the variations in the structure's estimated modal properties over the duration of the shaking suggests that nonlinear behavior was not a strong contributor to this parking structure's seismic response during the Northridge earthquake.

The finite element computer model described in this report was able to reasonably predict the main dynamic characteristics of the structure. It is clear that the cracked diaphragm model provides better correlation with the results obtained from Mode-ID method, particularly for the modes sensitive to in-plane diaphragm motion (i.e. Mode 1 and Mode 4 which correspond to the modes in the North-South direction). It was shown that the first fundamental modes in the North-South and East-West directions are almost linear. The Second order modes are typical double curvature modes. This result compares very well with the results obtained from the Mode-ID method. In addition, a good fit between the computed an recorded spectra curves were obtained.

Tables 6.1 through Tables 6. 11 provide a comparison between the results obtained from different computer model and the code provisions. The following main observations were made:

- It is shown that the base shear obtained from the code response spectrum curve, and the recorded ground motion are 8.46 and 5.88 times the code base shear, respectively. These factors correspond to the ductility which is required to be supplied by the structural elements of the Garage.

- The inter-story drift based on the finite element results is approximately 0.2%, and did not result in noticeable damage to the nonstructural elements such as the exterior veneer or the stair towers.

- Although the ground motion did not result in noticeable damage, the maximum deflection obtained from Run #1 is approximately 2.85 times the code deflection. This indicates that possibly, at a higher level of ground shaking, the ratio may exceed the value recommended by the current provisions of the code which is based on the $3(R_w/8)$ factor. Therefore, an increase of this factor to reflect the nonlinear response of the structure at higher levels of ground shaking is recommended.

- The finite element model indicates that diaphragm deflection is approximately 10% higher than the deflection at the end shear walls. Finite element mode with cracked diaphragms, indicate that this ratio increases to 16%.

- The computer results indicate that the shear walls experienced noticeable uplift. Maximum uplift forces of 2225 kips and 1763 kips in the E-W walls and N-S walls, exceeded the estimated 1210 kips uplift resistance forces. The resulting upward displacements along the E-W and N-S directions, are 0.31" and 0.29", respectively. It is noted that the code uplift forces are less than the uplift resistance forces, indicating that code stress checks will not predict this uplift behavior.

- The computer results indicate that the top roof will experience flexural cracking, and provides more flexible response. The computer model with cracked sections, resulted in a more flexible response, with a slight increase in the seismic forces.

- Another stress check was performed to examine the upper coupling beams connecting the N-S shear walls. It is shown that these beams were overstressed using both Code equivalent static forces, and the response spectrum analysis using the recorded response spectrum curves. The shear D/C is 2.84 and the flexural D/C is 1.94. The proposed ATC-33 (75% draft, Table 6-15) recommends the use of D/C for shear and flexural as 1.0 and 2.0, respectively, for immediate occupancy performance. Higher values of 2.0 and 4.0 are recommended for behavior based on life-safety based performance.

- The study of the coil inserts connecting the precast columns and the concrete floors indicated that D/C ratios up to 5.25 can be obtained at some of these connections, when using the Code response spectrum. It is highly questionable that these connections will sustain such large demands without experiencing excessive damage. Failure of these connections may lead to the separation of the columns from the slab, which may result in columns' instability.

- It appears that 5% damping is a reasonable estimate for the structures in the lateral direction. However, 2% damping is recommended in the vertical direction.

- For large span girders (65 ft long), effective floor vertical acceleration in the middle of the girder can be significant (up to 3.5 times the peak ground vertical acceleration). This large acceleration produces significant vertical loading that should be included in the design. Both the increase and the decrease of the total loads action on the girder should be considered.

- The current building codes do not provide simplified formulas to consider the effect of the vertical acceleration on the floor girders or beams. It appears that guidelines to consider such an effect are required. One design approach would be to increase or decrease the gravity loads acting on the beam with 2.5 times the peak ground vertical acceleration (in %g) times the gravity loads.

- A computer model was able to predicted the large acceleration recorded at the top of the roof parapet at the north side of the parking structure. It was shown that in this building the design of the parapet, based on the code formula, is conservative and should produce satisfactory results.

8.2 RECOMMENDATION FOR IMPROVED INSTRUMENTATION FOR PARKING STRUCTURES

The recorded instrumentation arrays in the parking structure appear to provide a reasonably complete representation of the translational and torsional response of the structure. The only apparent limitations appear to be the following:

(a) a lack of free-field instruments and instrumentation of the drilled caissons that would indicate the importance of soil-structure interaction. It is noted that a free field sensor has been placed at the parking structure after the Northridge earthquake.

(b) a lack of instrumentation to indicate the rocking rotations about the structure's east-west axis.

(c) no instrumentation along the length of the first and fourth floor diaphragms that could indicate their in-plane deformations.

(d) There was only one sensor to measure floor vertical acceleration in this parking structure. We recommend the installation of additional sensors to measure the vertical response of one of the coupling beams between the north-south shear walls.

REFERENCES

Beck, J.L. (1978). Determining Models of Structures from Earthquake Records, Report No. EERL 78-01, Earthquake Engineering Research Laboratory, California Institute of Technology, Pasadena CA., June.

Beck, J.L. (1990). "Statistical System Identification of Structures", Structural Safety and Reliability, ASCE, New York, Aug, pp 1395-1402.

Beck, J.L. and Dowling, M.J. (1988). "Quick Algorithms for Computing Either Displacement, Velocity, or Acceleration of an Oscillator" J. of Earthq. Eng. and Struct. Dyn., Vol. 16, No. 2, February, pp. 245-253.

Engelkirk, R. and Beres, A. (1994), "The Need to Develop Shear Ductility in Presetressed Members", Concrete International, Vol. 16 No. 10, October 1994, pp 49-56

Hilmy, S. and Masek, J. (1993). "Seismic Retrofit of Parking Structures in California (Recent Case Studies), Proceedings of the First Egyptian Earthquake Engineering Conference, Egypt, 1993.

Hilmy, S. and Masek, J. (1994). "Failure Mechanisms of Parking Structures during the Northridge Earthquake, Proceedings of the first Cairo Earthquake Engineering Symposium on Seismic Risk Assessment, Egypt, Dec. 3-5, 1994.

Porush, A., Hilmy, S. and Grigorian, C. (1995) "CSUN Parking Structure C, Causes of Failure and Code Issues", Proceedings of the 1995 SEAOC Convention, Idian Wells, California, October 19-21.

Hilmy, S . and Porush, A. (1995) "Seismic Strengthening of Non-ductile R/C Gravity Columns, Retrofit Strategies and Code Considerations", Proceedings of the Second Cairo Earthquake Engineering Symposium on Seismic Design Codes, December 1995, Cairo, Egypt.

Holmes, W. T. and Somers, P. (1996) " Northridge Earthquake of January 17, 1994 Reconnaissance Report, Vol. 2", Earthquake Spectra, Supplement C to Volume 11, January, pp. 75-98.

Werner, S.D., Beck, J.L., and Levine, M.B. (1987). "Seismic Response Evaluation of Meloland Road Overcrossing using 1979 Imperial Valley Earthquake Records", J. of Earthq. Eng. and Struct. Dyn., Vol. 15, No. 2, Feb., pp. 249-274.

Werner, S.D., Beck, J.L., and Nisar, A. (1990). "Dynamic Tests and Seismic Excitation of a Bridge Structure" Proc. of Fourth U.S. Nat. Conf. on Earthq. Eng., Palm Springs, CA., Vol. 1, May 20-24, pp. 1037-1046.

Werner, S.D., Nisar, A., and Beck, J.L. (1992a). Assessment of UBC Seismic Design Provisions using Recorded Building Motions from Morgan Hill, Mount Lewis, and Loma Prieta Earthquakes, Dames & Moore, Oakland CA, Report to National Science Foundation, Washington D.C., April.

Werner, S.D. and Nisar, A. (1992b). Use of Strong Motion Records in Buildings to Evaluate 1991 NEHRP Seismic Design Provisions, Dames & Moore, Oakland CA, Report to Building Seismic Safety Council, Washington D.C., December.

Werner, S.D., Crouse, C.B., Katafygiotis, L., and Beck, J.L. (1993). Model Identification and Seismic Analysis of Meloland Road Overcrossing, Dames & Moore, Oakland CA and Seattle WA, Report to California Department of Transportation, Sacramento CA, May.

LIST OF CSMIP DATA UTILIZATION REPORTS

California Department of Conservation
Division of Mines and Geology
Office of Strong Motion Studies
California Strong Motion Instrumentation Program (CSMIP)

The California Strong Motion Instrumentation Program (CSMIP) publishes data utilization reports as part of the Data Interpretation Project. These reports were prepared by investigators funded by CSMIP. Results obtained by the investigators were summarized in the papers included in the proceedings of the annual seminar. These reports and seminar proceedings are available from CSMIP at nominal cost. Requests for the reports, seminar proceedings and/or for additional information should be addressed to: Data Interpretation Project Manager, Office of Strong Motion Studies, Division of Mines and Geology, California Department of Conservation, 801 K Street, MS 13-35, Sacramento, California 95814-3531. Phone: (916)322-3105

CSMIP/92-01 **"Evaluation of Soil-Structure Interaction in Buildings during Earthquakes,"** by G. Fenves and G. Serino, June 1992, 57 pp.

CSMIP/92-02 **"Seismic Performance Investigation of the Hayward BART Elevated Section,"** by W. Tseng, M. Yang and J. Penzien, September 1992, 61 pp.

CSMIP/93-01 **"Influence of Critical Moho Reflections on Strong Motion Attenuation in California,"** by P. Somerville, N. Smith and D. Dreger, December 1993, 84 pp.

CSMIP/93-02 **"Investigation of the Response of Puddingstone Dam in the Whittier Narrows Earthquake of October 1, 1987,"** by J. Bray, R. Seed and R. Boulanger, December 1993, 60 pp.

CSMIP/93-03 **"Investigation of the Response of Cogswell Dam in the Whittier Narrows Earthquake of October 1, 1987,"** by R. Boulanger, R. Seed and J. Bray, December 1993, 53 pp.

CSMIP/94-01 **"Torsional Response Characteristics of Regular Buildings under Different Seismic Excitation Levels,"** by H. Sedarat, S. Gupta, and S. Werner, January 1994, 43 pp.

CSMIP/94-02 **"Degradation of Plywood Roof Diaphragms under Multiple Earthquake Loading,"** by J. Bouwkamp, R. Hamburger and J. Gillengerten, February 1994, 32 pp.

CSMIP/94-03 **"Analysis of the Recorded Response of Lexington Dam during Various Levels of Ground Shaking,"** by F. Makdisi, C. Chang, Z. Wang and C. Mok, March 1994, 60 pp.

LIST OF CSMIP DATA UTILIZATION REPORTS (continued)

CSMIP/94-04 **"Correlation between Recorded Building Data and Non-Structural Damage during the Loma Prieta Earthquake of October 17, 1989,"** by S. Rihal, April 1994, 65 pp.

CSMIP/94-05 **"Simulation of the Recorded Response of Unreinforced Masonry (URM) Infill Buildings,"** by J. Kariotis, J. Guh, G. Hart and J. Hill, October 1994, 149 pp.

CSMIP/95-01 **"Seismic Response Study of the Hwy 101/Painter Street Overpass Near Eureka Using Strong-Motion Records,"** by R. Goel and A. Chopra, March 1995, 70 pp.

CSMIP/95-02 **"Evaluation of the Response of I-10/215 Interchange Bridge Near San Bernardino in the 1992 Landers and Big Bear Earthquakes,"** by G. Fenves and R. Desroches, March 1995, 132 pp.

CSMIP/95-03 **"Site Response Studies for Purpose of Revising NEHRP Seismic Provisions,"** by C.B. Crouse, March 1995, 68 pp.

CSMIP/96-01 **"An Investigation of UBC Serviceability Requirements from Building Responses Recorded During the 1989 Loma Prieta Earthquake,"** by C.-M. Uang and A. Maarouf, September 1996, 140 pp.

CSMIP/96-02 **"Evaluation of Displacement Amplification Factor for Seismic Design Provisions,"** by C.-M. Uang and A. Maarouf, September 1996, 167 pp.

CSMIP/00-01 **"Prediction of Ground Motions for Thrust Earthquakes,"** by P. Somerville and N. Abrahamson, February 2000, 56 pp.

CSMIP/00-02 **"Quantifying the Effect of Soil-Structure Interaction for Use in Building Design,"** by C. Poland, J. Soulages, J. Sun and L. Mejia, February 2000, 99 pp.

CSMIP/00-03 **"Seismic Performance and Design Considerations of Long Span Suspension Bridges,"** by W.D. Liu, A. Kartoum, K. Chang and R. Imbsen, February 2000, 132 pp.

CSMIP/00-04 **"Analyses of Strong-Motion Records from a Parking Structure during the 17 January 1994 Northridge Earthquake,"** by S. Hilmy, S. Werner, A. Nisar and J. Beck, March 2000, 117 pp.

LIST OF CSMIP DATA UTILIZATION REPORTS (continued)

SMIP89	"SMIP89 Seminar on Seismological and Engineering Implications on Recent Strong-motion Data," Preprints, Sacramento, California, May 9, 1989
SMIP90	"SMIP90 Seminar on Seismological and Engineering Implications on Recent Strong-motion Data," Preprints, Sacramento, California, June 8, 1990
SMIP91	"SMIP91 Seminar on Seismological and Engineering Implications on Recent Strong-motion Data," Preprints, Sacramento, California, May 30, 1991
SMIP92	"SMIP92 Seminar on Seismological and Engineering Implications on Recent Strong-motion Data," Proceedings, Sacramento, California, May 21, 1992
SMIP93	"SMIP93 Seminar on Seismological and Engineering Implications on Recent Strong-motion Data," Proceedings, Sacramento, California, May 20, 1993, 114 pp.
SMIP94	"SMIP94 Seminar on Seismological and Engineering Implications on Recent Strong-motion Data," Proceedings, Los Angeles, California, May 26, 1994, 120 pp.
SMIP95	"SMIP95 Seminar on Seismological and Engineering Implications on Recent Strong-motion Data," Proceedings, San Francisco, California, May 16, 1995, 105 pp
SMIP96	"SMIP96 Seminar on Seismological and Engineering Implications on Recent Strong-motion Data," Proceedings, Sacramento, California, May 14, 1996, 130 pp.
SMIP97	"SMIP97 Seminar on Utilization of Strong-Motion Data," Proceedings, Los Angeles, California, May 8, 1997, 127 pp.
SMIP98	"SMIP98 Seminar on Utilization of Strong-Motion Data," Proceedings, Oakland, California, September 15, 1998, 175 pp.
SMIP99	"SMIP99 Seminar on Utilization of Strong-Motion Data," Proceedings, Los Angeles, California, September 15, 1999, 154 pp.